

CALIFORNIA INSTITUTE OF TECHNOLOGY

EARTHQUAKE ENGINEERING RESEARCH LABORATORY
Center for Research on the Prevention of Natural Disasters

**ENGINEERING STUDIES OF
THE SAN FERNANDO EARTHQUAKE**

by
Charles B. Crouse

EERL 73-04

A Report on Research Conducted under Grants
from the National Science Foundation and
the Earthquake Research Affiliates Program
at the California Institute of Technology

Pasadena, California
March, 1973

ENGINEERING STUDIES OF
THE SAN FERNANDO EARTHQUAKE

Thesis by

Charles Brian Crouse

In Partial Fulfillment of the Requirements
for the Degree of
Doctor of Philosophy

California Institute of Technology

Pasadena, California

1973

(Submitted July 25, 1973)

ACKNOWLEDGMENTS

The author wishes to thank Professor P. C. Jennings for guidance and assistance in the preparation of this report. Suggestions from Professors G. W. Housner, R. F. Scott, M. D. Trifunac, and Dr. F. E. Udwadia are gratefully acknowledged.

The author is also appreciative of the financial support provided by the California Institute of Technology and the National Science Foundation.

ABSTRACT

A number of accelerograms obtained during the San Fernando earthquake were analyzed to investigate the nature of the strong motion. The particular features studied were soil-structure interaction and the relative influence of local site conditions versus the source mechanism and travel paths of earthquake waves.

Evidence of soil-structure interaction in the EW fundamental mode of the Hollywood Storage building is seen in the earthquake data. General agreement exists up to ~ 5 c.p.s. in both lateral directions between theoretical, base to free field transfer functions and transfer functions derived from accelerograms obtained in the basement and adjacent parking lot. There was no evidence of soil-structure interaction in the Millikan Library and Athenaeum buildings on the Caltech campus, and this effect could not account for the major differences in their accelerograms.

Accelerogram, Fourier Amplitude Spectra, and Response Spectra data were compared from a group of six tall buildings close together near Wilshire Blvd. and Normandie Ave. in Los Angeles and from seven surrounding buildings, two to three miles away. The data indicated that local site conditions and soil-structure interaction were not major contributors to the observed differences in the response at these sites. There was correlation between the degree of similarity in the response at two sites and their distance apart. A simple wave superposition model with numerical examples confirms this correlation.

TABLE OF CONTENTS

<u>Chapter</u>	<u>Title</u>	<u>Page</u>
I	INTRODUCTION	1
II	STUDIES OF SOIL-STRUCTURE INTERACTION	4
III	ANALYSIS OF SELECTED BASEMENT ACCELEROGRAMS IN LOS ANGELES	64
IV	STUDIES OF WAVE SUPERPOSITION AND INTERPRE- TATION OF DIFFERENCES IN THE ACCELEROGRAMS	126
V	GENERAL CONCLUSIONS	142
	APPENDIX	145
	REFERENCES	149

I. INTRODUCTION

The San Fernando earthquake of February 9, 1971, provided an unprecedented amount of strong-motion data, previously unavailable. From an engineering standpoint, the lack of informative data on the destructive nature of strong earthquake-generated ground motions has resulted in a number of theoretical attempts to predict the character of the ground motion. Up until the San Fernando event such theories could not be tested well because of the lack of necessary data. For purposes of aseismic design of structures, some theoretical models have been beneficial in reducing the risk of damage. However, there has been speculation about the importance and applicability of certain features and assumptions of the theories.

A major portion of this thesis is devoted to the study of strong-motion accelerograms obtained during the San Fernando earthquake. Detailed comparisons among the records themselves, in addition to comparisons between the data and results from theoretical applications, have determined the capabilities of theories of soil-structure interaction and soil layer modification in predicting the nature of observed motions. The results of the study offer insights into the uncertain nature of the ground motion and have implications on future aseismic design of structures.

Chapter II is the study of soil-structure interaction. A theoretical soil-structure model consisting of a multi degree of freedom system supported on a rigid circular disc resting on an elastic half space is used in the analysis. The model is adapted to the Hollywood

Storage site in Los Angeles and the Millikan Library and Athenaeum buildings on the campus of the California Institute of Technology. For the Hollywood Storage site theoretical transfer functions between the base and free field motions were compared with a transfer function derived from accelerograms obtained in the basement and adjacent parking lot during the San Fernando (1971) and Arvin-Tehachapi (1952) earthquakes. The actual transfer functions derived from the earthquake data were calculated from the Fourier Amplitude Spectra (F.A.S.) of 20 sec. portions of the accelerograms. Basement accelerograms obtained from the Millikan Library and Athenaeum during the San Fernando earthquake were the basis for comparisons between the recorded motions and the results expected from soil-structure models of both buildings.

Chapter III examines accelerogram data obtained from the basements of buildings within a three mile radius centered near the intersection of Wilshire Blvd. and Normandie Ave. in Los Angeles. Most of the chapter is devoted to the study of accelerogram data from 6 tall buildings within a 200 yard X 700 yard area near Wilshire Blvd. and Normandie Ave. Comparisons of accelerograms, F.A.S., and Response Spectra are made to determine the nature of the observed similarities and differences in the data. The effects of local site conditions were studied by comparing the data with theoretical results from layered half space models based on data from pre-construction soil borings. The role of soil-structure interaction was examined by

comparing the responses of several buildings in both the time and frequency domains.

Accelerograph data from 7 buildings surrounding the Wilshire-Normandie group were compared with the Wilshire-Normandie data to identify general similarities that might be related to the source mechanism and travel paths of the earthquake waves as opposed to local site conditions. Also, the ground motion data of the surrounding buildings were inspected to determine the character of the ground motion with distance from the center of the earthquake. Implications of the data on earthquake resistant design were discussed.

Chapter IV investigates dispersion and wave superposition as possible explanations of the observed differences in the data studied in the previous chapters. A simple, wave superposition model is developed with numerical examples to show the differences in response at two locations as a function of their separation. Results of the analysis are compared with the observed motions during the San Fernando earthquake at sites close together.

II. STUDIES OF SOIL-STRUCTURE INTERACTION

II.1 Introduction

Soil-structure interaction has been recognized by research engineers and designers as an important factor in the behavior of some structures during strong earthquake motion. Of prime importance to the engineer are the extent the soil beneath a building modifies the structural response, and any differences between the motion of the building at ground level and the motion that would have resulted at that point had there been no building present.

Housner was one of the first to investigate the problem. He and Merritt (1) studied the rocking motion of a building on a flexible soil. Housner (2) then analyzed basement accelerograms from the Hollywood Storage building and those recorded on the ground nearby during the Arvin-Tehachapi earthquake of July 21, 1952. Based on a comparison of the relative velocity response spectrum curves for both records, he concluded that the effect of soil-structure interaction was not appreciable.

The soil-structure model studied by Housner and Merritt consisted of a lumped-mass and spring system with a rotational spring at the base to approximate the rocking of the structure on the soil. They subjected this model to four different recorded earthquake motions. The results indicated that the maximum base shear would almost always be less than that obtained from a rigid base model.

More realistic models of the coupling between the soil and foundation have since been developed to approximate the dimensional

effects of the foundation. Reissner (3) first studied the problem of a vertical harmonic excitation applied to a rigid circular disc resting on an elastic half space. Arnold, Bycroft, and Warburton (4), Bycroft (5), and Warburton (6) considered the same problem but extended the work to include three other types of vibration, horizontal translation, torsion, and rocking. In all cases a form of the stress distribution at the contact surface was assumed to obtain solutions.

Numerical results for the dynamic problem of a rigid disc perfectly bonded to an elastic half space have never been obtained. A perfect bond means that the stresses and displacements are continuous at the interface between the disc and the half space. This problem is commonly referred to as the complete mixed boundary value problem.

If it is assumed that at least one of the components of surface traction at the interface is zero, then a relaxed mixed boundary value problem results. The relaxed problem, extensively studied so far, assumes that for vertical and rocking vibrations the contact surface is frictionless, while for horizontal vibrations the contact surface is free of normal tractions. Consequently, the horizontal displacements under the disc are unconstrained for vertical and rocking vibrations, and the vertical displacements are unconstrained for horizontal vibrations.

Veletsos and Wei (7) and Luco and Westmann (8) have obtained numerical results for this relaxed problem and have devised approximate techniques to show that rotational displacements due to lateral

forces and vice-versa are small in comparison with displacements in the same direction as the applied forces. Solutions from the rigid disc-elastic half space model have been justified to a certain extent experimentally (5), (9), (10) as close approximations to the actual behavior of footings on soil.

In practice, circular foundations are rarely encountered. The more typical geometry of a rectangular plate on an elastic half space was studied by Kobori et al. (11), (12). His numerical results for typical length to width ratios are similar to Bycroft's solutions for a circular plate of equal area in the range of small excitation frequencies. The numerical analysis of one of Kobori's solutions was extended by Sarrazin (13) to include higher frequencies. Sarrazin concluded that the irregular behavior and departure of his numerical results from the results for an equivalent circular disc needed further investigation.

Trifunac (14) obtained analytical solutions for the surface motion in the vicinity of a semi-cylindrical inclusion in an elastic half space for incident plane SH waves. This model offers some insight into the nature of wave scattering around a building with sub-ground level stories.

The previously mentioned studies were preliminary to the construction of elaborate soil-structure interaction models.

Trifunac (15) expanded his earlier work (14) to account for an infinitely long shear wall atop a rigid cylindrical inclusion. Trifunac's model was a generalization of an earlier study by Luco (16)

to the case of SH waves at arbitrary angles of incidence (Fig. 1a). Trifunac calculated the differences in surface displacements on both sides of the shear wall from the scattering of waves off the foundation (inclusion). The results give some indication of the extent to which surface motion near the building might be modified by the presence of the structure.

Sarrazin (13) and Sarrazin, Roesset, and Whitman (17) have modeled the coupling between the foundation and soil with equivalent springs and dashpots (Fig. 1b) in accordance with the foundation compliances of the relaxed problem of a rigid massless plate on an elastic half space. They have extensively studied the interaction of this foundation model supporting a single degree of freedom structure. Parmelee et al. (18) investigated a soil-structure interaction model consisting of a multi-degree of freedom system supported by a rigid disc on an elastic half space (Fig. 1c). Parmelee assumed constant values for the frequency dependent compliance functions between the disc and half space to obtain solutions to the problem. Bielak (19) was the first to obtain explicit solutions of this model subjected to vertically incident shear waves. Other studies of multi degree of freedom structures with soil-structure interaction have been recently published by Fagel and Liu (20) and Wood (21). Wood used a model similar to Fig. 1b to investigate possible soil-structure interaction of a nine-story steel frame building during the San Fernando earthquake. In the analysis he used constant values for the foundation springs and dashpots as suggested by Veletsos and Wei and others. The

model studied by Wood is a simplified version of the one studied by Bielak.

There have been several soil-structure interaction studies using the finite element approach. A finite element model developed by Finn and Reimer (22) (Fig. 1d) can be useful in instances where alluvial soil overlies bedrock. The analysis of their particular soil-structure system indicated that the coupling between the soil and structure gave conservative estimates of the maximum base shear.

Another aspect of interaction which might be significant in the downtown area of cities is the coupling between buildings through the soil. Warburton et al. (23) studied the effects of the response of a vertically excited mass from another mass nearby. Both masses were discs of equal area resting on an elastic half space. The distance between their centers was 5 times the disc's diameter. The main conclusion drawn was that under certain circumstances, namely, at excitation frequencies near the resonant frequencies of the unexcited mass-soil system, the displacements of the unexcited mass are amplified. A less obvious but perhaps a more significant result was that the presence of the second mass had virtually little effect on the response of the excited mass.

II.2 Bielak's Solutions

This section is devoted to the application of Bielak's soil-structure interaction solutions to the measured response of the Hollywood Storage building, the Millikan Library, and the Athenaeum during the San Fernando earthquake. A comparison with the Arvin-Tehachapi

earthquake data from the Hollywood Storage site was also included. The Millikan Library and the Athenaeum are on the campus of the California Institute of Technology.

A diagram of the model studied by Bielak appears in Fig. 2a. It consists of a linear, viscously damped, n-story structure supported on a rigid circular foundation of radius, a , which is bonded to a linearly elastic, homogeneous, isotropic half space. In its general form the system has $n + 2$ degrees of freedom, translation of each story mass, translation of the base, and rotation of the entire system. The system, initially at rest, is subjected to vertically incident plane shear waves. It is assumed that there is no scattering of waves off the rigid foundation and nearby surface.

The equations used in the analysis (see Appendix) were developed under the assumption that the superstructure possesses classical normal modes. This assumption has been shown to be sufficiently accurate for most engineering purposes. For the case of classical normal modes, a model equivalent to that shown in Fig. 2a can be constructed (Fig. 2b) (19). It consists of n oscillators attached to the rigid circular base; each oscillator defined by a natural frequency, ω_j , critical damping ratio, η_j , modal mass, M_j , modal moment of inertia, \bar{I}_j , and modal height, H_j (see Appendix).

For small displacements the equations of motion for the model shown in Fig. 2a are (19)

$$M\ddot{\underline{v}}^t + c\dot{\underline{v}} + K\underline{v} = 0 \quad (2.1a)$$

$$\sum_{j=1}^n m_j \ddot{v}_j^t + m_o(\ddot{v}_o + \ddot{v}_g) + P(t) = 0 \quad (2.1b)$$

$$\sum_{j=1}^n m_j h_j \ddot{v}_j^t + I_t \ddot{\phi} + Q(t) = 0 \quad (2.1c)$$

In these equations: v_j^t = total horizontal displacement of the j^{th} mass with respect to a fixed vertical axis, i.e., $v_j^t = v_g + v_o + h_j \phi + v_j$, I_t = sum of the centroidal moments of inertia of the $n + 1$ masses, and $P(t)$ and $Q(t)$ are the horizontal restoring force and moment, respectively, at the interface between the base mass and the half space. A complete description of the symbols is given in the Appendix.

A relationship between the generalized interaction forces and generalized base displacements can be written as (4), (5), (11)

$$\begin{Bmatrix} \frac{\bar{P}(s)}{\mu a^2} \\ \frac{\bar{Q}(s)}{\mu a^3} \end{Bmatrix} = \begin{bmatrix} K_{hh} & K_{hm} \\ K_{mh} & K_{mm} \end{bmatrix} \begin{Bmatrix} \frac{\bar{v}_o(s)}{a} \\ \bar{\phi}(s) \end{Bmatrix} \quad (2.2)$$

In equation (2.2), $\bar{P}(s)$ and $\bar{Q}(s)$ are the Laplace transforms of $P(t)$ and $Q(t)$, respectively, while K_{hh} , K_{hm} , K_{mh} , K_{mm} are the dimensionless, complex impedance functions and are functions of frequency and Poisson's ratio. K_{hm} and K_{mh} are equal by virtue of the reciprocity theorem and are small in comparison with the diagonal terms, K_{hh} and K_{mm} . For the analysis in the next section K_{mh} and K_{hm} will be set equal to zero. The functions

K_{hh} and K_{mm} used in the analysis are found from solutions to the relaxed mixed boundary value problem discussed in section II.1. These functions have not been evaluated for the case of a perfectly bonded, massless, rigid plate on an elastic half space; however, some experimental evidence (5), (9), (10) indicates that the differences in these two cases are small enough to not affect the problem appreciably.

For steady-state harmonic excitation of the disc, K_{hh} and K_{mm} can be expressed as (5), (24)

$$\begin{aligned} K_{hh}(ia_0) &= k_{hh}(a_0, \sigma) + ia_0 c_{hh}(a_0, \sigma) \\ K_{mm}(ia_0) &= k_{mm}(a_0, \sigma) + ia_0 c_{mm}(a_0, \sigma) \end{aligned} \quad (2.3)$$

where $i = \sqrt{-1}$, $a_0 = \frac{\omega a}{V_s}$ and ω is the frequency of excitation. k_{hh} , c_{hh} , k_{mm} , and c_{mm} are real, and can be written as (25)

$$\begin{aligned} k_{hh}(a_0, \sigma) &= \frac{8}{2 - \sigma} \beta_h(a_0, \sigma) \\ c_{hh}(a_0, \sigma) &= \xi_h(a_0, \sigma) k_{hh}(a_0, \sigma) \\ k_{mm}(a_0, \sigma) &= \frac{8}{3(1 - \sigma)} \beta_m(a_0, \sigma) \\ c_{mm}(a_0, \sigma) &= \xi_m(a_0, \sigma) k_{mm}(a_0, \sigma) . \end{aligned} \quad (2.4)$$

The functions β_h , β_m , ξ_h , ξ_m were evaluated from the numerical results in the form of graphs presented by Luco and Westmann (8), for values of the frequency parameter, a_0 , up to 6 and Poisson's ratio, $\sigma = 1/4$. β_h , β_m , ξ_h , ξ_m are not affected appreciably for different values of σ in the range $0 \leq \sigma \leq 1/3$, (8). A plot of these functions for $\sigma = 1/4$ is shown in Fig. 3.

Solution of Equations of Motion

The equations used in the analysis (section II.3) will now be presented. Details of the solution to equations (2.1) can be found in Bielak's work (19). Since the superstructure is assumed to possess classical normal modes, equations (2.1) can be solved for the base displacement in terms of the free field acceleration and transfer functions involving the modal quantities, M_j , H_j , \bar{I}_j , the natural frequencies, ω_j , and the modal damping ratios, η_j , of the superstructure. The result, expressed in terms of Laplace Transformations, is

$$\bar{y}_o(s) = \bar{v}_g(s) \frac{\Delta_o(s)}{\Delta(s)} + \bar{v}_g(s) \quad (2.5)$$

where $y_o(=v_o + v_g)$ is the total lateral displacement of the base mass. Taking the base mass to be initially at rest, equation (2.5) becomes (replacing the transform variable s by $i\omega$)

$$\frac{\bar{y}_o(\omega)}{\bar{v}_g(\omega)} = \frac{-\omega^2 \Delta_o + \Delta}{\Delta} \quad (2.6)$$

Expressions for Δ_o and Δ are given in the Appendix. Equation (2.6) will be used for comparisons with data derived from specific accelerograms from the San Fernando and Arvin-Tehachapi earthquakes.

Behavior of Transfer Function

Before making any comparisons between the theoretical model and the earthquake data, some basic characteristics and consequences of the basic model and equation (2.6) will be discussed. The model

developed in this section is equivalent to a model shown in Fig. 1b which utilizes frequency-dependent springs and dashpots for the interaction between the soil and foundation. The spring-dashpot model becomes equivalent if the impedance functions, K_{hh} and K_{mm} , are expressed as equation (2.3). The functions, k_{hh} and k_{mm} would be the stiffnesses of the translational and rotational interaction springs, respectively, while the functions, c_{hh} and c_{mm} , would represent the viscous damping constants of the translational and rotational interaction dashpots. k_{hh} and c_{hh} are nearly constant over a wide frequency range, while the rotational compliances, k_{mm} and c_{mm} , vary significantly with frequency (see equation (2.3) and Fig. 3).

To visualize the basic differences between the translational motion of the base and free field motion in the same direction, it is convenient to examine an equivalent oscillator shown in Fig. 4. Temporarily neglecting the rotation (assume K_{ϕ} and C_{ϕ} are infinite) and excluding any effects of the dynamic base shear, S_b , and moment, M_b , the transfer function, $\bar{y}_o(\omega)/\bar{v}_g(\omega)$, for a harmonic excitation, $v_g = e^{i\omega t}$, can easily be computed by elementary vibration theory. A plot of $|\bar{y}_o(\omega)/\bar{v}_g(\omega)|$ for the simple case is shown by a dashed line in Fig. 5 for an actual building-soil site (21). Since K_x and C_x are nearly constant over the range of frequencies considered, average values of these parameters were used. The frequency-dependent base shear distorts the transfer function in the neighborhood of the natural frequencies of the superstructure (Fig. 5). The amount of

distortion depends mainly on the natural frequencies, modal damping, and mode shapes of the superstructure. It will be demonstrated by examples in section II.3, that the transfer function, $\bar{y}_o(\omega)/\bar{v}_g(\omega)$, can be sensitive to different choices of mode shape. Fig. 5 clearly shows that the base response can be greater than the free field motion at the lower end of the frequency scale, and for larger frequencies the base response can be attenuated. The radiation damping into the soil from the building basically determines the maximum amplitude of the transfer function, although in some instances, higher modes from the superstructure can contribute significantly.

The addition of the overturning moment, M_b , and the rocking flexibility have a negligible effect on the transfer function for horizontal motion, $\bar{y}_o(\omega)/\bar{v}_g(\omega)$, other than to decrease the fundamental frequency of the system further (Fig. 6), (21). Soil-structure interaction due to translation and/or rocking of the base mass reduces the natural frequencies of the superstructure (25), but in most cases the only appreciable reduction occurs to the fundamental frequency. For tall buildings, where M_b is large, this reduction is primarily due to rocking.

II.3 Applications of Model to Earthquake Data

The first soil-structure interaction study of earthquake response was Housner's analysis of accelerograms obtained from the site of the Hollywood Storage building during the Arvin-Tehachapi earthquake (2). His conclusions about possible interaction were based on the comparisons between the basement records and free field records

obtained in a nearby parking lot. No comparisons were made between the data and a theoretical model.

Duke et al. (26) compared the Hollywood Storage data to a theoretical model of the building-soil system adapted from Luco (16), (Fig. 1a). Luco's model was restricted to buildings that behaved as infinitely-long shear walls; however, natural frequency calculations of the superstructure in the EW direction indicated that the Hollywood Storage building closely approximated a cantilevered shear wall. Comparisons were made between the basement to free field transfer function for the model and an actual transfer function computed from a smoothed version of the ratio of the Fourier Amplitude Spectra of the accelerograms. The actual transfer function did not give much indication of the presence of modal contributions from the superstructure as predicted by the model. The only resemblance to the theoretical model appeared beyond 5 c.p.s. where the transfer function was less than unity.

Duke's approach assumed the accelerogram from the parking lot was representative of the free field motion. This assumption is considered valid for the frequency range of interest used in the analysis and is further discussed in the conclusions (section II.4).

Hollywood Storage

The Hollywood Storage building is located near the corner of Santa Monica Blvd. and Highland Ave. in Los Angeles (Fig. 7). The building is about 18 miles south of the center of energy release of the San Fernando earthquake. The building is a 14-story reinforced

concrete frame structure, 150 ft. tall, with a basement 9 ft. beneath the ground story. The foundation consists of concrete piles 10 ft. to 30 ft. long spaced every 17 ft. in each direction. Lateral dimension of the building are 51 ft. (NS) by 217 ft. (EW). A soil boring to a depth of 100 ft. revealed a soft, sandy clay mixture with a density varying from 100 p.c.f. at the surface to roughly 130 p.c.f. (27).

Adjoining the main building is a long, narrow, one-story structure used as a loading dock and storage area. Just north of the main structure and east of the loading dock is a film studio, 30 ft. tall, with base dimensions, 120 ft. by 60 ft. Directly west 112 ft. from the southwest corner of the main building is a small shed with aluminum siding and a 9 ft. by 6 ft. concrete base. This shed contains a Standard Strong-Motion accelerograph instrument. The accelerograph in the basement of the building is located at the southwest corner and is also a Standard.

The major portions of the horizontal components of the accelerograms obtained during the San Fernando earthquake from the basement and the shed (hereafter referred to as the free field record) are shown in Fig. 8. The peak free field accelerations in the hard shaking portions from 1 to 8 sec. are generally 0.05 g to 0.1 g greater than corresponding peaks of the basement accelerations. The free field accelerograms also show a higher frequency content in this 1 to 8 sec. segment. Following the portion of hard shaking are smaller amplitude, longer period accelerations in both records that gradually diminish to peak values of about 0.025 g at 20 sec.

The Fourier Amplitude Spectra (F.A.S.) of the 20 sec. accelerograms were calculated using a fast Fourier transform technique based on the Cooley-Tukey algorithm. Graphic comparisons of the F.A.S. (Fig. 9) show close agreement between the basement and free field F.A.S. for frequencies up to 4 c.p.s. in both the NS and EW directions. For frequencies larger than 4 c.p.s. the free field F.A.S. is significantly larger than the corresponding basement F.A.S. For visual purposes the F.A.S. plots were smoothed one cycle with the Hanning spectral window weighted $\frac{1}{4}, \frac{1}{2}, \frac{1}{4}$, i.e., if F_i represents a point in the unsmoothed F.A.S., then a point, \bar{F}_i , in the smoothed F.A.S. is given by $\bar{F}_i = \frac{1}{4} F_{i-1} + \frac{1}{2} F_i + \frac{1}{4} F_{i+1}$. The frequency spacing of the ordinate is 0.05 c.p.s.

A transfer function between the basement and free field was achieved by dividing the once-smoothed basement F.A.S. by the once-smoothed free field F.A.S. and smoothing this ratio 10 times. The additional smoothing of the transfer function was done to emphasize the overall trend and to eliminate large fluctuations. Data reduction of Arvin-Tehachapi accelerograms was identical to the process just described for the San Fernando data.

The calculation of the necessary parameters for the theoretical model was based on data collected by Duke (26), (27). A representative value of the shear wave velocity was derived from an experimentally determined P-wave velocity for the soil. A P-wave velocity of 2400 f.p.s. was measured at the site at depths from 9 ft. to 60 ft. (27). If a Poisson's ratio, $\sigma = \frac{1}{3}$, is assumed, then the theory for a linear, homogeneous, isotropic half space predicts that the shear wave velocity is

half the P-wave velocity, or 1200 f.p.s. However, during an earthquake the elastic behavior of the soil is nonlinear. Experimental evidence indicates that the shear modulus of soil determined by velocity tests can be reduced by half during an earthquake (28). For an ideal half space then, the shear velocity would be reduced by a factor of $1/\sqrt{2}$. The earthquake shear wave velocity would be $V_s \simeq 800$ f.p.s. The average density, ρ , from the soil borings was 115 p.c.f. The equivalent base radius, a , for a circle whose area is equal to the cross-sectional area of the main building was 59.4 ft. The story masses and equivalent interstory stiffnesses were taken from Duke (26), who calculated these quantities from the structural drawings. The lumped-story masses varied from a minimum of 1.47×10^6 lbs. to a maximum of 2.06×10^6 lbs. The total mass of the superstructure, from the 2nd floor up, was 25.8×10^6 lbs. The EW direction of the building was significantly stiffer than the NS direction. The EW stiffnesses varied from 230×10^6 lbs./ft. at the top to $1,070 \times 10^6$ lbs./ft. near the bottom, while the NS stiffnesses varied between 46×10^6 lbs./ft. and 496×10^6 lbs./ft.

The natural frequencies and mode shapes of the superstructure were found by solving the eigenvalue problem for a 14 degree of freedom, linear, spring-mass system. The first 4 natural frequencies in the NS direction were 1.05, 2.74, 4.30, and 5.84 c.p.s. Vibration tests before the San Fernando earthquake (29) gave resonant frequencies at 0.83, 2.7, and 4.5 c.p.s. for the NS direction. The EW natural frequencies, calculated from the eigenvalue problem, were within 5% of 2, 6, and 10 c.p.s., the natural frequencies of an appropriate cantilevered

shear beam. The EW fundamental frequency from vibration tests was 2.0 c.p.s. (29).

Figures 10 through 15 compare the basement to free field transfer functions, $|\bar{y}_o/\bar{v}_g|$, derived from the F.A.S. of the earthquake acceleration data and the theoretical model. For the theoretical transfer function the parameters ρ , V_g , a , and the natural frequencies were fixed, while m_o (and hence I_t), η_j , and the mode shapes were varied. Different choices of the base masses, m_o , modal damping ratio, η_j , and mode shapes, X_{ij} , were made to indicate their effect on the transfer function and to obtain the "best fit" with the actual transfer function.

Figures 10 and 11 show how two different orthogonal mode shapes can affect the shape of the theoretical transfer function. The size of the distortions in the transfer function from higher modes, through the modal quantities, M_j , \bar{I}_j , H_j , depends on the mode shape chosen. For example, mode shapes measured by Jennings et al. (30) at another building give modal mass values, $M_1 = 19.6 \times 10^6$ lbs., $M_2 = 5.8 \times 10^6$ lbs., and $M_3 = 0.4 \times 10^6$ lbs. (Fig. 10). Mode shapes calculated from the superstructure using Duke's data (26) give modal mass values, $M_1 = 21.4 \times 10^6$ lbs., $M_2 = 2.8 \times 10^6$ lbs., and $M_3 = 0.9 \times 10^6$ lbs. Variations in the modal quantities for different mode shapes are more pronounced in the transfer function for the higher modes where the distortions are spread over a wide frequency band. The distortions in the transfer function at the fundamental frequency are confined to a much narrower band.

A comparison of the theoretical transfer functions in Figs. 11 and 12 or Figs. 14 and 15 shows the basement response greatly attenuated with a 6 fold increase in the base mass. The smaller value of m_0 , 5×10^6 lbs., was an estimate of the weight of the basement and ground level floor slabs and the weight of the concrete walls in the basement. The larger value, $m_0 = 3.1 \times 10^7$ lbs., included an estimate of the weight of the soil and clustered foundation piles between the basement floor and the rock layer supporting the piles. This value of the base mass was thought to be an upper bound for m_0 .

An example of how the modal damping, η_j , in the superstructure modifies the transfer function can be seen in Figs. 12 and 13. Larger values of η_j tend to smooth the distortions for all modes; but, as might be expected, variations in η_j do not alter the overall shape of the transfer function.

The partial agreement between the theoretical and actual transfer functions in the EW direction is limited to frequencies between 0 and ~ 5 c.p.s. There appears to be strong evidence of soil-structure interaction in the fundamental mode for the San Fernando earthquake but not the Arvin-Tehachapi event. A distortion in the San Fernando transfer function centered at 1.5 c.p.s. conforms in shape and size with the theoretical prediction. Beyond 5 c.p.s. it does not appear that any combination of parameters previously discussed is consistent with the observed behavior. Using the upper bound for m_0 in the theoretical model will attenuate the amplitude of the transfer function enough to give reasonable agreement for frequencies beyond 11 c.p.s.

for the San Fernando data (Figs. 12 and 13). The trend of the Arvin-Tehachapi transfer function shows reasonable agreement with the theoretical curve for frequencies beyond 4 c.p.s. In both cases, however, this choice of m_0 reduces the agreement in the low frequency range.

There is general agreement in amplitudes between the theoretical and both earthquake transfer functions in the NS direction for frequencies between 0 and 4 c.p.s. for the smaller value of the base mass, $m_0 = 5 \times 10^6$ lbs. (Fig. 14). Neither of the earthquake transfer functions however, gives positive indication of interaction in any of the modes. For frequencies beyond 4 c.p.s. both earthquake transfer functions attenuate in roughly the same manner, with the amplitude levels of Arvin-Tehachapi slightly larger on the average than San Fernando. The same general trend was observed in the EW direction. Substituting the upper limit for m_0 into the model to achieve amplitude attenuation for larger frequencies improves the agreement; however, as previously noted for the EW direction, this worsens the agreement for frequencies less than 4 c.p.s.

To further investigate the likelihood that the theoretical model does not adequately explain the observed behavior over a large frequency range, comparisons were made between the San Fernando free field accelerogram and a theoretical free field accelerogram. The theoretical free field accelerogram was computed by transforming the San Fernando EW basement accelerogram through theoretical transfer functions by appropriate Fourier analysis and synthesis. Two theoretical transfer functions, whose amplitudes are plotted in Figs. 10 and 12, were selected. They were chosen because of their dissimilarity

to illustrate that the differences they cause between the computed free field accelerograms and the input basement accelerogram are almost negligible. Figures 16 and 17 clearly show the differences between the computed free field and recorded basement motions are relatively minor. Local variations do exist in the size and shape of a few peaks. Overall then, the calculated free field accelerogram is virtually the same as the recorded basement accelerogram and is thus quite different from the recorded free field accelerogram (Fig. 8).

Millikan Library and Athenaeum

The Millikan Library and Athenaeum buildings are located on the main campus of the California Institute of Technology in Pasadena, approximately 21 miles southeast of the center of energy release during the San Fernando earthquake. The Athenaeum is due east of Millikan Library a distance of 1220 ft. Fig. 18 shows their location with respect to other buildings on campus, the majority of which are 3 story reinforced concrete structures with 2 basement levels.

The Millikan Library is a nine-story reinforced concrete building 144 ft. tall with a basement level 14 ft. below the ground floor. The plan dimensions are 79 ft. x 69 ft. with an additional 8 ft. x 23 ft. area on the east side and a 14 ft. x 29 ft. stairwell on the west side (Fig. 19). Lateral load resistance is provided in the NS direction primarily by reinforced concrete shear walls and in the EW direction by a central reinforced concrete elevator shaft. The north and south faces consist of precast concrete window wall panels. The foundation is basically a central pad 32 ft. wide by 4 ft. deep,

extending from the east curved wall to the west curved wall (Fig. 19). The foundation rests on alluvium composed of firm to dense sand mixed with gravel with an average density of 115 p.c.f. The alluvium on campus extends about 900 ft. to bedrock.

The Athenaeum is a $2\frac{1}{2}$ -story reinforced concrete structure of fairly complex geometry (Fig. 20). The building is asymmetric and non-uniform in height. The basement floor area is approximately 127 ft. \times 138 ft. with an additional 69 ft. \times 32 ft. on the north side. The main support of the structure is provided by square reinforced concrete columns numbering 120 to 150 depending on the floor level. The foundation consists of conventional spread footings, 7 ft. \times 7 ft. \times 2 ft. thick on the average, and rests on the same type of alluvium as the Millikan Library. A P-wave velocity of 2200 f.p.s. to a depth of 100 ft. was determined by experimental velocity tests (27).

A SMA-1 accelerograph recorded the basement accelerations at the Athenaeum during the San Fernando earthquake, and an RFT-250 obtained a record in the basement of Millikan Library. There were no other ground or basement level stations on campus. Figs. 21 and 22 compare the lateral components of the basement acceleration of each building while Fig. 23 represents the Fourier Amplitude Spectra (F.A.S.) of the 20.48 sec. portions of the accelerograms. The F.A.S. plots have been smoothed 10 cycles (an arbitrary choice) with the Hanning spectral window. Accelerogram comparisons reveal the peak accelerations during the hard shaking are generally larger in the Millikan Library record. A comparison of the F.A.S. shows that the

basement motion was more intense in Millikan, especially in the NS direction.

To test whether soil-structure interaction could account for the differences noted in the F.A.S. and the accelerograms, the free field motions near each building were assumed to be identical. For vertically incident waves this would be a valid assumption discounting any local geological irregularities and the influence of other nearby structures. The modulus of a transfer function, $|\bar{y}_o(\omega)/\bar{v}_g(\omega)|$, was calculated for each building. The moduli were then divided to give the amplitude of a theoretical transfer function between the basements of each building, i.e., $|\bar{y}_o(\omega)_{\text{MILLIKAN}}/\bar{y}_o(\omega)_{\text{ATHENAEUM}}|$. The amplitude of this transfer function was then compared with the ratio of the F.A.S. calculated from the accelerograms. A brief discussion of the modeling of each building-soil structure precedes the analysis of the results.

The Athenaeum was modeled two ways because of its relatively high stiffness. One method was to consider the entire building as a rigid plate; the other way was to approximate it as an equivalent one-story structure resting on a foundation base mass. The weight of the building and foundation determined from structural drawings was 18×10^6 lbs. This value was obtained by estimating the weights of the reinforced concrete walls, columns, floor slabs, beams, and spread footings. Nominal values were added for the live load, but the weight of the architectural elements was neglected. For the single-story approximation the total weight was divided so that the base mass, m_o , weighed 13×10^6 lbs. and the first story, m_1 , 5×10^6 lbs. The height between m_o and m_1 was estimated to be 20 ft. The equivalent base

radius was 80 ft. A fundamental frequency of 4 c.p.s. was chosen for both directions and the modal damping was assumed to be 5% of the critical value.

The masses of each story for the Millikan Library were taken from Kuroiwa (31). The total weight of the superstructure, 18.7×10^6 lbs., was divided fairly evenly among the 9 stories. Values estimated for the base mass and radius were 7×10^6 lbs. and 45.9 ft., respectively. The fundamental frequencies, based on pre-earthquake ambient and forced vibration tests (31), were 2.0 c.p.s. (NS direction) and 1.5 c.p.s. (EW direction). A forced vibration test (31) also obtained the 2nd natural frequency in the EW direction of 6.2 c.p.s. The 3rd natural frequency (EW direction) was chosen as 13.5 c.p.s., an intermediate value between the theoretical values for a fixed-end shear beam and a bending beam based on a fundamental frequency of 1.5 c.p.s. The 2nd natural frequency in the NS direction, 10 c.p.s., was based on the F.A.S. analysis of earthquake accelerograms from the roof and basement (21). Fundamental mode shapes for the superstructure were taken from Kuroiwa's forced vibration tests (31). The measured translation of the ground floor was subtracted from the measured values at the upper levels. The new modal displacements were then normalized with respect to the roof and the resulting values were used as the fundamental mode shape.

To complete the modeling of the superstructure, interstory stiffnesses were calculated from the fundamental frequency and mode shape plus the story masses. The formula used to estimate the inter-story stiffnesses (32) was

$$k_s = \frac{\omega_1^2 \sum_{i=s}^n m_i X_{1,i}}{X_{1,s} - X_{1,s-1}}, \quad s = 1, 2, \dots, n \quad (2.7)$$

where ω_1 is the fundamental frequency in rad./sec., m_i is the mass of the i^{th} story, and $X_{1,i}$ is the fundamental modal value of the i^{th} story. Knowledge of the interstory stiffnesses and mass of each story enabled the calculation of the higher mode shapes by solving the eigenvalue problem. The higher natural frequencies obtained from the solution did not agree very well with the values mentioned previously, thus indicating a discrepancy between the calculated and actual stiffnesses. However the effect of these differences on the mode shapes and hence the theoretical transfer function will not be significant when comparisons are made with the transfer function calculated from the earthquake data.

Soil parameters used were the same for both soil-structure systems. Values for the soil density and Poisson's ratio were $\rho = 115$ p.c.f. and $\sigma = 0.25$. For strain levels associated with earthquake response, an appropriate shear wave velocity of 800 f.p.s. was calculated in a manner similar to that done for the Hollywood Storage site.

Theoretical transfer functions, $|\bar{y}_o(\omega)/\bar{v}_g(\omega)|$, are shown in Figs. 24, 25, 26 for both directions of the Millikan Library and the Athenaeum. The dashed line in Fig. 26 represents the Athenaeum treated as a rigid circular plate with a weight equal to the total weight of the building. The curve is nearly flat which theoretically means the basement and free field motions are very nearly identical. No reasonable increase in base mass or moment of inertia, by including

the weight of the soil between the bottom of footings and basement floor, could alter the Athenaeum's theoretical transfer function enough so that the theoretical free field motion would be noticeably different from the basement motion. Based on the Hollywood Storage analysis, it can also be concluded that the Millikan Library transfer function would not produce significant differences between the recorded basement motion and theoretical free field motion, because the transfer function is fairly close to unity over a frequency range containing most of the energy of the strong motion. Thus, the theoretical free field accelerations for the Millikan Library and Athenaeum are essentially the same as their respective basement accelerograms.

Figs. 27, 28, and 29 compare the ratio of theoretical transfer functions to the ratio of the basement F.A.S. smoothed an additional 10 cycles. The agreement between the theoretical ratios and those from the earthquake response in Figs. 27, 28, and 29 is extremely poor. There is no reasonable way to adjust the parameters of the soil-structure model of either building to improve the agreement substantially.

II.4 Conclusions

Evidence of soil-structure interaction appeared in EW direction of the Hollywood Storage building during the San Fernando earthquake for frequencies less than 5 c.p.s. The distortion in the theoretical transfer function from interaction of the fundamental mode of the building-soil system resembles the shape of the earthquake transfer function around 1.5 c.p.s. There was no positive evidence of

soil-structure interaction in the fundamental mode (EW direction) during the Arvin-Tehachapi earthquake. There seemed to be no indication of interaction from the higher modes during either earthquake.

In the NS direction there was no concrete evidence of soil-structure interaction from any mode during either earthquake. However, the theoretical transfer function for a base mass equal to the weight of the structure beneath ground level was similar in amplitude to both earthquake transfer functions for frequencies less than 4 c.p.s.

In general the San Fernando and Arvin-Tehachapi transfer functions exhibit basically the same character. Beyond ~ 5 c.p.s. both transfer functions attenuate to amplitude levels less than unity. This filtering of higher frequencies by the building was greater during the San Fernando earthquake than the Arvin-Tehachapi event.

During the earthquakes, the building somehow filtered out the higher frequencies observed in the free field accelerograms. The theoretical model was unable to predict satisfactorily this filtering which occurred for frequencies above ~ 5 c.p.s. in both directions. One obvious revision of the model would be to replace the circular base plate with a rectangular plate of the same dimensions as the building's foundation. However, the numerical results for the compliance functions for large frequencies, as noted earlier (13), need further investigation. The stress distribution beneath the plate becomes less accurate for higher excitation frequencies, and hence smaller wavelengths of the order of the plate's dimensions. According to Sarrazin (13) the differences in the compliance functions between a 2×1 rectangular plate and a circular plate of equal

area become large for dimensionless frequencies, $a_o = \frac{\omega a}{V_s}$, above 2. It is interesting to note that for the Hollywood Storage building during an earthquake (with $V_s = 800$ f.p.s. and $a = 59.4$) this value of a_o corresponds to a frequency of 4 c.p.s. which is close to the frequency that the theoretical and earthquake transfer functions diverge. This is possibly a coincidence, and should not be seriously considered as an explanation of the observed differences until the theory for larger frequencies has been examined in a more rigorous manner.

Another possible explanation of the building's filtering of higher frequencies can be given assuming most of the earthquake waves were incident upon the foundation at angles other than 90° (vertical waves). Unfortunately, no mathematical theory of soil-structure interaction has been developed to account for P or SV waves at arbitrary angles of incidence or surface waves. The idea of foundation filtering for incident waves can be visualized from Fig. 30. Notice that for certain wavelengths, λ , and angles of incidence, α , the soil beneath the building can be moving in opposite directions as indicated by the arrows. Because of its relatively large rigidity in the transverse direction, the foundation would suppress lateral movements in opposite directions at the same time. It might be reasonable to assume that the building will filter out all wavelengths smaller than the one shown in Fig. 30. For this case the building is at an impasse since equal areas beneath the foundation tend to move in opposite directions. For example, in the case of the Hollywood Storage building in the EW direction, $L \simeq 200$ ft. If the velocity, V , and angle of incidence, α , of the incoming waves were 800 f.p.s. and 45°

respectively, then the frequency corresponding to the wavelength shown in Fig. 30 would be $f = \frac{V}{L \cos \alpha} = \frac{800 \text{ f.p.s.}}{200 \text{ ft.} (.707)} \approx 5.6 \text{ c.p.s.}$ For waves traveling along the surface at this velocity, $f = 4 \text{ c.p.s.}$ For waves from the NS direction, f would be about 4 times larger since the foundation dimension of the building is only 50 ft. in this direction. However, the adjoining one-story structure and the structure 78 ft. to the north of the main building may increase the effective length of the building in the NS direction from a filtering standpoint. Waves arriving from a direction other than NS or EW would presumably cause similar filtering. The expected filtered frequencies, then, are of the same order as the observed frequencies filtered by the building during the earthquakes.

The inability of the theoretical model to incorporate any type of wave at arbitrary incidence may be its most serious limitation in describing observed soil-structure interaction effects.

There are other obvious inadequacies of the mathematical model in conforming to reality. A homogeneous, isotropic, linearly elastic soil is never encountered. These assumptions are recognized as mathematically convenient and hopefully can approximate the actual soil behavior for practical engineering purposes.

The modeling of the foundation by a flat plate resting on the surface is another debatable issue. This simplification would intuitively seem more accurate for shallow foundations as opposed to buildings with a number of underground stories. In the case of deep foundations, wave scattering off the underground portion of the building would alter the sub-ground story response and nearby free field

motions. Also, the compliance functions for the rigid plate problem, expressing the nature of the radiative damping and the soil stiffness, would no longer be valid. For the Hollywood Storage building the basement level was only 9 ft. beneath the surface. The size and orientation of the building and location of the parking lot accelerograph with respect to the epicenter of both earthquakes should rule out wave scattering off the building's foundation as a reason for doubting the representation of the parking lot accelerogram as the free field motion.

The reinforced concrete piles, depending on their number and size, could be another contributing factor to the basement response. In the analysis of the Hollywood Storage building, their presence was accounted for by an increase in the foundation mass only. This consideration did not improve the overall agreement between the theoretical and earthquake transfer functions.

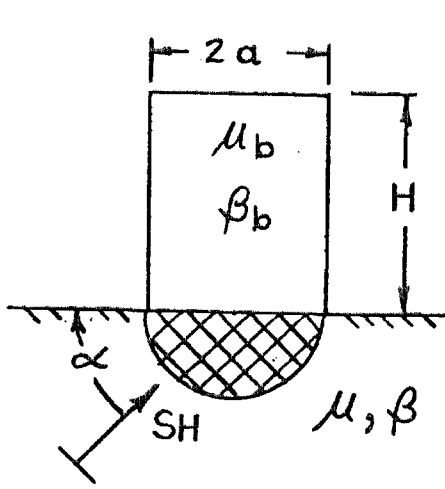
In the case of the Millikan Library and Athenaeum the main question is: Can the differences in the basement accelerograms be explained by the present state of art of soil-structure interaction theory? The answer is simply no. The distance between the buildings and their relative orientation with respect to the epicentral area, coupled with the possibility that many incoming waves may have been incident at angles other than 90° , could perhaps account for the major differences. The concepts of wave superposition and dispersion can also conceivably explain the major differences between the basement accelerograms recorded in the Millikan Library and the Athenaeum. Wave superposition and dispersion are discussed in Chapter IV.

If soil-structure interaction in some form did result in the major differences between the library and Athenaeum, then the general character of the interaction phenomenon must be significantly different than considered by the present theory.

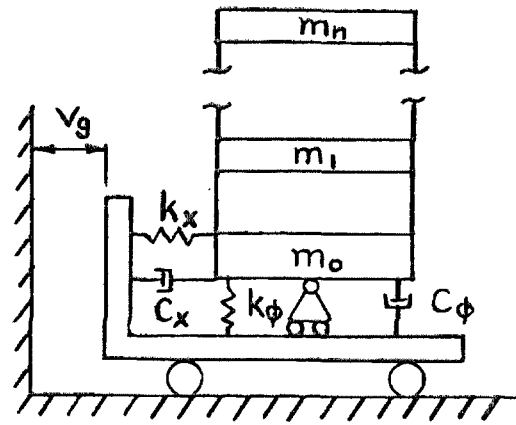
For a better understanding of the interaction phenomenon during earthquakes, it would be beneficial to know more precisely the ground motion near a particular building. It was assumed that the parking lot accelerogram from the Hollywood Storage site was representative of the surface motion at the location of the building with the building absent (i.e., the true free field motion). The ground motion is expected to vary from point to point, but based on accelerograms studied in Chapter III and the wave superposition analysis in Chapter IV, the degree of similarity in surface motions at any two points increases as their distance apart decreases. From the examples presented in Chapter IV on wave superposition, with due regard to the distance between the accelerographs in the parking lot and the Hollywood Storage building, and their orientation with respect to the direction of incoming waves for both earthquakes, the error in assuming the parking lot record is the free field motion should be small in the frequency ranges containing most of the earthquake's energy.

The distance between the Millikan Library and Athenaeum is roughly 10 times the distance between the accelerographs in the main building and parking lot at the Hollywood Storage site. The free field motions at these sites were probably different over a significant frequency range. A knowledge of the differences in ground motion at various locations near these buildings would be of value in understand-

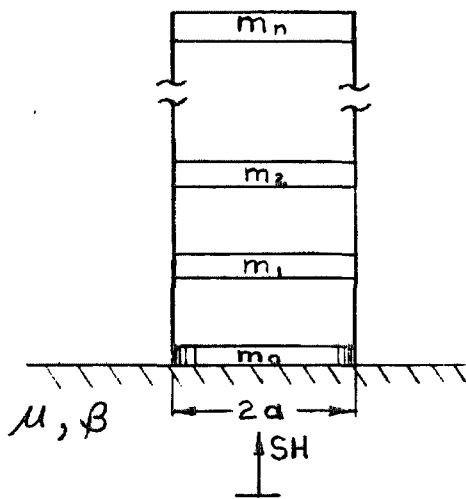
ing the actual nature of interaction, as well as the relationship between ground motions as a function of their separation. During future earthquakes, a well instrumented site of this nature might determine whether there is consistency in observed soil-structure interaction behavior and whether any site periodicities exist.



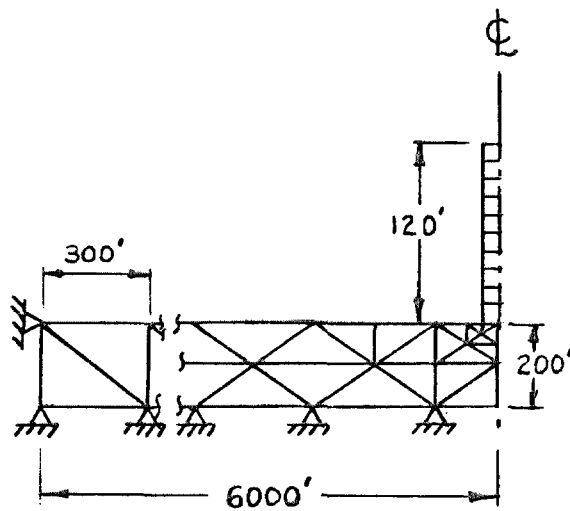
(a)



(b)



(c)



(d)

Fig. 1 Models of Soil-Structure Interaction.

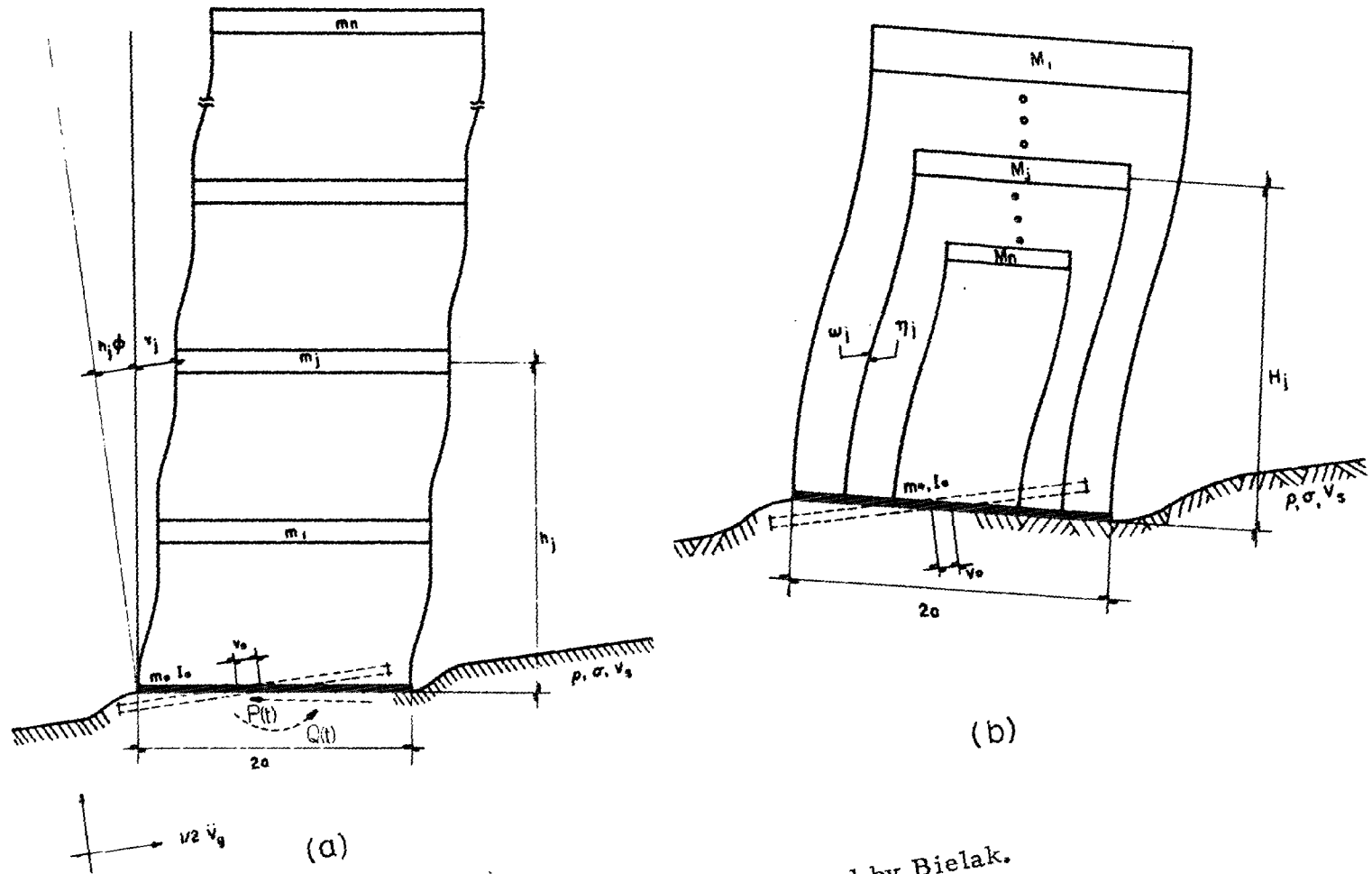


Fig. 2 Soil-Structure Models Studied by Bielik.

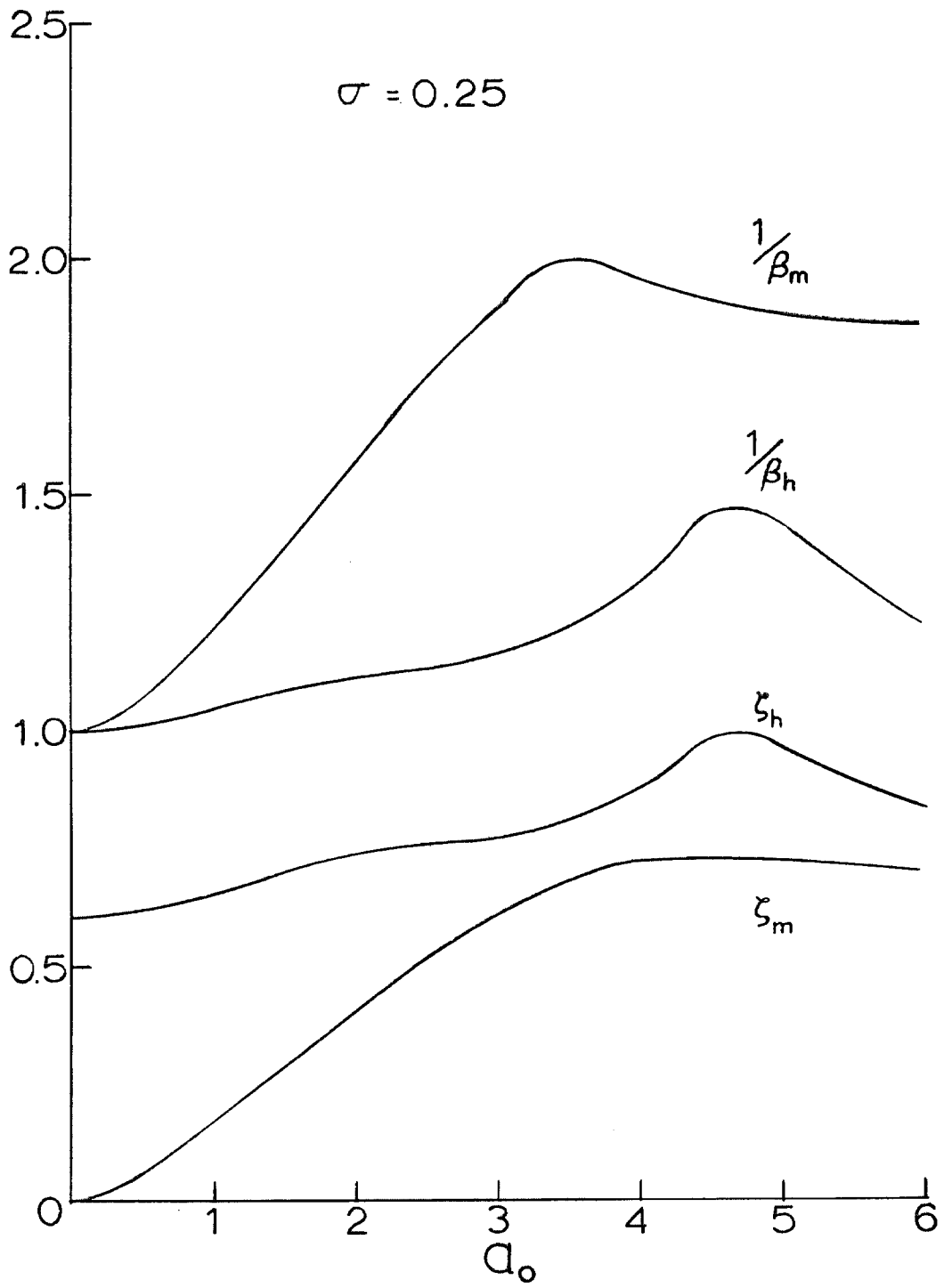


Fig. 3 Values of $1/\beta$ and ξ for $\sigma = 1/4$.

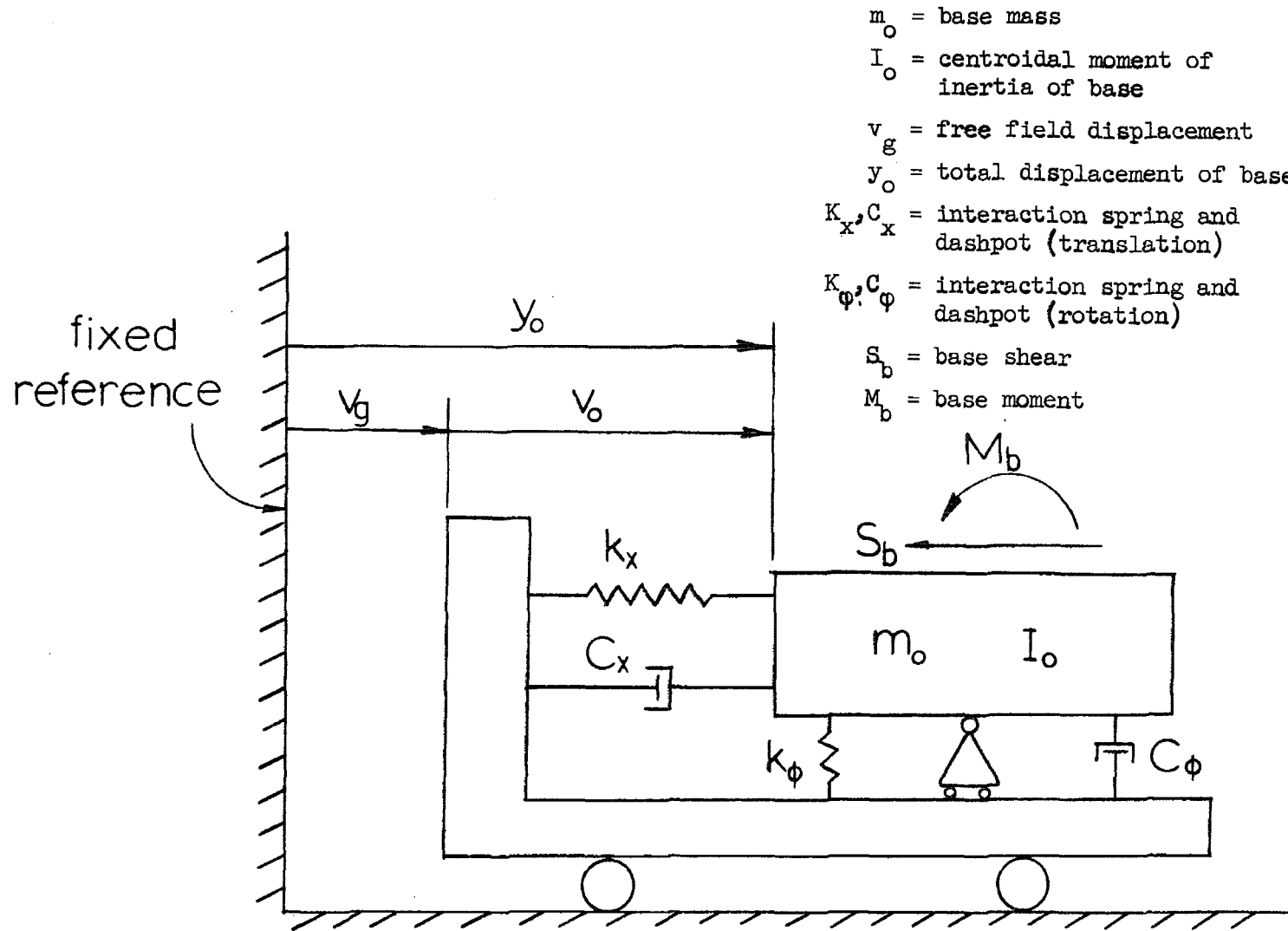


Fig. 4 Soil-Structure Model with Springs and Dashpots.

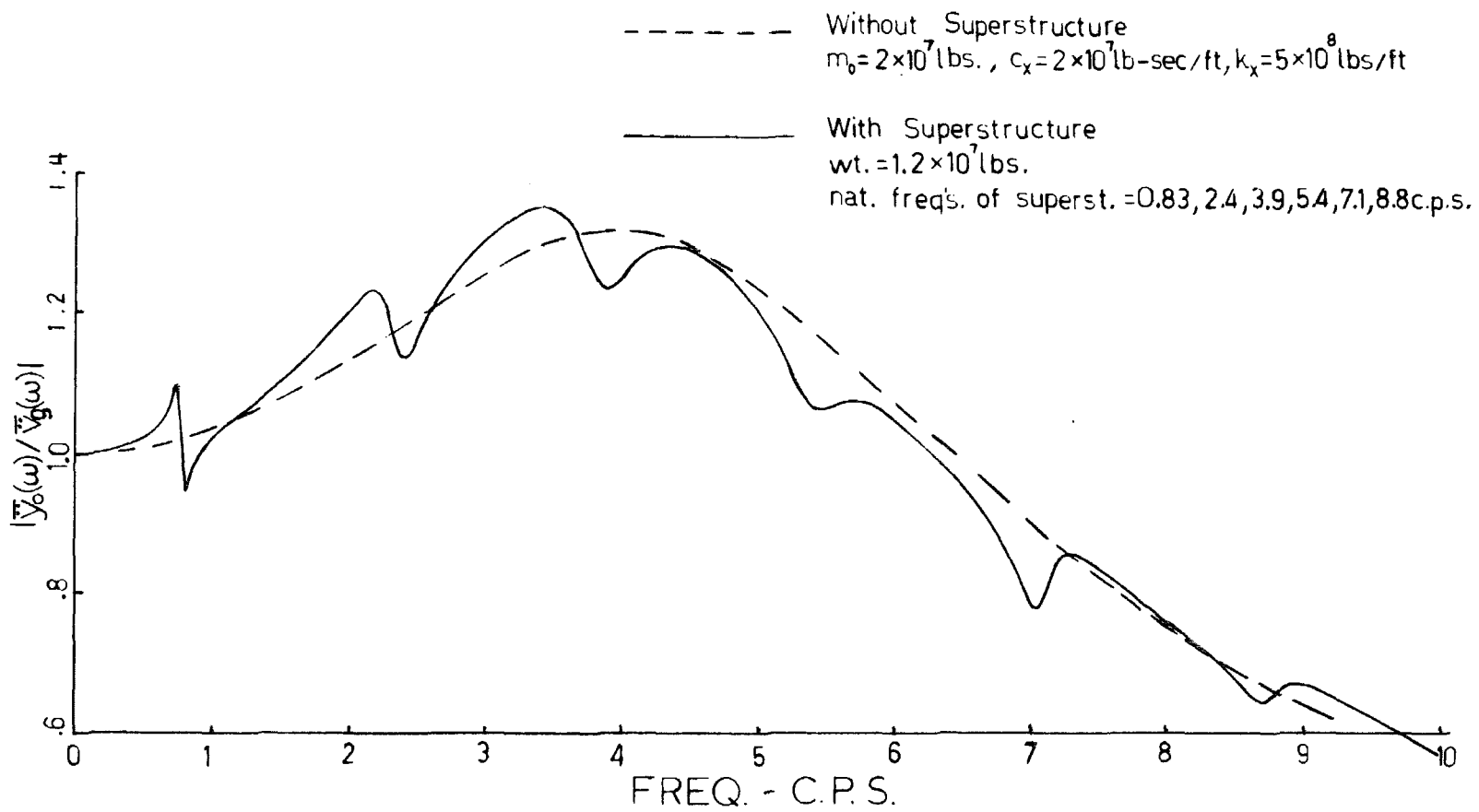


Fig. 5 Transfer Function for Translation of Oscillator Shown in Fig. 4.

MILLIKAN LIBRARY N-S DIRECTION.

RATIO OF FOURIER AMPLITUDE SPECTRA. BASE MOTION/FREE FIELD MOTION.

— MODEL WITH NO BASE ROCKING
-- MODEL WITH BASE ROCKING

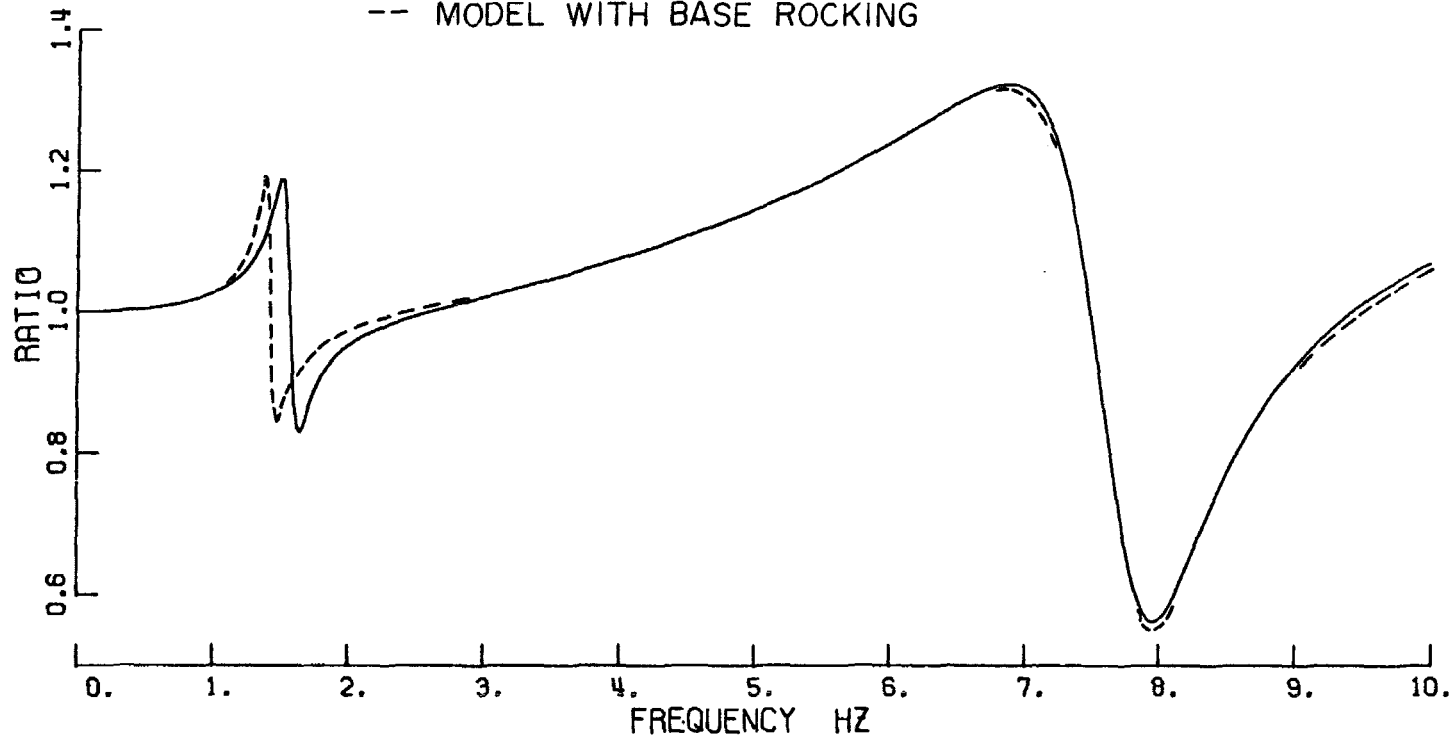


Fig. 6 Differences in Transfer Function with and without Rocking.



View Looking Southeast. Arrow Shows Location of Shed in Parking Lot Containing an Accelerograph.

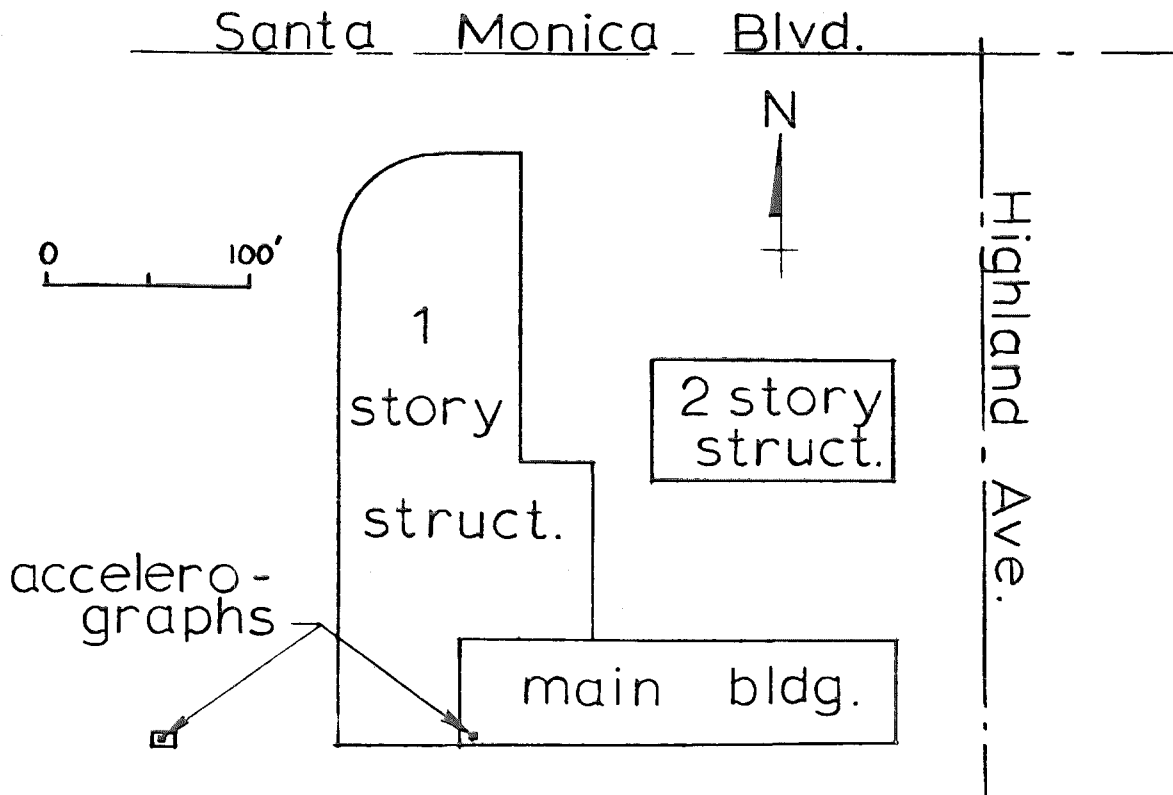


Fig. 7 Hollywood Storage Site in Los Angeles.

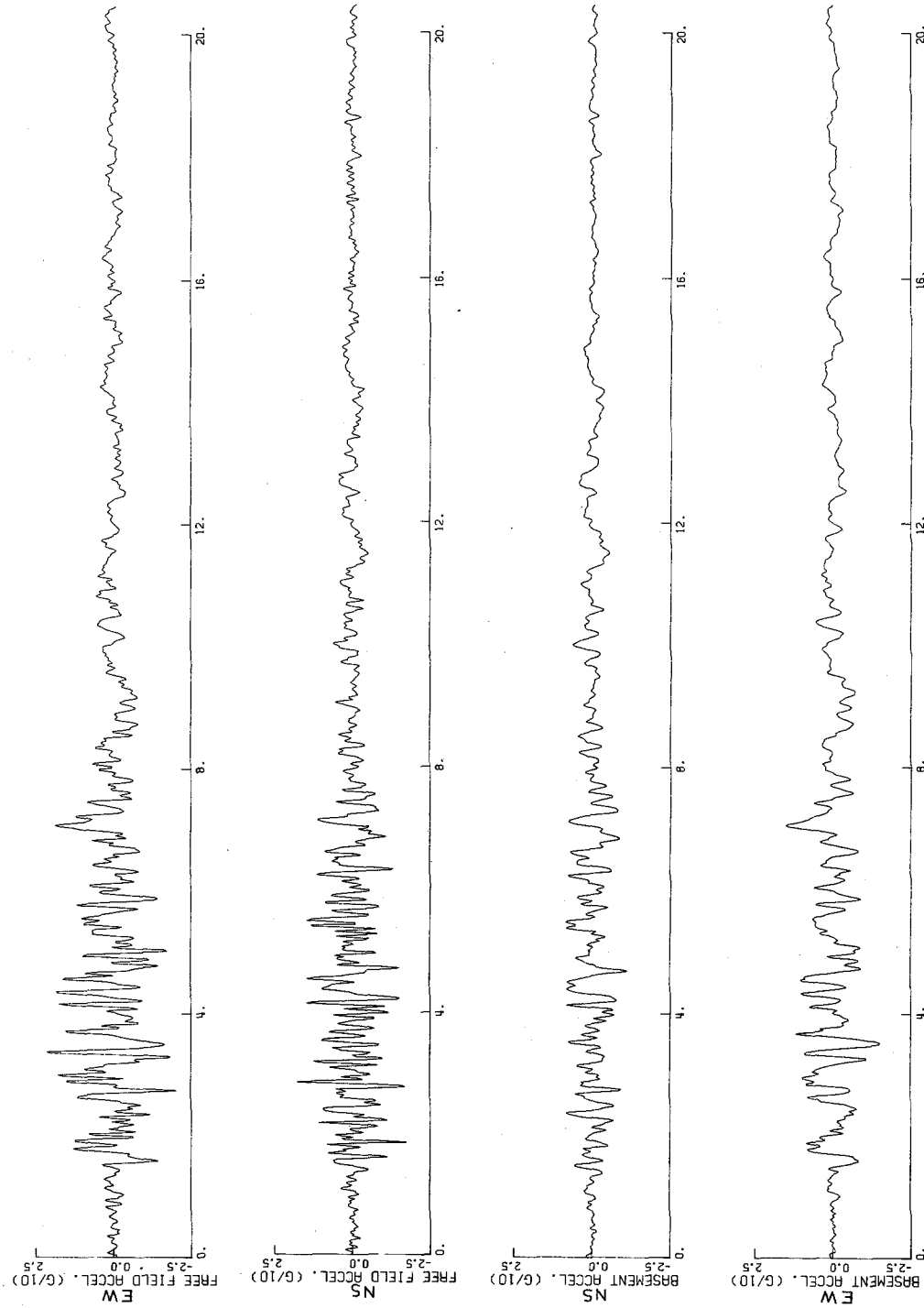


Fig. 8 Recorded Accelerations at Hollywood Storage Site.

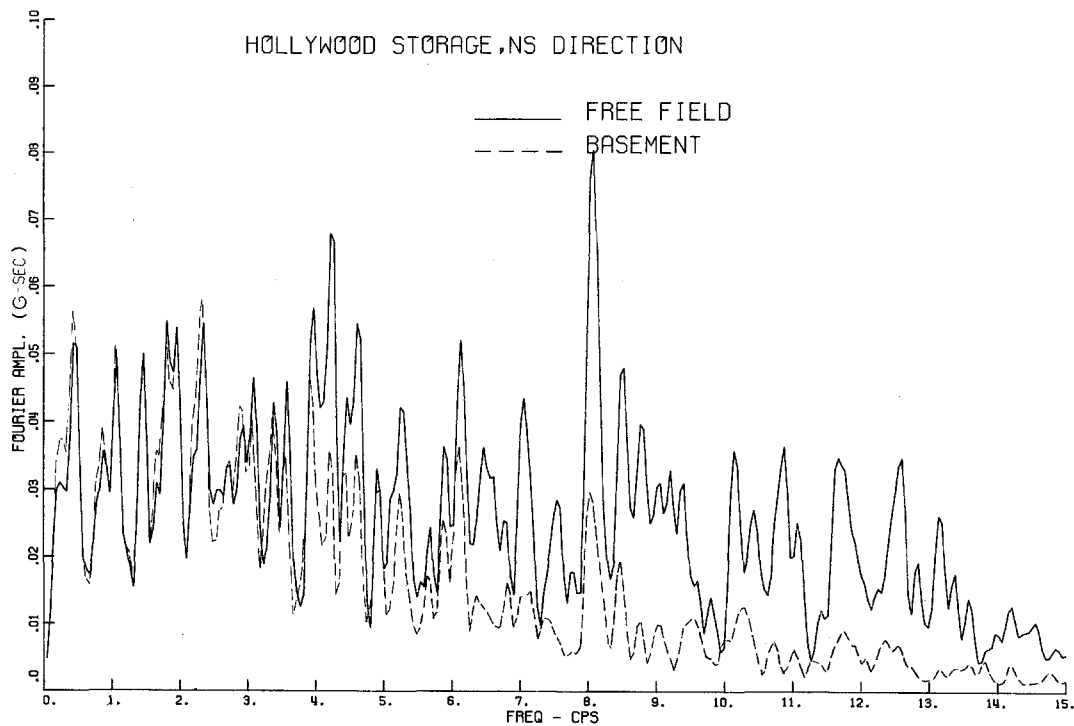
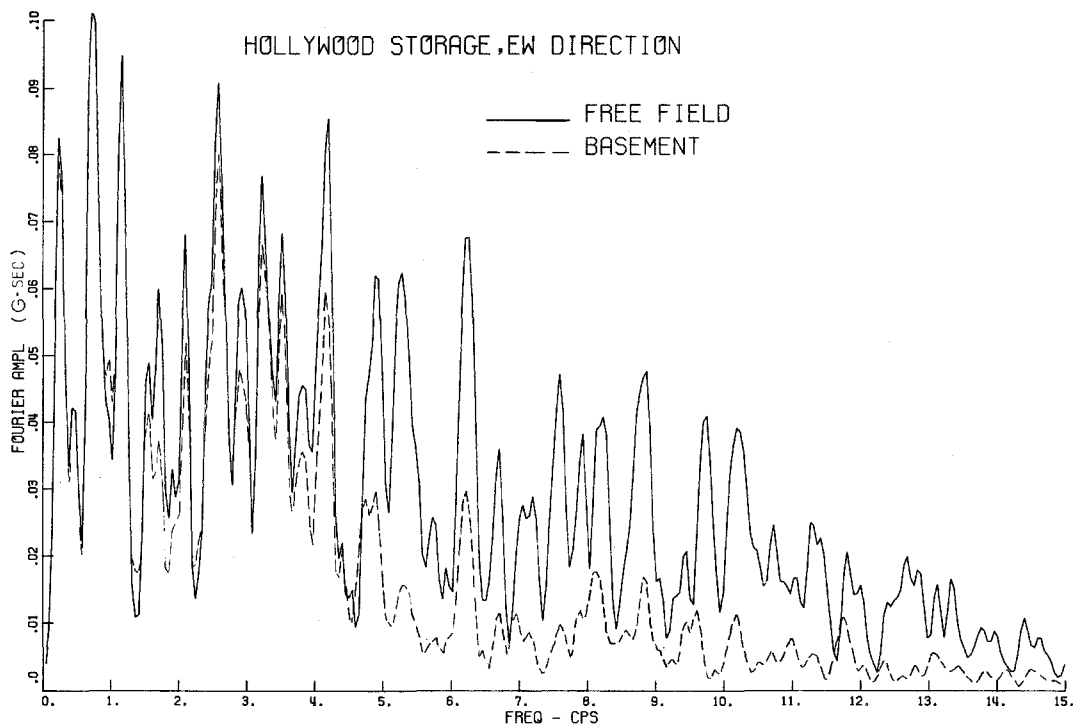
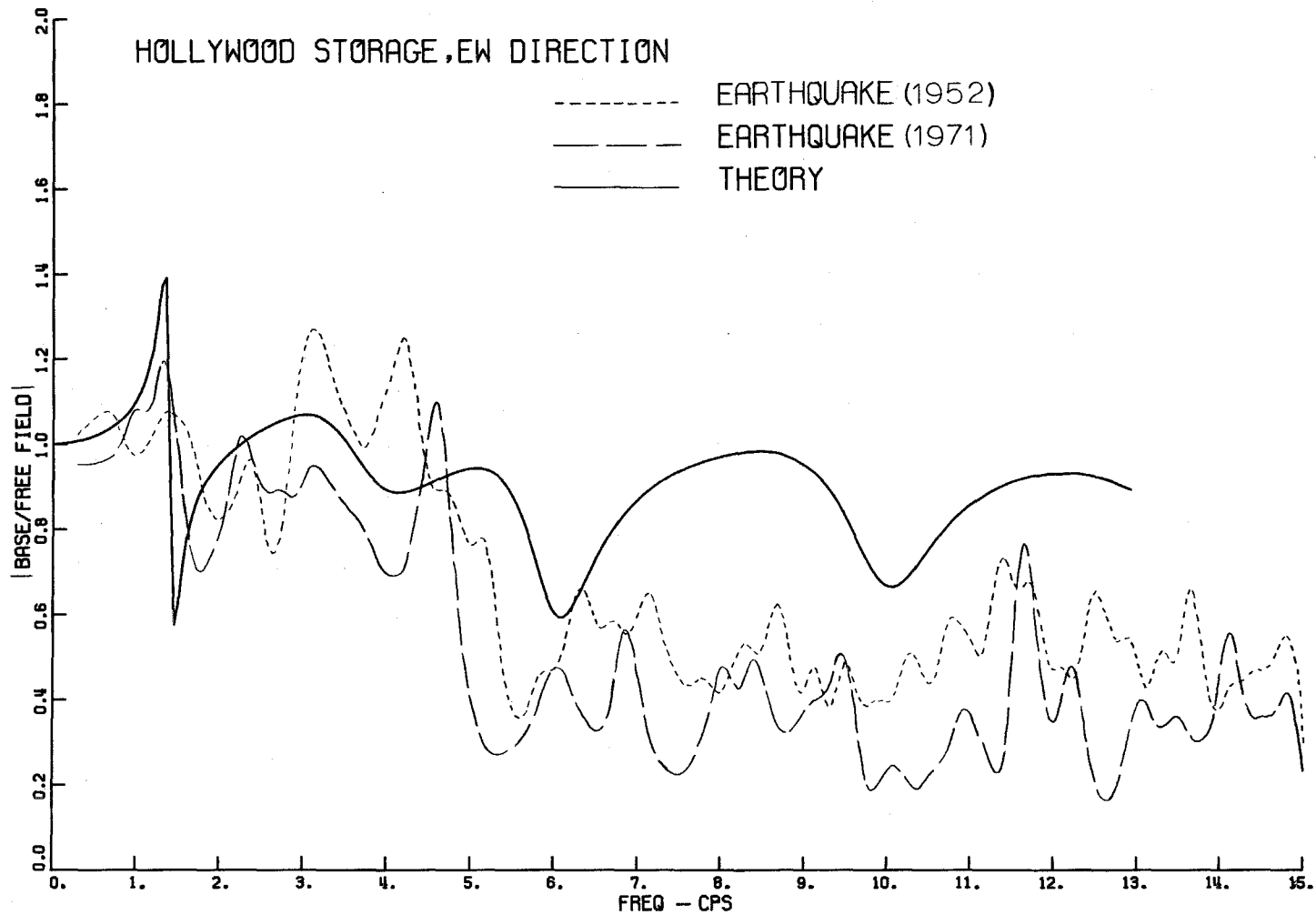


Fig. 9 Fourier Amplitude Spectra of Accelerograms from Hollywood Storage Site.



-43-

Fig. 10 Comparison of Transfer Functions. Model: $m_o = 5 \times 10^6 \text{lb.}$, $I_t = 1.21 \times 10^{11} \text{lb.-ft.}$, $\eta = .05$, Mode Shapes from (30), $M_1 = 19.6 \times 10^6 \text{lb.}$, $M_2 = 5.8 \times 10^6 \text{lb.}$, $M_3 = .4 \times 10^6 \text{lb.}$

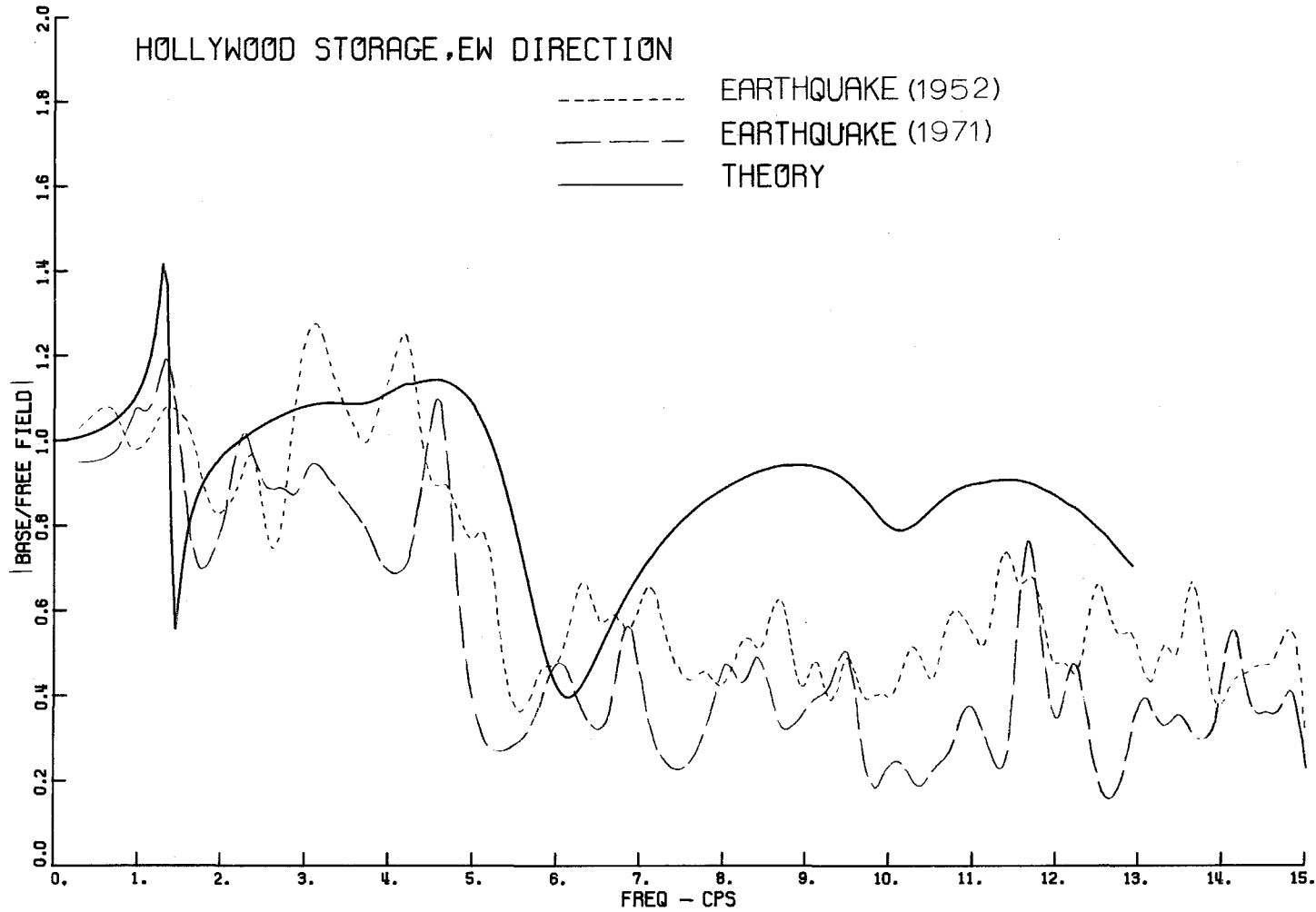


Fig. 11 Comparison of Transfer Functions. Model: $m_o = 5 \times 10^6$ lb., $I_t = 1.21 \times 10^{11}$ lb.-ft., $\eta = .05$,
 Mode Shapes Calculated from (26), $M_1 = 21.4 \times 10^6$ lb., $M_2 = 2.8 \times 10^6$ lb., $M_3 = .9 \times 10^6$ lb.

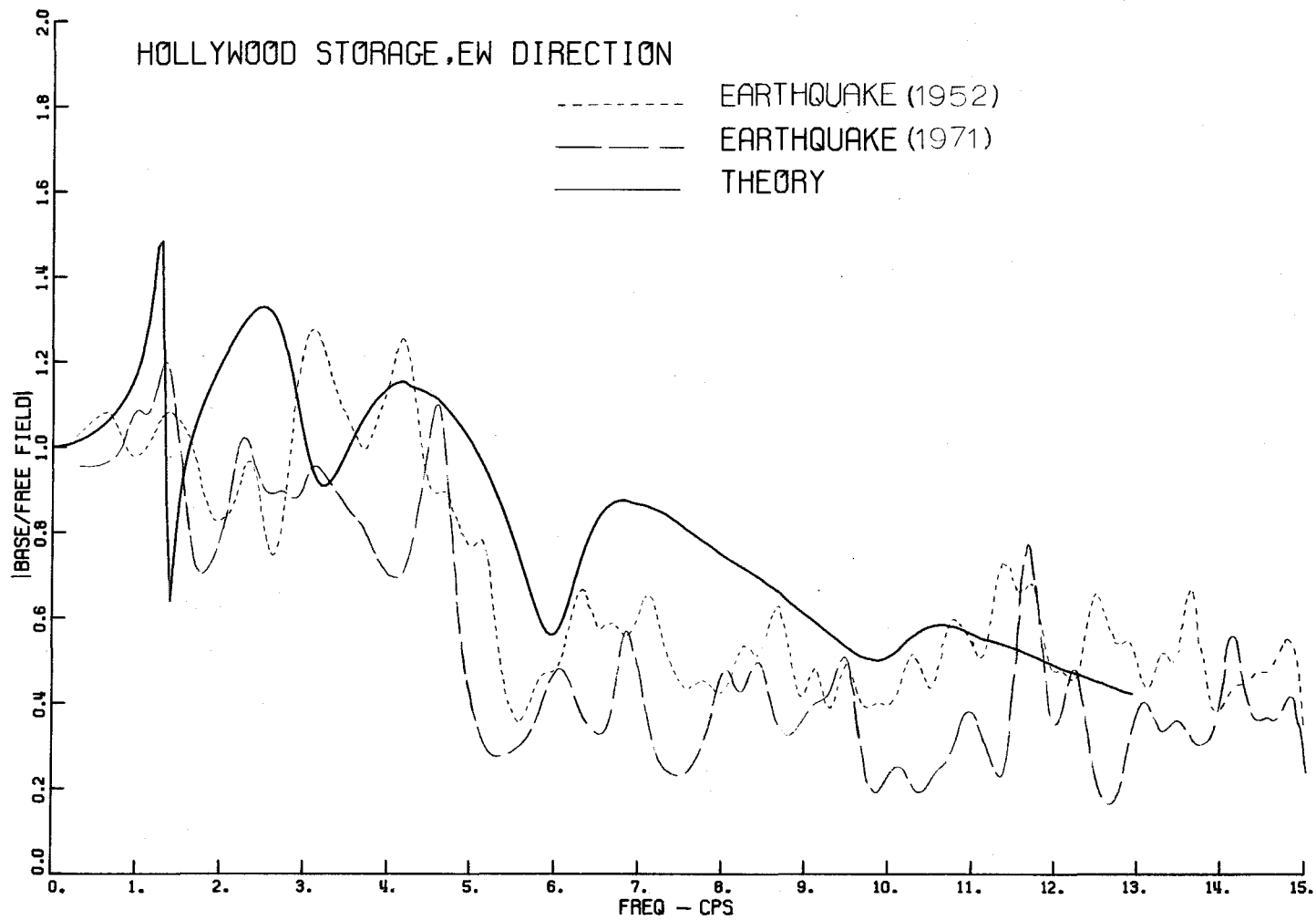


Fig. 12 Comparison of Transfer Functions. Model: $m_o = 3.1 \times 10^7$ lb., $I_t = 2.2 \times 10^{11}$ lb.-ft., $\eta = .05$, Mode Shapes Calculated from (26).

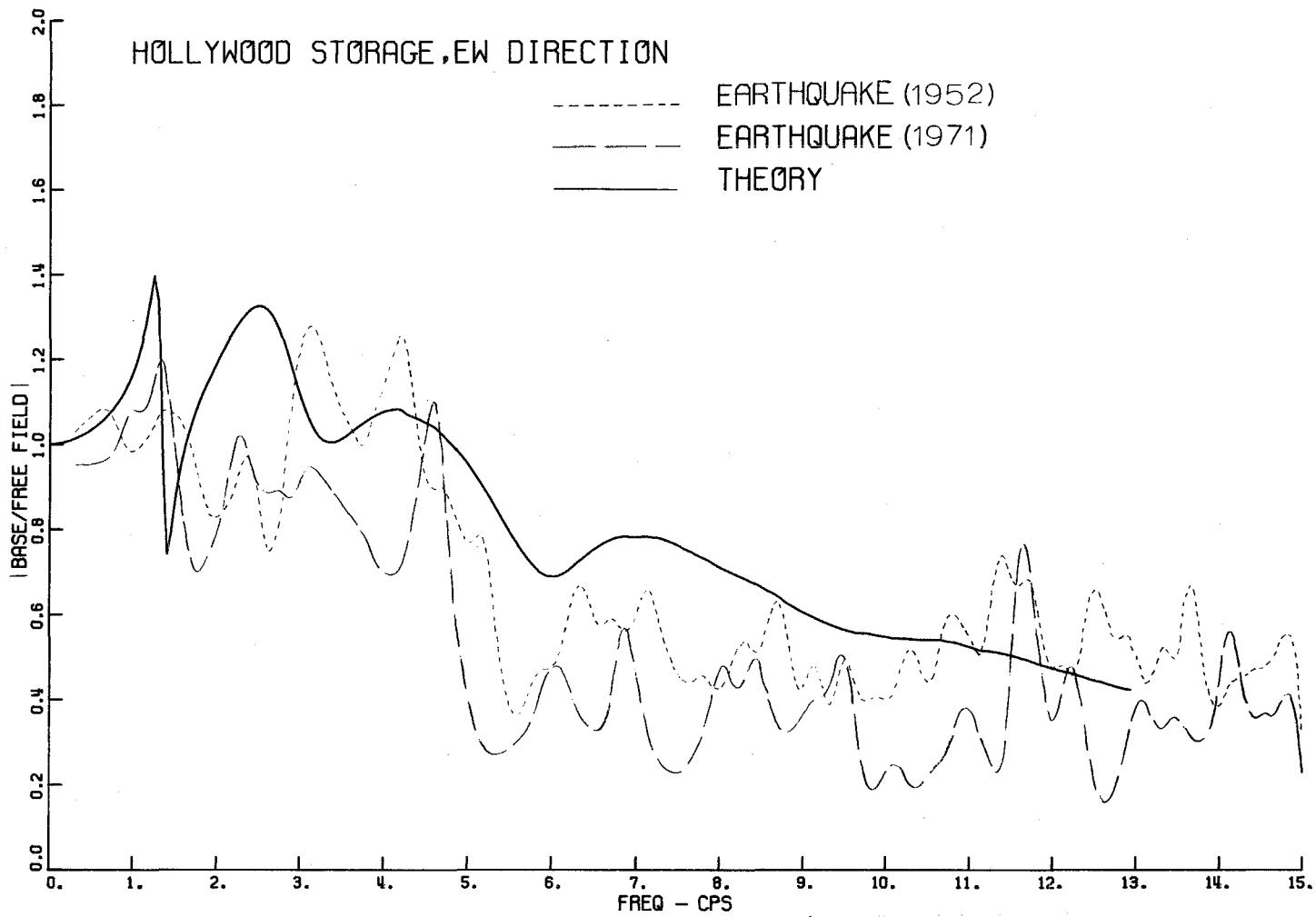


Fig. 13 Comparison of Transfer Functions. Model: $m_o = 3.1 \times 10^7$ lb., $I_t = 2.2 \times 10^{11}$ lb.-ft., $\eta = .10$, Mode Shapes Calculated from (26).

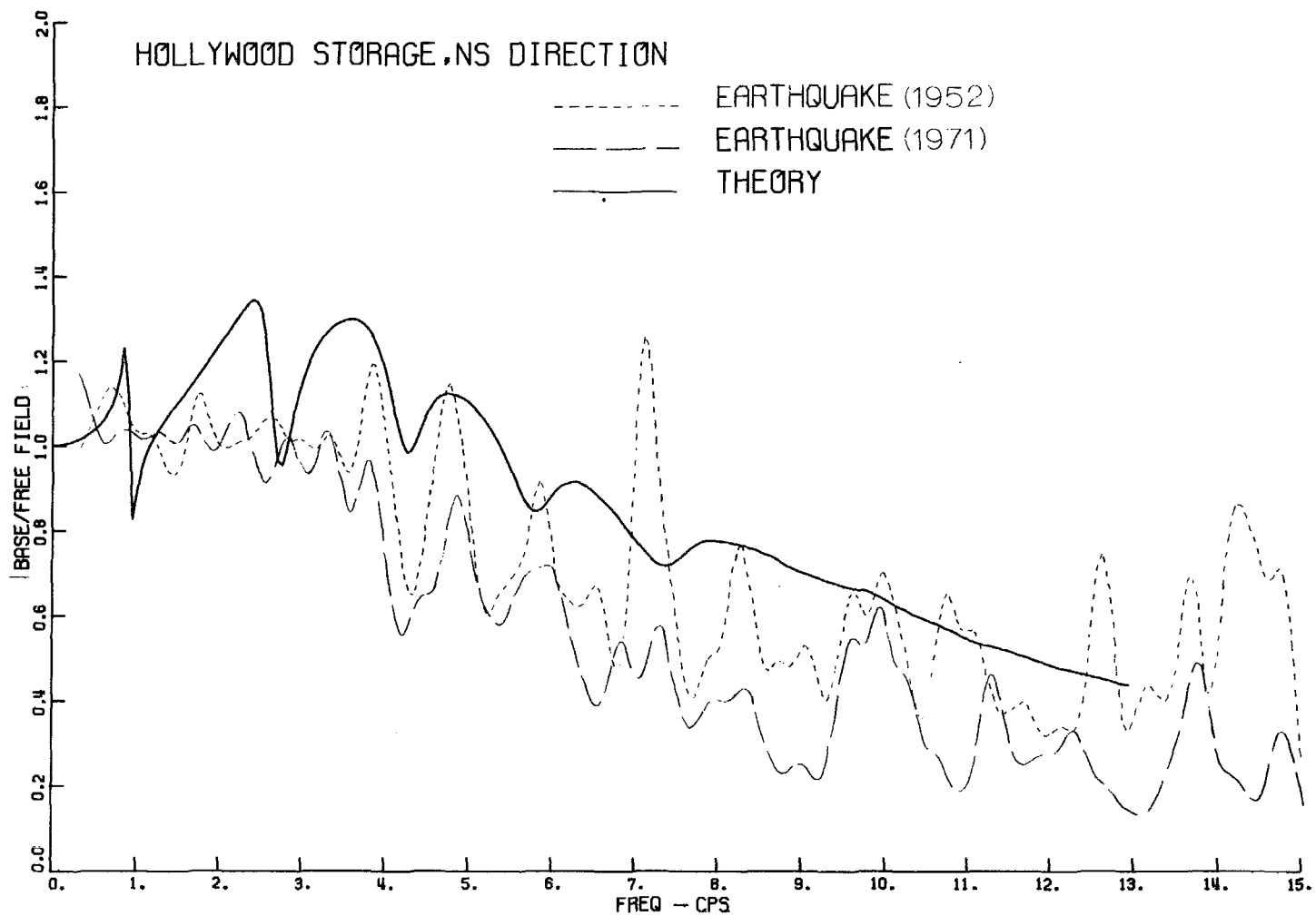


Fig. 14 Comparison of Transfer Functions. Model: $m_o = 3.1 \times 10^7$ lb., $I_t = 1.22 \times 10^{10}$ lb. ft., $\eta = .05$, Mode Shapes Calculated from (26).

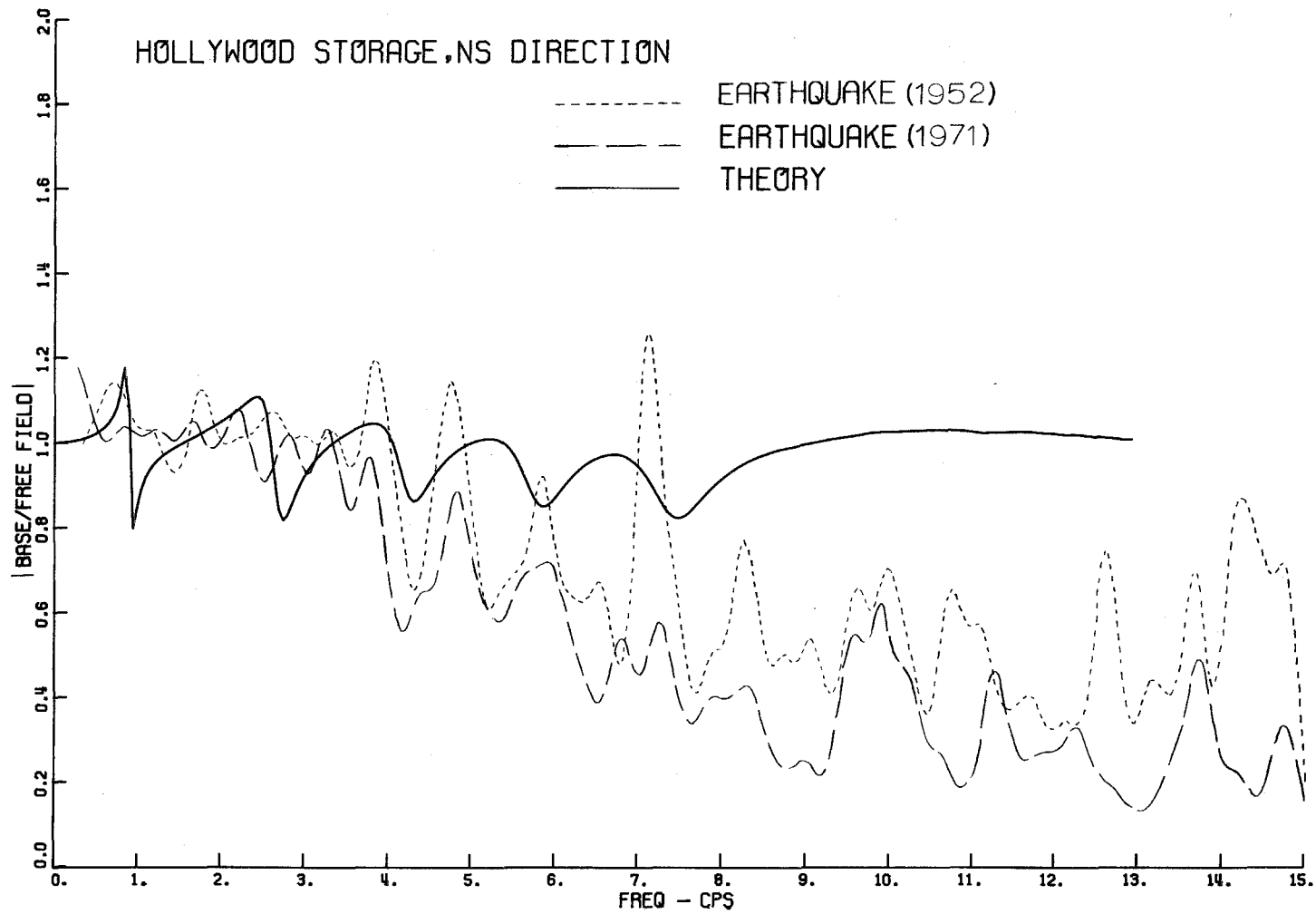


Fig. 15 Comparison of Transfer Functions. Model: $m_o = 5 \times 10^6$ lb., $I_t = 6.7 \times 10^9$ lb.-ft., $\eta = .05$. Mode Shapes Calculated from (26).

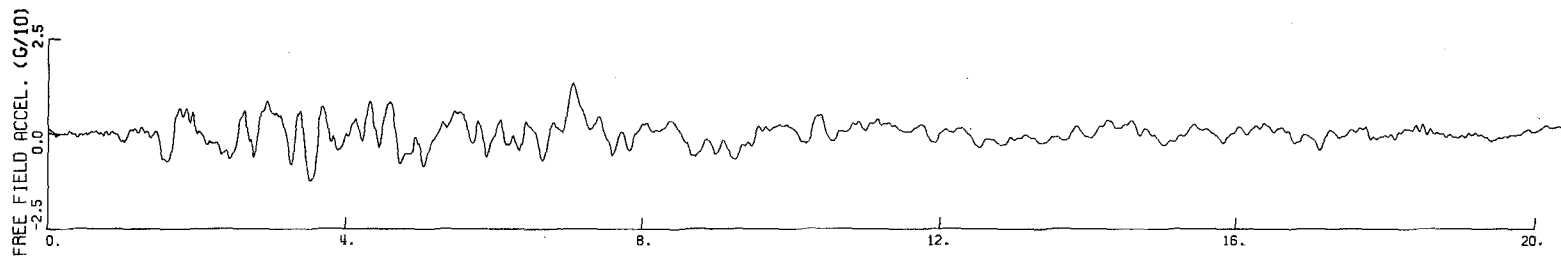
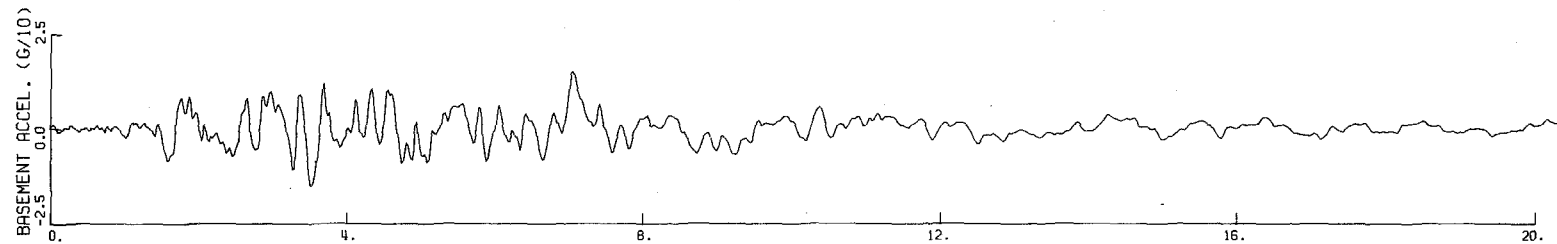


Fig. 16 Hollywood Storage Site. Computed Free Field Acceleration vs. Recorded Basement Acceleration. Modulus of Transfer Function Used Shown in Fig. 10.

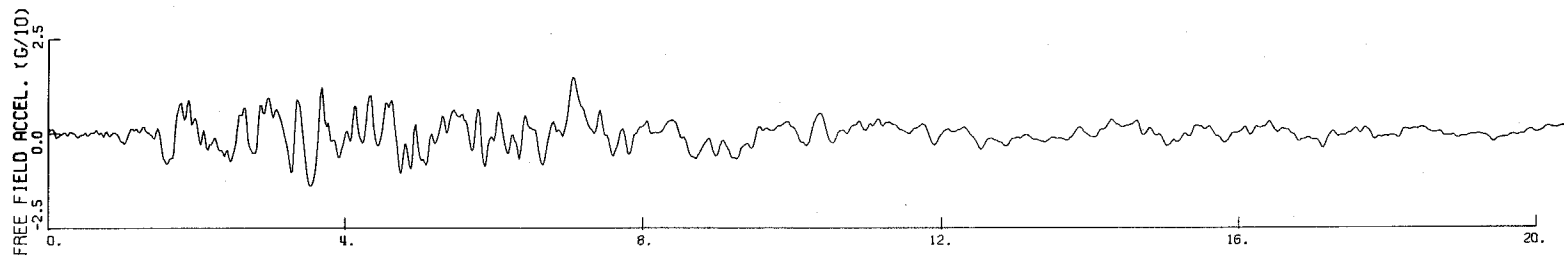
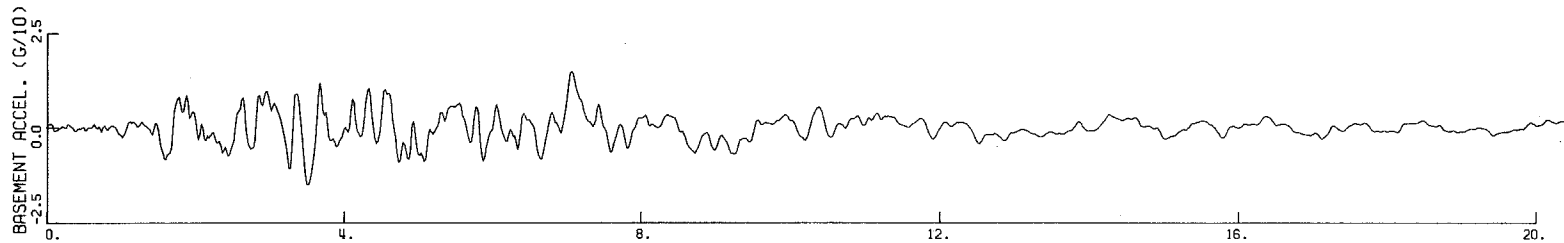


Fig. 17 Hollywood Storage Site. Computed Free Field Acceleration vs. Recorded Basement Acceleration. Modulus of Transfer Function Used Shown in Fig. 12.

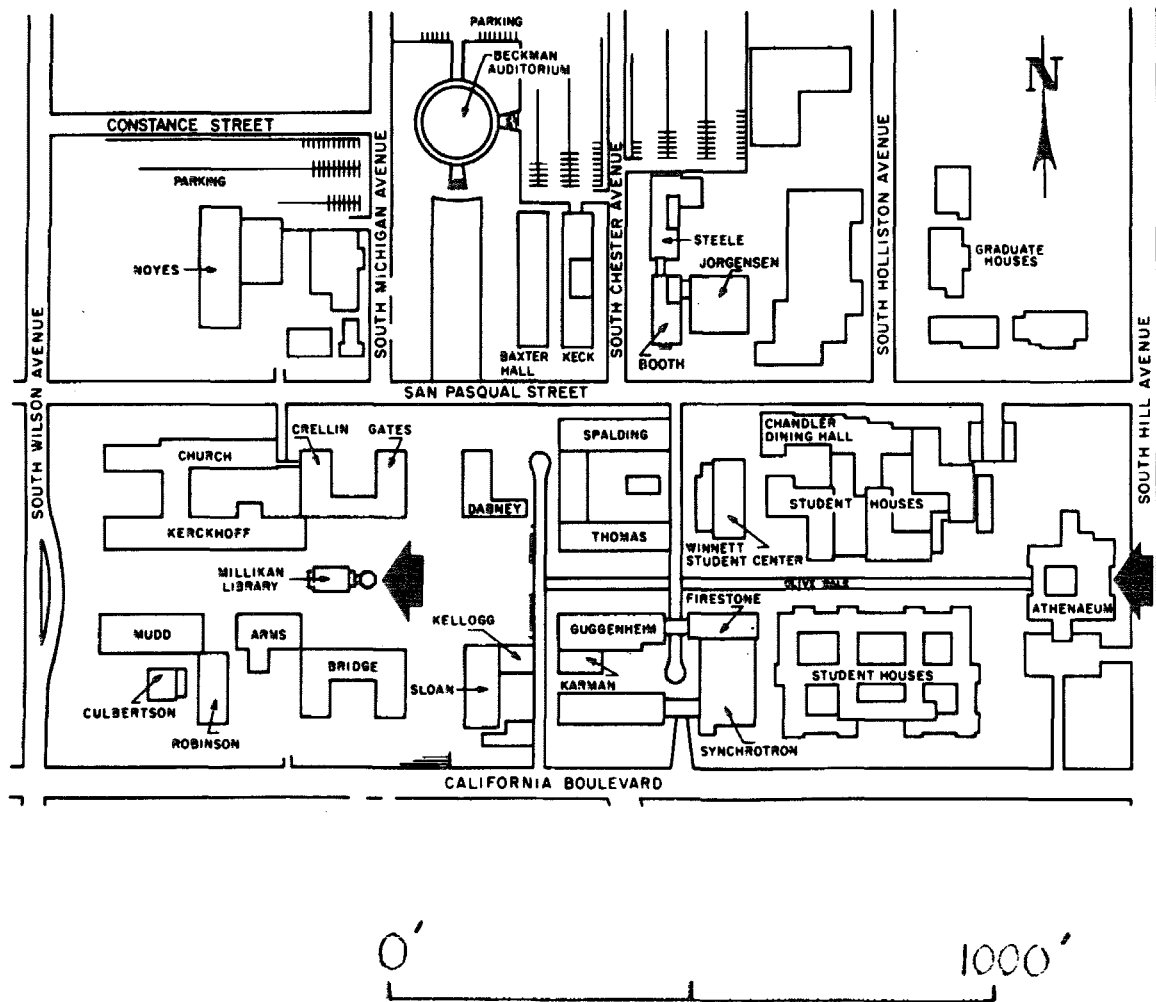


Fig. 18 Location of Athenaeum and Millikan Library Buildings on Campus of California Institute of Technology.

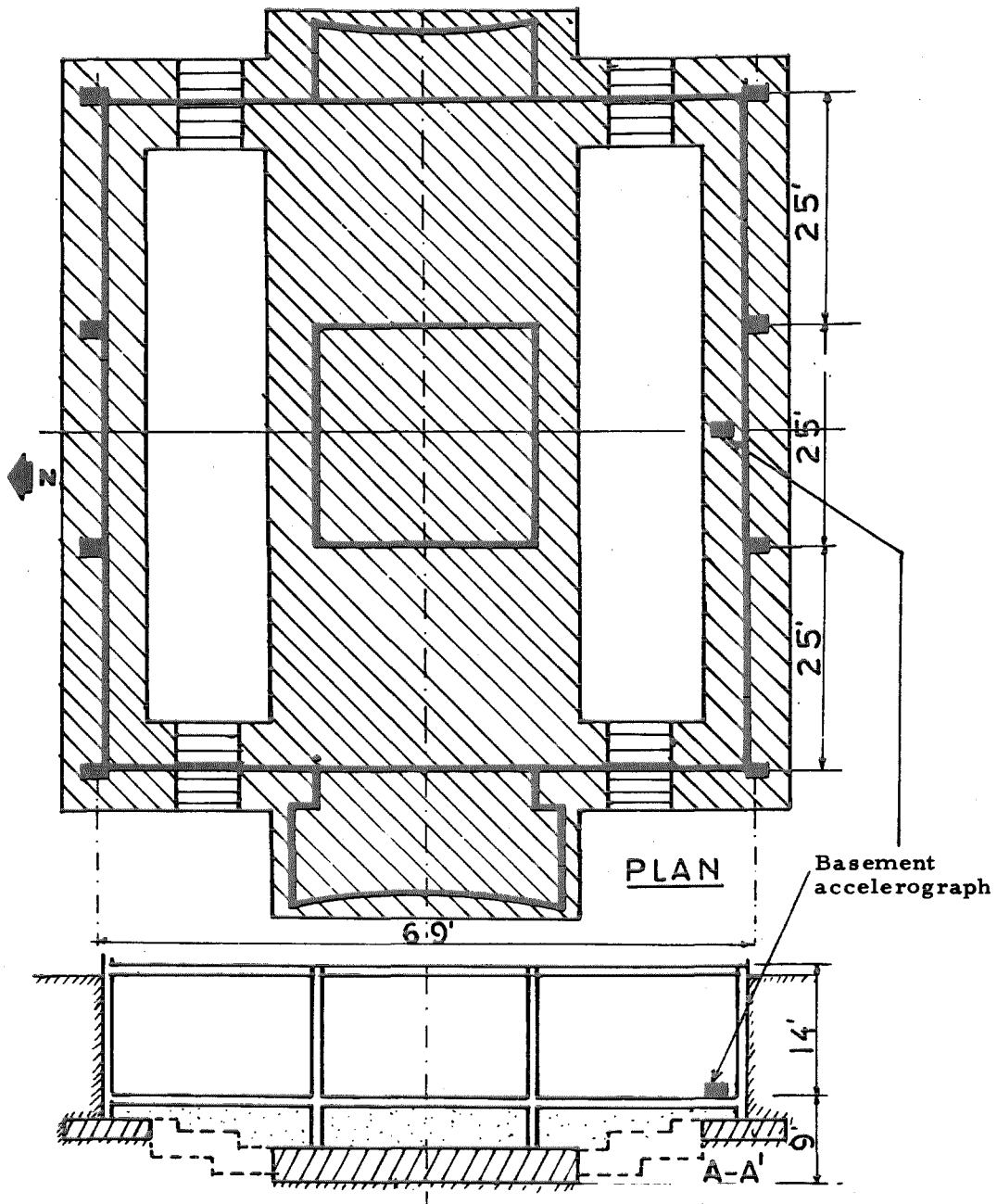


Fig. 19 Millikan Library



View Looking Northeast.

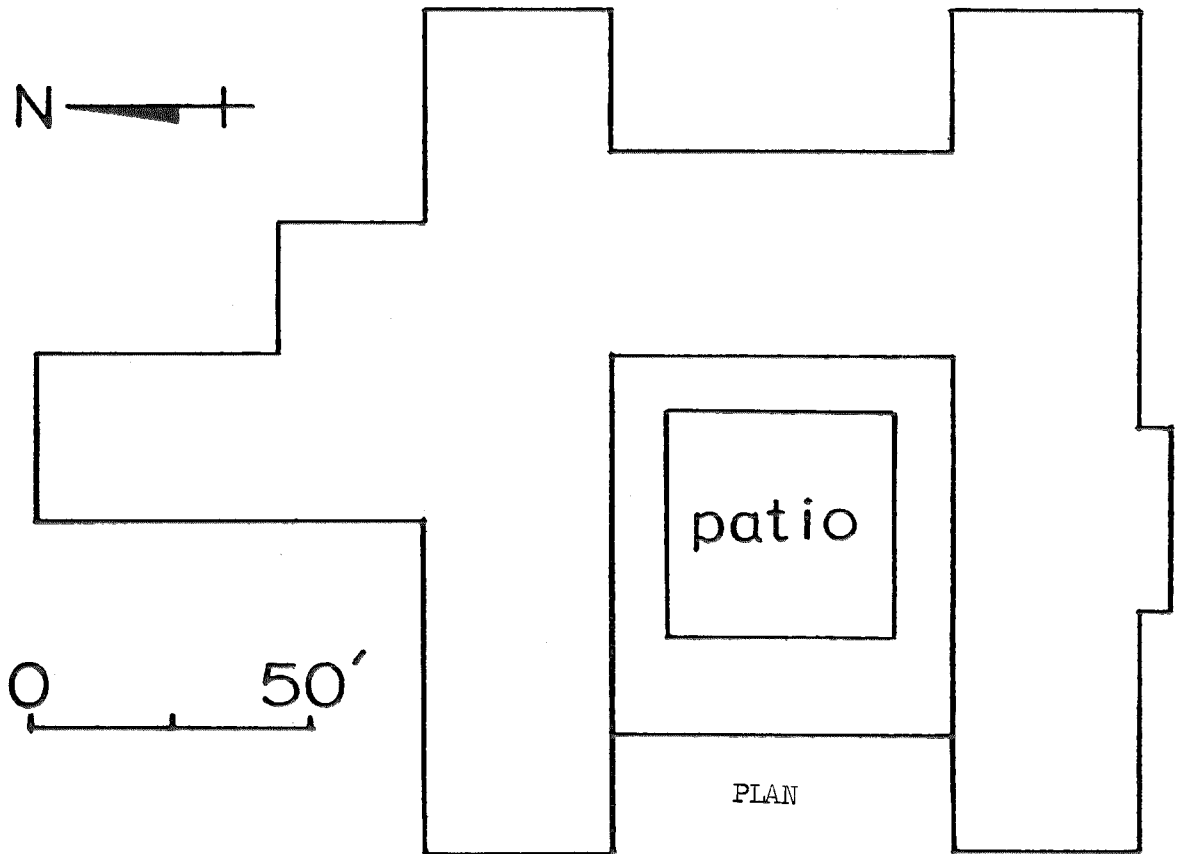


Fig. 20 Athenaem.

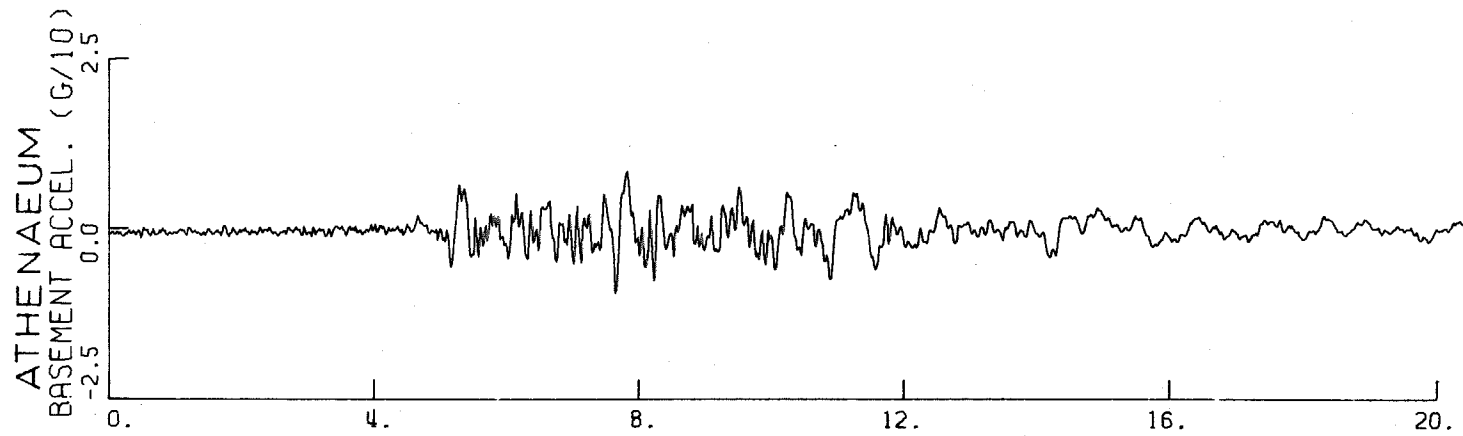
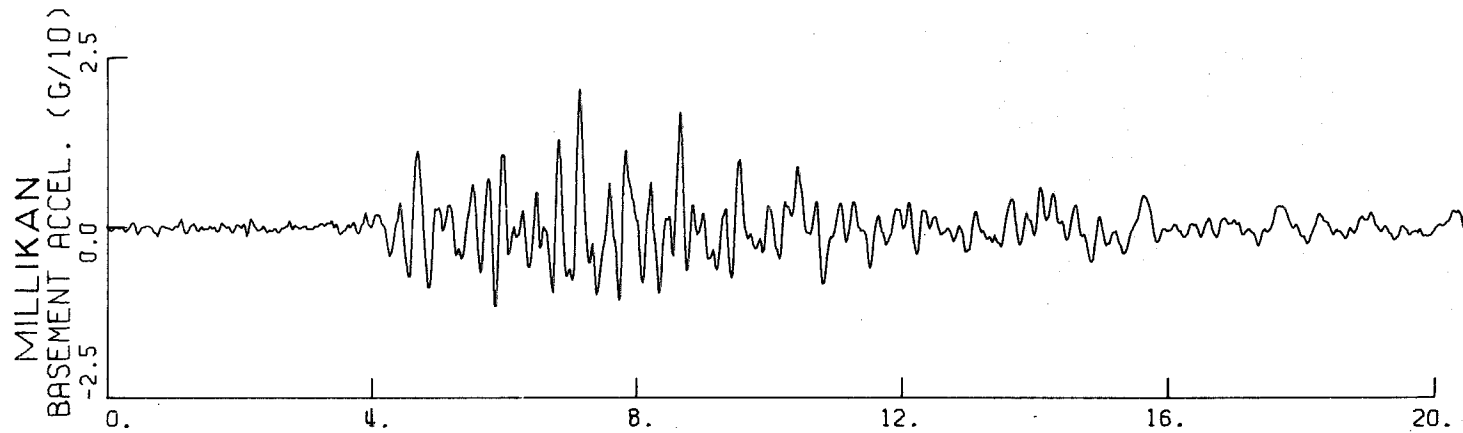


Fig. 21 Comparison of Recorded Accelerograms from Millikan Library and Athenaeum. NS Direction.

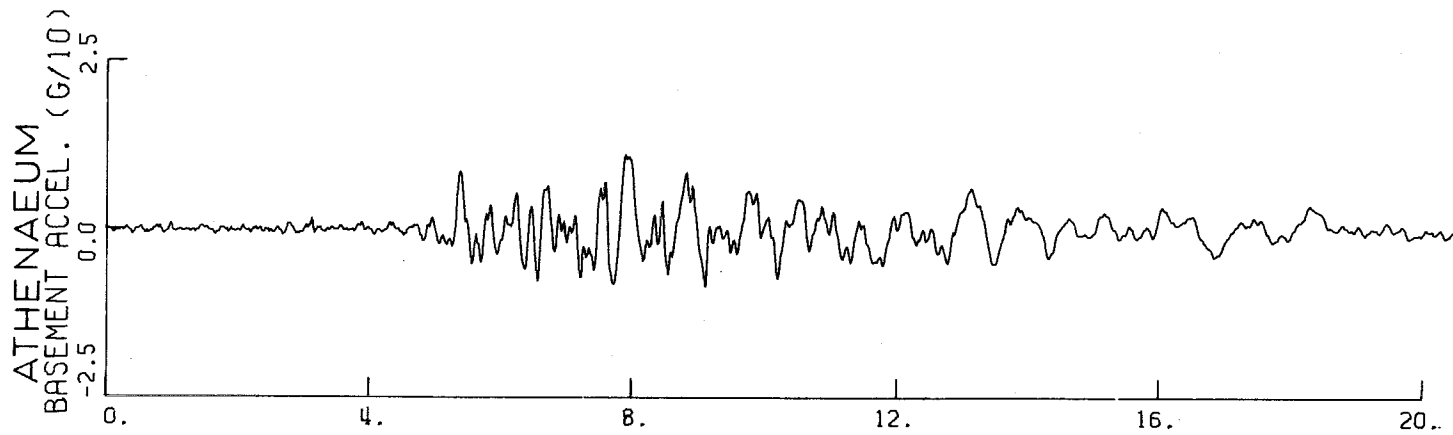
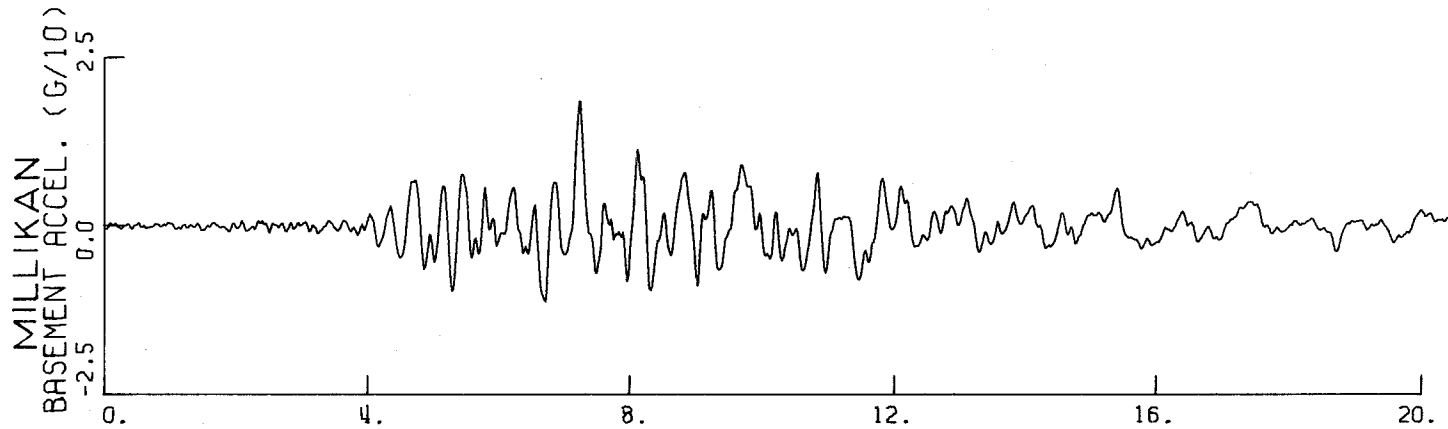


Fig. 22 Comparison of Recorded Accelerograms from Millikan Library and Athenaeum. EW Direction.

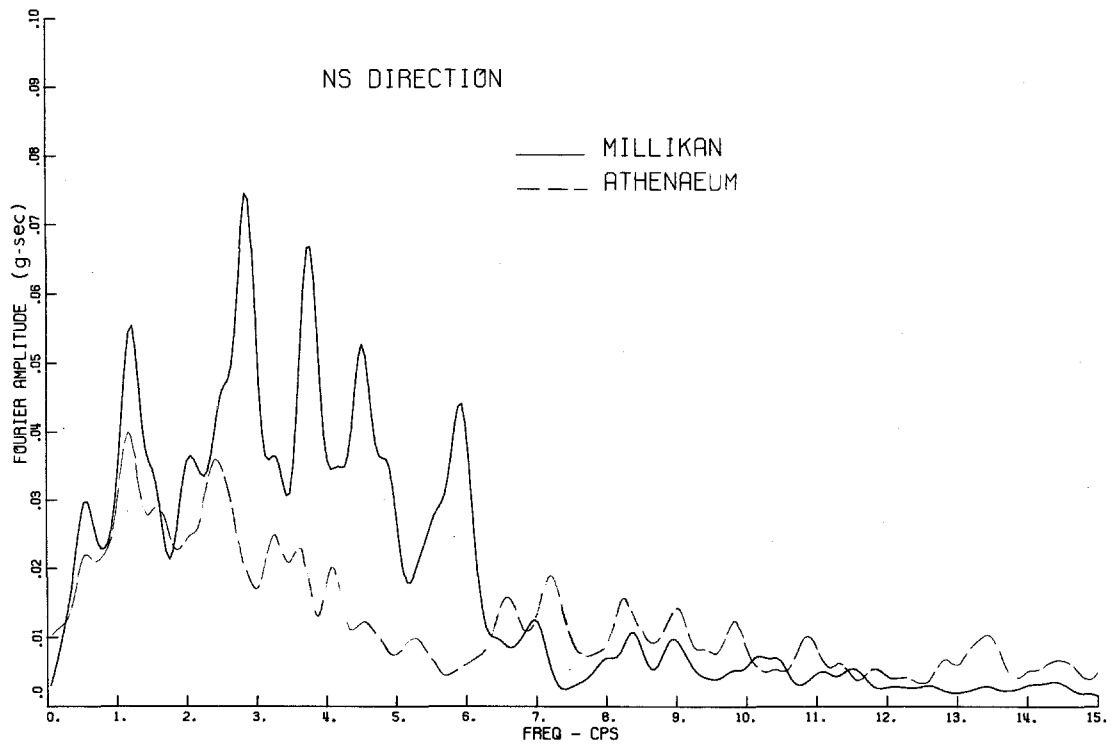
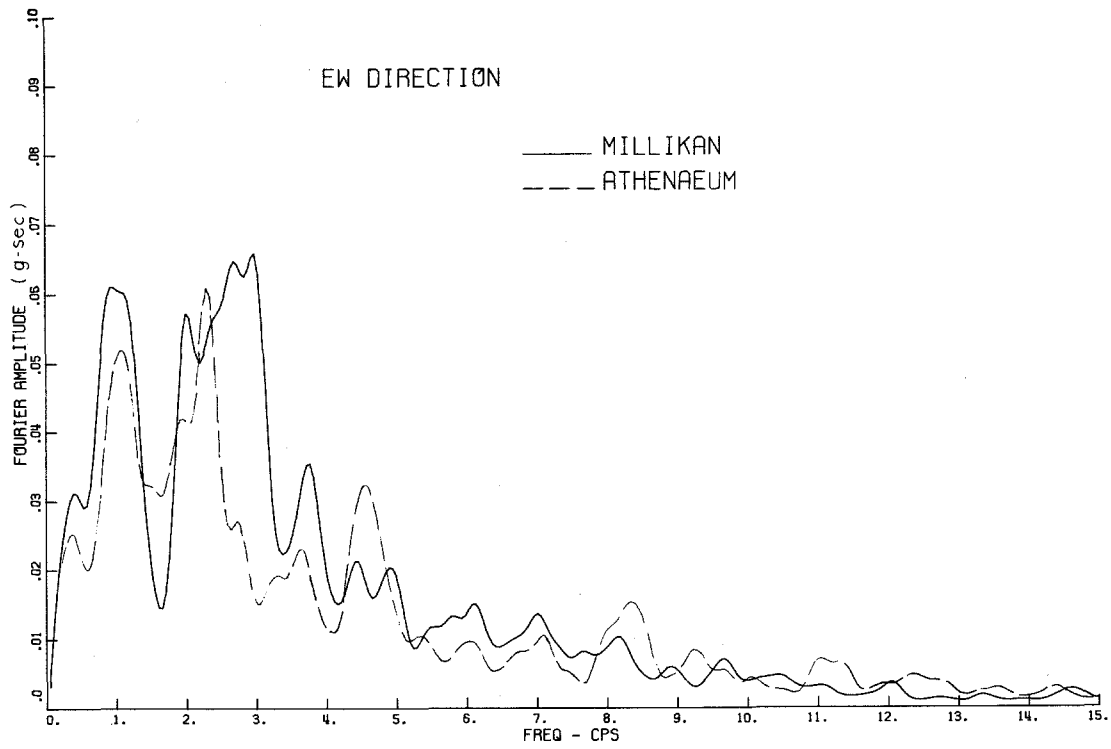


Fig. 23 Fourier Amplitude Spectra.

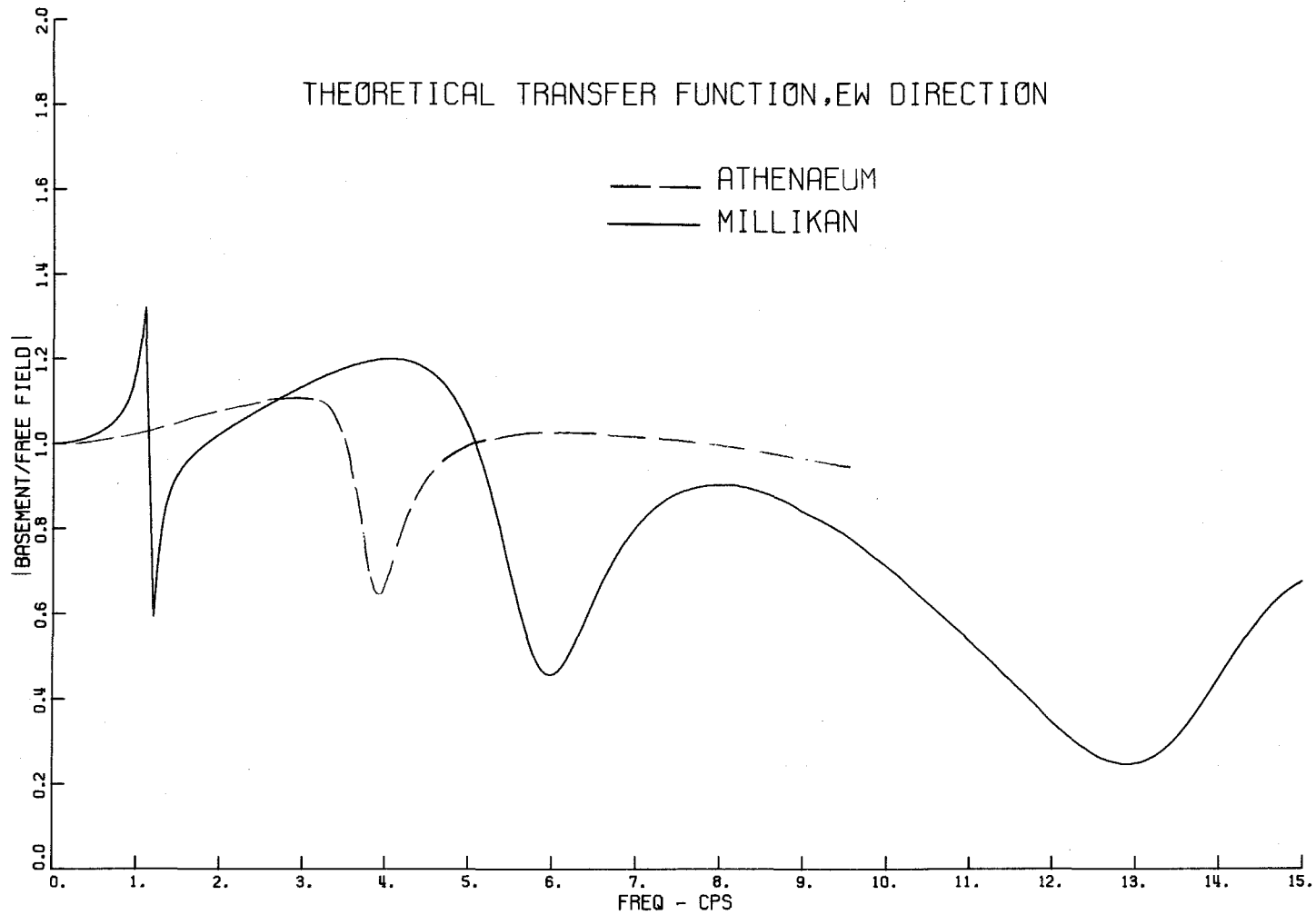


Fig. 24 Comparison of Transfer Functions. Millikan: $m_o = 7 \times 10^6 \text{ lb.}$, $I_t = 1.21 \times 10^{10} \text{ ft. - lb.}$, $\eta = .05$. Athenaeum: $I_t = 2.52 \times 10^{10} \text{ ft. lb.}$, $m_o = 13 \times 10^6 \text{ lb.}$, $m_1 = 5 \times 10^6 \text{ lb.}$, $f_1 = 4 \text{ c. p. s.}$, $\eta = .05$.

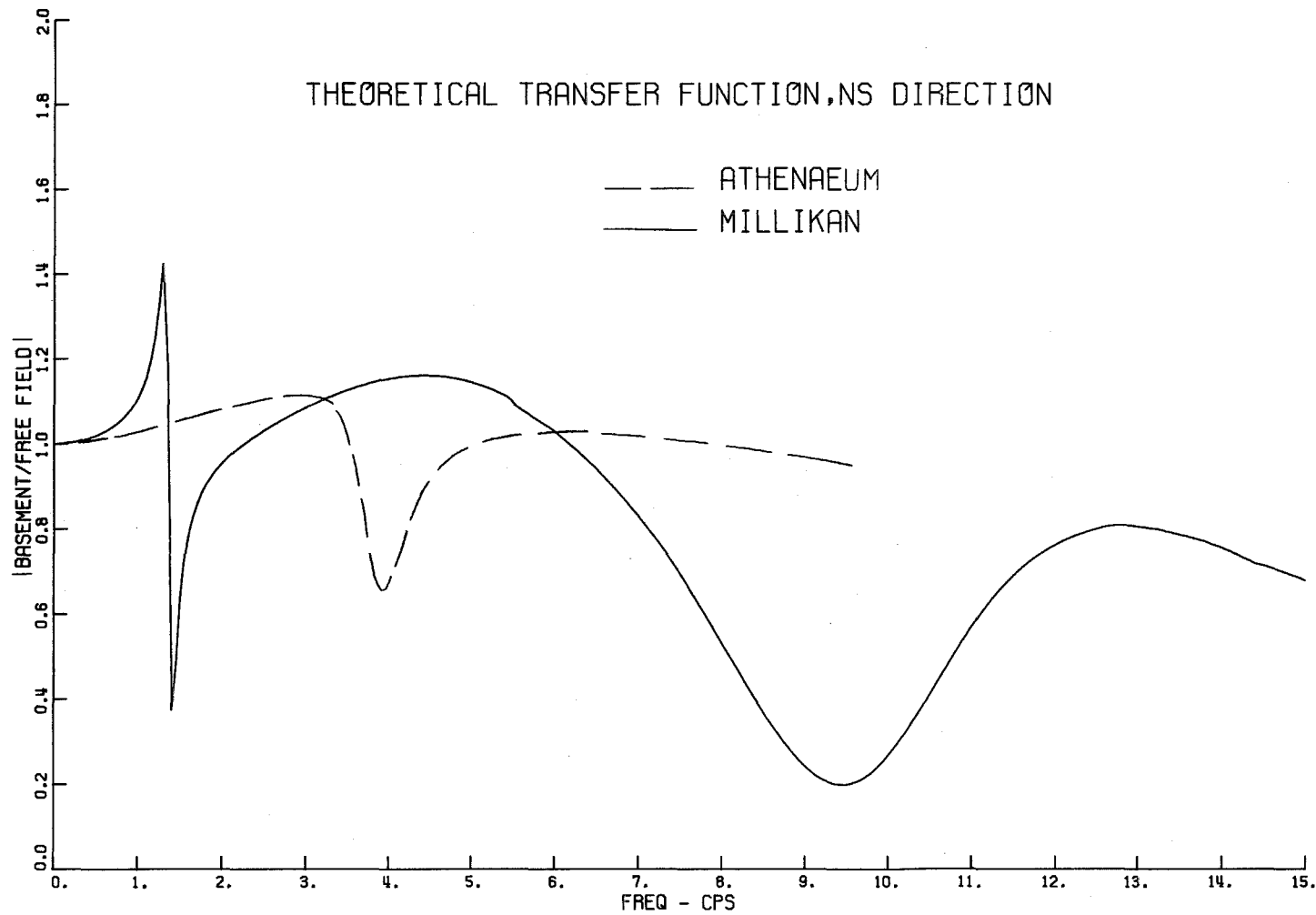


Fig. 25 Comparison of Transfer Functions. Millikan: $m_o = 7 \times 10^6$ lb., $I_t = 1.02 \times 10^{10}$ ft.-lb., $\eta = .05$. Athenaeum: $m_o = 13 \times 10^6$ lb., $m_1 = 5 \times 10^6$ lb., $I_t = 3.4 \times 10^{10}$ ft.-lb., $f_1 = 4$ c.p.s., $\eta = .05$.

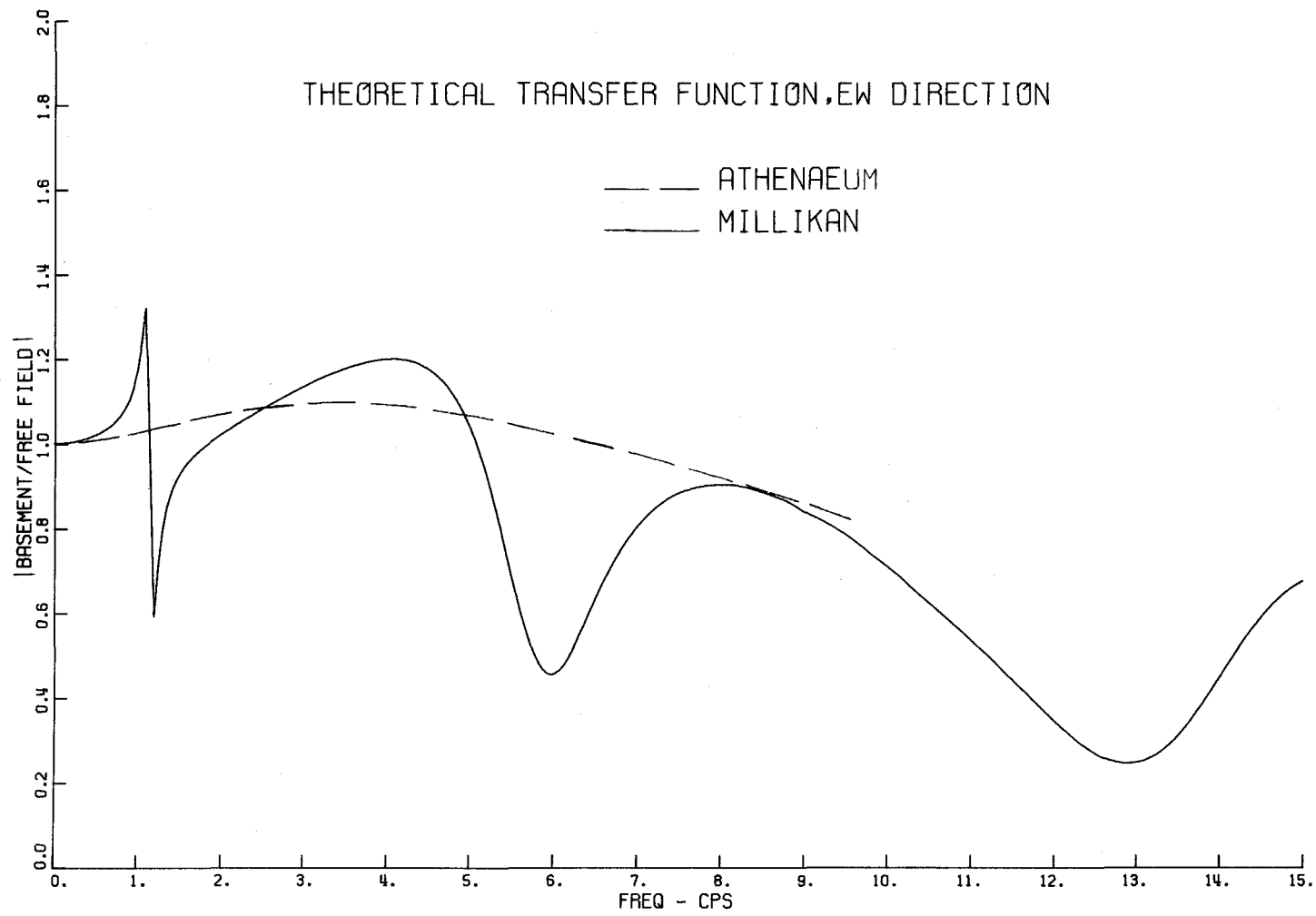


Fig. 26 Comparison of Transfer Functions. Millikan: same as Fig. 24.
 Athenaeum: $m_o = 18 \times 10^6$ lb., $I_t = 2.52 \times 10^{10}$ ft. -lb.

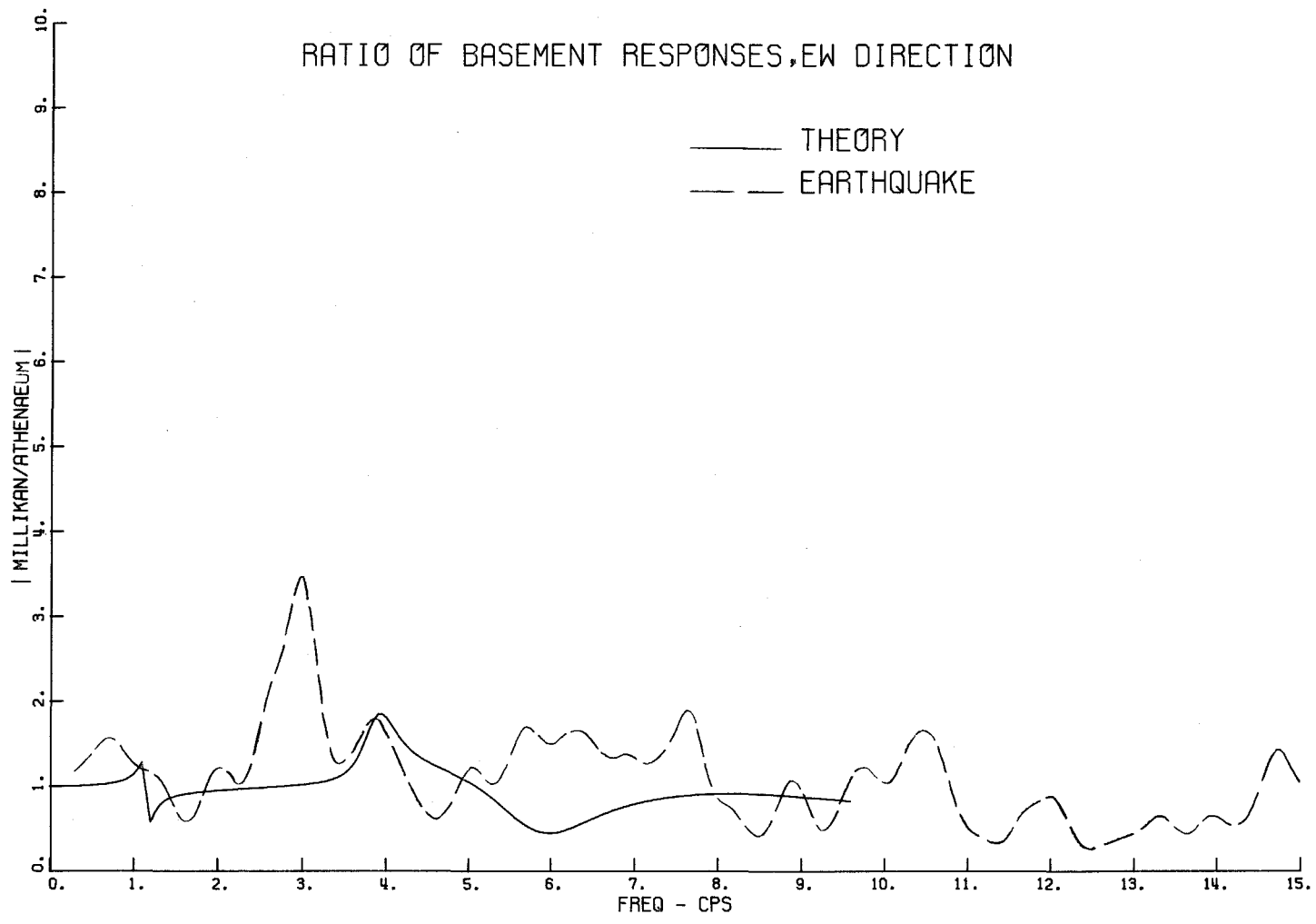


Fig. 27 Comparison of Transfer Functions. Theoretical Transfer Function Calculated From Fig. 24.

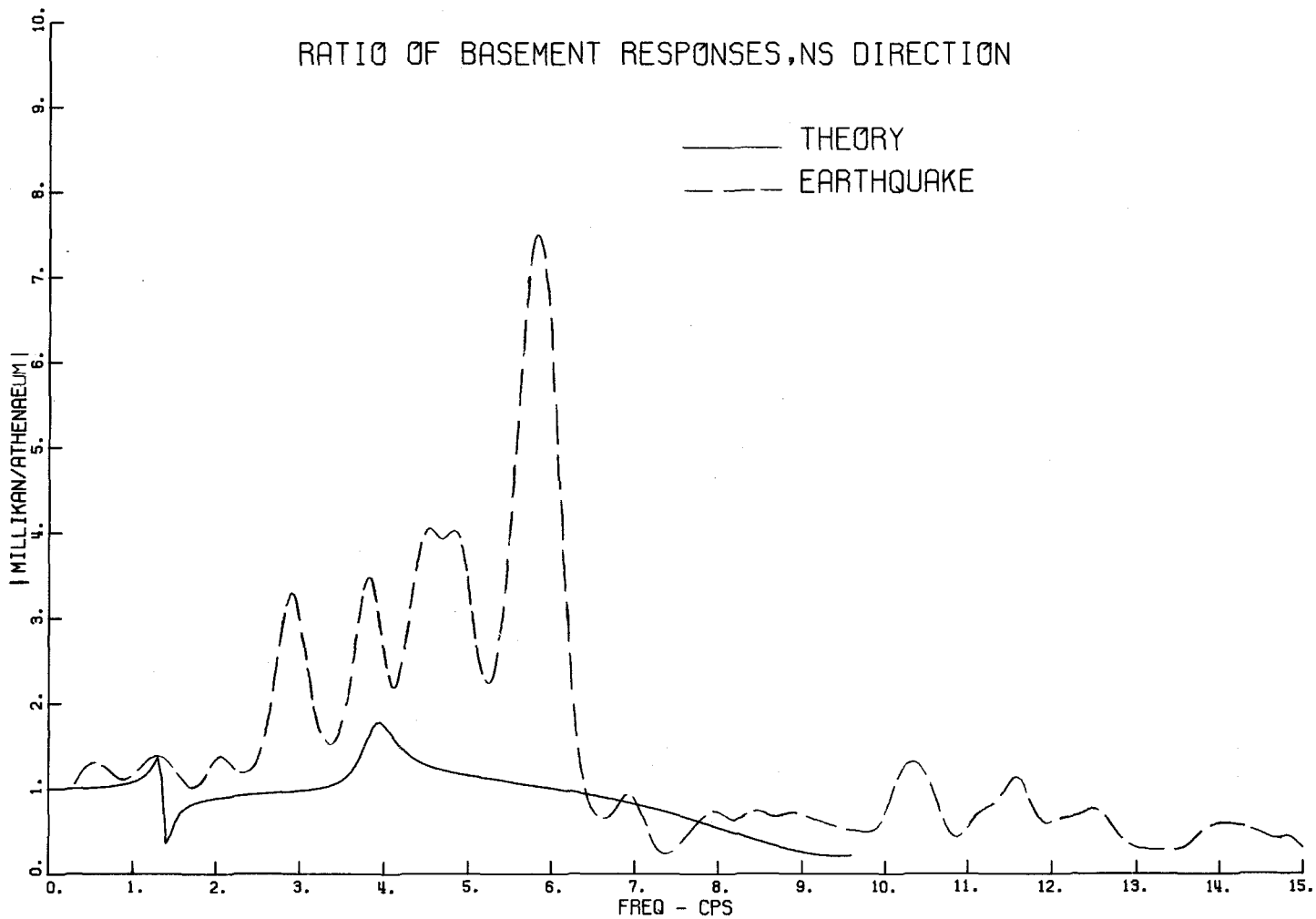


Fig. 28 Comparison of Transfer Functions. Theoretical Transfer Function Calculated From Fig. 25.

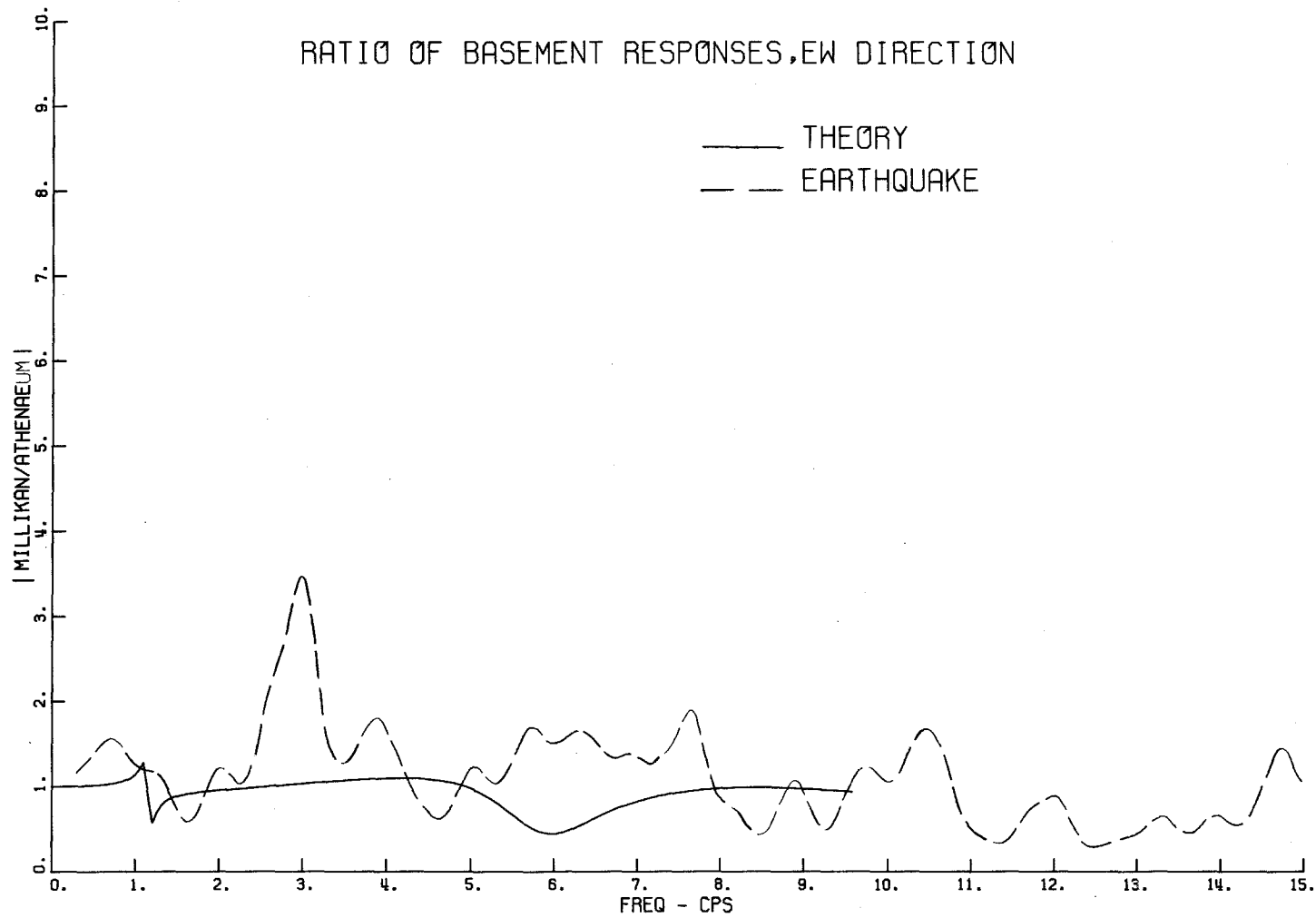


Fig. 29 Comparison of Transfer Functions. Theoretical Transfer Function Calculated From Fig. 26.

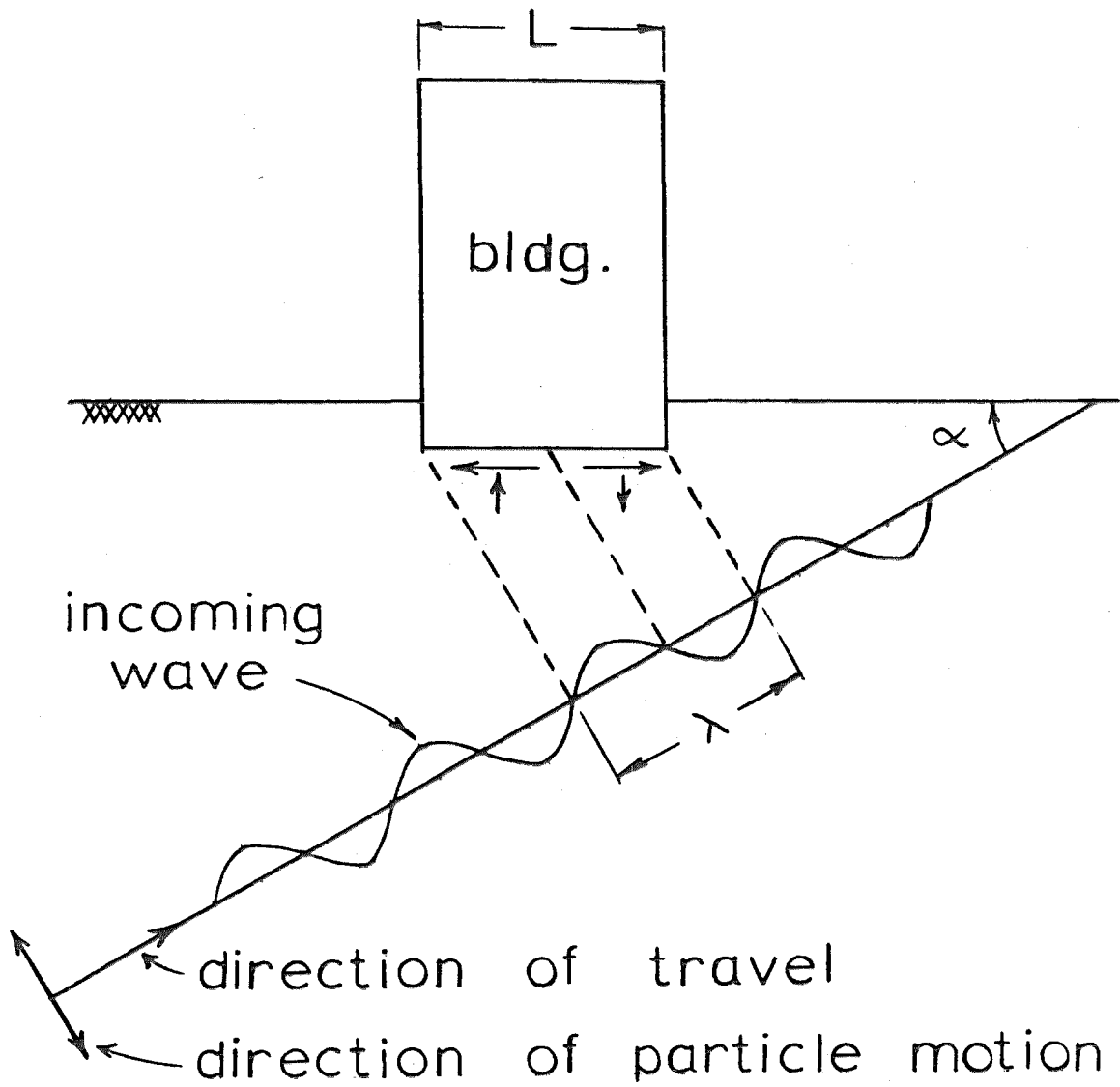


Fig. 30 Plane Harmonic Wave Incident at an Angle.

III. ANALYSIS OF SELECTED BASEMENT ACCELEROGRAMS IN LOS ANGELES

III.1 Introduction

This chapter is devoted to the study of selected accelerograms obtained in basements of buildings in the city of Los Angeles during the San Fernando earthquake. The first portion of the chapter deals with accelerograms from a group of 6 tall buildings in the vicinity of Wilshire Blvd. and Normandie Ave. (Fig. 31). The buildings, varying in size and foundation design, are clustered in a 200 yd. × 700 yd. area. A description of the size, structural type, foundation design, and underlying soil is included for each building for the purposes of investigating the possibility of trends in the acceleration data that might be related to similarities or differences in structural and soil characteristics at the sites. Analysis of the acceleration data, in addition to visual comparisons of the accelerograms, also includes comparisons in the frequency domain by means of Fourier Amplitude Spectra (F.A.S.) and relative velocity response spectra. The major differences in the data are compared with results expected from existing theories of soil-structure interaction and theories describing the effects of soil deposits on the ground motion.

The second part of this chapter examines acceleration data from buildings surrounding the group of buildings in the Wilshire-Normandie area. The seven accelerograms studied were taken from buildings approximately 2 to 3 miles from the center of the Wilshire-

Normandie group. The locations of all of the accelerographs are shown in Fig. 31.

III.2 Analysis of Basement Accelerograms from
the Wilshire Blvd.-Normandie Ave.
Area in Los Angeles

The ground motion during the San Fernando earthquake was recorded in a group of 6 tall buildings clustered near the intersection of Wilshire Blvd. and Normandie Ave. The location is 21 miles from the center of the San Fernando earthquake (i.e., center of energy release), at a direction of S 12° E. The most prominent structure of the group is the 31-story Equitable Life Assurance building at 3411 Wilshire, which is centrally located with respect to the other 5 buildings. Fig. 32 is an aerial photograph showing 5 of the buildings within a dense array of other multistory structures.

The surface topography of the overall area is relatively flat. The Santa Monica mountains can be seen in the background. This chain runs east-west and begins at a point roughly 5 miles to the north of the Equitable building. Beyond the Santa Monica mountains to the north is the San Fernando valley and the epicentral region. To the northeast of the Equitable building about one mile is the southwestern extent of the Elysian Hills, not visible in the photo.

The 6 buildings are located on the eastern edge of a geologic feature called the La Brea Plain, composed of preconsolidated Pleistocene sediments (33). Five of the buildings are supported on a layer of sedimentary rock, 30 ft. to 60 ft. beneath the surface of the overlying alluvium. The sedimentary rock at these sites is the same

geologic formation from the Miocene era (33) and has a density of roughly 90 p.c.f. The rock is nearly horizontal beneath the 5 sites. The thickness of the rock layer could not be determined from the soil borings which only went to depths between 50 ft. and 100 ft. No rock layer was found at the westernmost site. The 9 soil borings at this site varied between 50 ft. and 100 ft. in depth. Variations with depth in the soil conditions of the alluvium, indicated by the soil borings, exist at each site. The soils in the alluvium also vary from site to site. The surface topography is fairly flat except for a gently sloping valley which runs southwesterly through the Equitable building site. This valley was formerly a river bed, most likely an extension of Ballona Creek, which begins just to the southwest (33).

The locations of the 6 buildings are shown in Fig. 33. The greatest distance between any two buildings is 2100 ft. while the shortest distance is 470 ft. The tallest structure, the Equitable building, at 3411 Wilshire, is 31 stories (439 ft.) from ground to roof. The shortest building of the group is located at 3407 W. 6th Street and is 7 stories (106 ft.) in height.

The basic features of the buildings, including column spacing, overall dimensions, foundation type, and the location of the basement accelerograph are shown in Figs. 34 through 39. The depth of the sedimentary rock is also shown and is an average value based on the soil borings.

The building at 3407 W. 6th (Fig. 34) is a composite structure; the first two stories are steel-frame construction, while the upper 5

stories are reinforced concrete. There is no basement as such, but the first floor on the western half of the building is sunk approximately 5 ft. beneath ground level. Belled caissons, 24 in. to 30 in. in diameter in the cylindrical portion, extend about 40 ft. to the sedimentary rock. The overlying alluvium consists of sandy silt fill at the surface at 110 p.c.f. and a combination of clayey silt and silty sand at 100 p.c.f. between the fill and the rock.

The Equitable building at 3411 Wilshire (Fig. 35) is a 31-story steel-frame structure with 4 to 5 sub-basement parking levels. The foundation consists of spread footings, 20 ft. x 20 ft. x 6 ft. on the average. The bottoms of the footings are nearly 25 ft. into the rock. Some hard, granite-like inclusions were encountered in the sedimentary rock during construction and had to be removed by jackhammers. Then sheets of water and sand are also present in the rock and were considered in the design of the foundation. The surface alluvium consisted of clayey and silty sand fill, 110 p.c.f. It is noted that the basement accelerograph is at the lowest level, essentially at the surface of the rock.

Just to the west of the Equitable building is a narrow 17-story reinforced concrete structure at 616 S. Normandie (Fig. 36). The building has one basement level 12 ft. beneath the first floor. Foundation support is provided by individual spread footings, 12 ft. x 12 ft. x 5 ft., with 2 to 4 friction piles extending an average of 10 ft. into the rock. The surface of the rock layer begins roughly 15 ft. beneath the bottom of the footings. The alluvium above is a

mixture of weathered rock, clay, and sand, with an average density of 105 p.c.f.

At 3345 Wilshire (Fig. 37) stands a 12-story reinforced concrete building with 3 sub-basement levels. The foundation, consisting of spread footings, 13 ft. × 18 ft. × 3 ft. 4 in. typically, rests on the rock approximately 30 ft. beneath the surface.

The only structure not supported on or over the sedimentary rock is the westernmost building of the group at 3550 Wilshire (Fig. 38). Although the site is only 500 ft. from the one at 3470 Wilshire, where the rock is 45 ft. beneath the surface, no rock layer was encountered to boring depths of 100 ft. The building is a 21-story steel-frame structure and has the largest cross-sectional area of the six and is the second tallest. The building has one basement and is supported by spread footings on firm to very firm silty sand and clay, 110 p.c.f.

The last of the group at 3470 Wilshire (Fig. 39) is the most complicated structure. It is basically an 11-story reinforced concrete building with interior shear walls. Adjoining the high rise portion are one-story annexes on the northern and western sides. There are two sub-basements. The first extends the entire length of the building and 90 percent of the width. The second basement is less than half the floor area of the first. Belled caissons, 3 ft. 6 in. to 4 ft. in diameter in the cylindrical portion, provide foundation support. The bells extend 5 ft. into the rock, 45 ft. beneath the surface and 25 ft. beneath the second basement floor level. The soils above the rock consist of a silty clay and sand with densities

between 100 p.c.f. and 115 p.c.f.

As shown in Figs. 34 through 39 each strong-motion accelerometer is located in the lowermost level of the building with the exception of the instrument located two levels above the third sub-basement at 3345 Wilshire. As is standard practice, all instruments are securely fastened to the concrete floors and are covered by a protective housing.

All six basement accelerographs triggered during the earthquake, but not all at the same time due to different starting sensitivities. The basement accelerograph array consisted of three AR-240's, two MO-2's, and one SMA-1 (34). The SMA-1 instrument at 616 S. Normandie ceased to function properly 18.6 sec. after initially triggering. The record does contain, however, all the hard shaking and some of the subsequent longer period motion, thus rendering it acceptable for the analysis. For purposes of meaningful comparisons, identical durations of similar portions of each accelerogram were chosen, the length of each record was limited by the abbreviated 616 S. Normandie accelerogram. Since this instrument triggered 5.5 sec. earlier than one of the other six accelerographs, the final length of accelerograms analyzed was 13 sec.

Accelerogram Comparisons

Comparisons of the accelerograms can be made by examining Figs. 40, 41, and 42 for vertical, NS, and EW acceleration components, respectively. The vertical transducer in the instrument at 3407 W. 6th

malfunctioned, so no vertical basement acceleration component was available for this site.

The amplitude levels and overall character of the vertical accelerograms, Fig. 40, are similar for all records. All of the acceleration records contain high frequency components in the first 6 sec. with amplitude levels near 0.05 g. Beyond 6 sec. the higher frequency content diminishes and longer period accelerations, between 1 and 2 seconds in period, clearly appear. The two vertical records which exhibit the best agreement are the ones from 616 S. Normandie and 3411 Wilshire, the sites closest together. There is a general resemblance in the smoothed appearance of the accelerograms from 3470 Wilshire and 3345 Wilshire due to lesser high frequency content than in the other three records.

The NS accelerograms, Fig. 41, have certain features in common. For instance, the character of the accelerations in the neighborhoods of 1.5, 3.3, and 6 sec. are similar in addition to the 2 sec. period motion at the tails of each record. Again the records from 616 S. Normandie and 3411 Wilshire have the most in common. Also, the amplitude levels for these two records are the smallest with peak accelerations of approximately 0.11 g. The largest amplitude levels occur in the 3407 W. 6th building, the shortest and possibly the lightest structure in the group, with a peak acceleration of about 0.17 g.

The EW accelerograms, Fig. 42, do not agree as favorably as the NS records. There are similarities in the EW records at about the same times (.7, 3.5, 6 sec., plus the longer period motion at the end)

as the NS records, but the similarities are generally not as strong. The agreement between the 616 S. Normandie and 3411 Wilshire EW accelerograms is not as striking as the comparisons of their NS components. The two accelerograms which appear to have the most in common are 3470 Wilshire and 3550 Wilshire. These buildings are the next closest pair of the group. Again the 3407 W. 6th record had the largest accelerations with one peak at 0.18 g. Table I summarizes the maximum recorded accelerations at each site for all components.

Fourier Amplitude Spectra Comparisons

Further comparisons of the accelerograms were made in the frequency domain by means of Fourier Amplitude Spectra (F.A.S.). In addition to quantitatively describing the frequency content of a given accelerogram, the modulus and phase of the Fourier transform have a simple physical interpretation in terms of the relative response of an undamped single degree of freedom oscillator excited by the acceleration. The modulus of the Fourier transform equals the square root of twice the energy per unit mass of the undamped oscillator at the end of the excitation (35).

The F.A.S. of the accelerograms in Figs. 40, 41, 42 were calculated by a Fast Fourier Transform (FFT) technique based on the Cooley-Tukey algorithm. The frequency interval between two successive F.A.S. points was about 0.05 c.p.s.¹ The F.A.S. were smoothed one cycle

¹The actual record analyzed was 20.48 sec. in length, 13 sec. of the real record plus an additional 7.48 sec. of zeros. The 20.48 sec. contained 1024 points, which is equal to 2^M , where M must be a positive integer in order to apply the FFT. The frequency interval is $1/20.48$ sec.⁻¹ or about 0.05 c.p.s.

with the ($\frac{1}{4}$, $\frac{1}{2}$, $\frac{1}{4}$) Hanning spectral window and are presented in Figs. 43, 44, 45. Only two plots are compared on each graph to maintain clarity in the presentation. The F.A.S. of the 3411 Wilshire and 616 S. Normandie records were paired on the same graph because the buildings are the two closest to one another. The F.A.S. for the 3407 W. 6th and 3550 Wilshire records were paired because those two buildings are the furthest apart. The basis for the final pairings was somewhat arbitrary; however, all F.A.S. plots have been extensively compared to one another.

The F.A.S. comparisons generally confirm the qualitative similarities and dissimilarities noted in the accelerograms. The F.A.S. of the vertical accelerograms, Fig. 43, agree closely in the low frequency range between 0.1 c.p.s. and 0.8 c.p.s., which corresponds to longer period motion. Above 0.8 c.p.s. there is little agreement in detail, except for overall amplitude levels, with one notable exception. The F.A.S. of 616 S. Normandie and 3411 Wilshire records are quite similar between 0.9 c.p.s. and 3 c.p.s.

The F.A.S. of the EW accelerograms, Fig. 44, are similar in the frequency range, 0.1 c.p.s. to 1.0 c.p.s. Above 1.0 c.p.s. the agreement deteriorates with increasing frequency. Fair agreement does exist up to 1.6 c.p.s. among the 3411 Wilshire, 616 S. Normandie, and 3345 Wilshire F.A.S. In certain instances the presence of large peaks beyond 1.0 c.p.s. can be seen in some of the spectra. For example, a large peak at 1.8 c.p.s. can be seen in the 616 S. Normandie and 3470 Wilshire spectra. In all of the spectra, the amplitude levels notice-

ably decrease at higher frequencies. For the majority of spectra the amplitude attenuation begins around 3 or 4 c.p.s. However, for the 3411 Wilshire spectrum the attenuation occurs beyond 10 c.p.s., while for the 3407 W. 6th spectrum, decay begins around 7 c.p.s. The largest overall amplitude levels are found in the 3407 W. 6th spectrum, while the smallest levels occur in the 3345 Wilshire spectrum.

All F.A.S. of the NS accelerograms, Fig. 45, agree reasonably well between 0.1 c.p.s. and 1.2 c.p.s. There is also good agreement between the 3550 Wilshire spectrum and 616 S. Normandie spectrum between 1.2 and 2.2 c.p.s., and fair agreement between the 3411 Wilshire and 616 S. Normandie spectra in this frequency range. With the exception of the 3411 Wilshire and 616 S. Normandie spectra, the spectra rapidly diminish in amplitude beyond 3 or 4 c.p.s. The 616 S. Normandie spectrum gradually decays beyond 3 c.p.s. while the spectral attenuation for 3411 Wilshire begins at approximately 8 c.p.s.; both spectra have similar amplitude levels beyond 5 c.p.s. The F.A.S. for 3407 W. 6th contain the largest overall amplitudes, an observation consistent with examination of the accelerograms.

Response Spectra Comparisons

Another standard tool useful in the analysis of strong-motion earthquake accelerograms is the relative response spectrum. Relative response spectra are the maximum relative responses of single degree of freedom oscillators over a range of natural periods and dampings for a given base acceleration. Plots of the spectra versus period show the maximum response of simple, single-story structures during

an earthquake and also give an indication of the frequency content of the accelerogram. Response spectrum methods are directly applicable to single degree of freedom structures and can also be applied to the design of multistory structures, in cases where modal superposition is valid, to determine important design parameters such as maximum base shear and overturning moment (36).

A program for calculating response spectra developed by Nigam and Jennings (37) was applied to the 6 basement accelerograms. Relative velocity response spectra curves were plotted for 2% critical damping over a period range, 0.2 sec. to 10 sec., in increments of 0.2 sec. Thus, the graphs tend to emphasize the longer period motion and suppress any detailed information in the higher frequency range, just the opposite of the information conveyed by the F.A.S. It was recognized that spectral values for the larger periods might be ill conditioned for accelerograms of only 13 sec. duration. Spectral calculations of a few accelerograms with an additional 7 sec. of record showed the differences to be negligible, however.

Figs. 46, 47, and 48 are the 2% damped relative velocity response spectra, S_v , for the vertical, EW, and NS accelerograms. The plots in each figure contain 3 spectra, one plot with spectra from the 3 buildings closest together and the other for the group furthest apart.

The response spectra for the vertical accelerations, Fig. 46, are quite similar over the entire period range. The largest variance between any two spectra occurs in a small neighborhood around 2.5 sec.

In general the spectral differences are small; the smallest differences are seen in the 616 S. Normandie and 3411 Wilshire spectra. It was noted that the F.A.S. of those accelerograms agreed better than any other combination for frequencies up to 3 c.p.s.

The EW response spectra, Fig. 47, closely agree up to periods of 3.5 sec., after which the divergence between the 616 S. Normandie and 3470 Wilshire spectra becomes evident up to 5.5 sec. The percentage differences between these spectra in that period range are as large as 70% with the smaller value used as the base. Differences among the spectra are small again beyond 5.5 sec.

The NS spectra, Fig. 48, are similar in character to the EW spectra. Again there is good agreement among all spectra except in the period range between 2.0 sec. and 3.6 sec., where the 3470 Wilshire and 616 S. Normandie spectra exhibit the greatest divergence, as large as 70% (again with the smallest value used as the base). The 616 S. Normandie and 3411 Wilshire spectra are practically identical over the entire period range. In the period range below 1.0 sec., the response spectra suggest that the 3407 W. 6th NS accelerogram had the largest frequency content between 1.0 c.p.s. and 5 c.p.s.; this is confirmed by the F.A.S. comparisons.

Soil-Structure Interaction Considerations

Examination of the accelerograms and their F.A.S. does not suggest that the major differences can be attributed to present theories of soil-structure interaction. For example, the buildings at 3407 W. 6th and 616 S. Normandie have roughly the same mass, height, foundation

support, and NS lateral dimension. Yet the basement accelerograms are clearly different for frequencies above 1.0 c.p.s. The amplitude levels of the F.A.S. and accelerograms are much larger for 3407 W. 6th. The EW F.A.S. for 3407 W. 6th is 2 to 3 times larger than the 616 S. Normandie F.A.S. between 5 c.p.s. and 8 c.p.s. Large contributions to the basement response from lightly damped higher modes of the 3407 W. 6th superstructure in this frequency range is not likely. A smoothed ratio of the F.A.S. of the roof and basement accelerograms of this building did not indicate the presence of any lightly damped modes beyond 5 c.p.s. In the NS direction the F.A.S. for 3407 W. 6th is 2 to 3 times larger in the frequency range, 1.5 c.p.s. to 3.5 c.p.s., than the F.A.S. of 616 S. Normandie. A smoothed ratio of the F.A.S. of the roof and basement for 3407 W. 6th in this direction revealed the second translational mode at 1.75 c.p.s. No other modes were present between 1.5 and 3.5 c.p.s. Only one peak at 1.8 c.p.s. in the F.A.S. for 3407 W. 6th is close to the second translational mode. Thus, it does not appear that interaction from the higher modes caused the differences observed in the basement accelerograms of these two buildings.

The unique feature of the 3407 W. 6th building, relative to the other five in the group, is the absence of a basement. The lowermost level, where the accelerograph is located, is no more than 5 feet beneath ground level. In essence the building is not embedded and the accelerograph is essentially at ground level. If this feature is the cause of differences observed in the accelerograms from this building and the one at 616 S. Normandie, say, then present theoretical models, such as the one studied by Bielak (19), cannot predict the differences for any

reasonable choices of the parameters involved. It is difficult from a theoretical standpoint to analyze embedded foundations without oversimplifying the problem. Theoretical and experimental results on the effects of embedment on the response of a footing (38) to harmonic excitation do not favorably agree, especially for high frequencies. One theoretical result which agrees with experiment is that the resonant response of a footing decreases with increased embedment (38). An embedment ratio, defined as the ratio of the depth of the building beneath the ground surface to the square root of the floor area, is presented in Table I for each building. It is difficult to determine if any definite correlation exists between embedment and the degree of hard shaking, determined from examination of the overall amplitude levels of the F.A.S. The building that experienced the strongest shaking, 3407 W. 6th, does have the least embedment. However, of the remaining buildings, it is difficult to clearly ascertain which ones experienced the stronger shaking.

A comparison of the F.A.S. for 616 S. Normandie and 3411 Wilshire tends to contradict the predictions from soil-structure models. The building at 3411 Wilshire is considerably different structurally from the building at 616 S. Normandie. It is three times taller, has larger lateral dimensions and completely different sub-ground level and foundation characteristics. If the effective base mass is taken as the weight of the structure beneath the ground or based on some value proportional to the basement floor area, then the base mass for 3411 Wilshire is considerably larger by an order of magnitude. For this case soil-structure interaction theory predicts that the base response at higher

frequencies would be significantly lower for 3411 Wilshire. Yet, the amplitude levels in their F.A.S. for the higher frequencies are nearly the same.

Effects of Soil Deposits above Rock

Soil borings at all sites except 3550 Wilshire revealed a layer of sedimentary rock 30 ft. to 45 ft. beneath the surface that provided partial if not total foundation support. Above the rock were softer soil layers of various compositions and properties. The layering and composition of the alluvium also varied from site to site. The buildings with shallow foundations near the rock, 3470 Wilshire, 3407 W. 6th, and 616 S. Normandie, had piles extending into rock. The building at 3411 Wilshire was embedded 25 feet into the rock, while the building at 3345 Wilshire was supported directly on the rock. Both of these buildings plus the building at 3550 Wilshire used spread footings for foundation support. The depths of the rock and foundation beneath the ground surface is included in Table I for each building.

The sub-surface conditions at the sites with soils between the rock and the foundation suggested examining whether these intermediate soils might have modified the basement response. Seed et al. (39) studied the effects of soil layers above rock on the surface response. They compared the response from a conventional one-dimensional, wave-propagation model, subjected to vertically incident shear waves, to motions recorded during the 1957 San Francisco earthquake. Their model was also used to study the ground motions during the El Centro earthquake. Their analysis indicated that the highest accelerations

can occur for relatively shallow soil deposits (30 ft. to 40 ft.) on rock, and that the maximum acceleration would be 2 to 3 times greater than that for deeper deposits of 100 ft. or more of the same soil.

To test whether the soil deposits at the Wilshire-Normandie sites had any major influence on the observed differences in the accelerograms, a model for the shearing behavior of a layered half space studied by Tsai was employed (40). The theoretical model, similar to the one developed by Seed, predicts the influence of horizontally stratified, linearly elastic soil layers on the surface response for vertically incident shear waves. Differences between an assumed rock motion and the resulting surface motion were examined for three sites, 3407 W. 6th, 3470 Wilshire, and 3550 Wilshire, to determine the extent to which the basement motion may have been modified. The site at 616 S. Normandie was similar to 3470 Wilshire and was not included in the analysis.

Because of the analogy between the governing differential equations of a shear beam and a layered half space, an appropriate model can be developed consisting of a continuous shear beam attached in some prescribed manner to a rigid foundation. The properties of the shear beam approximate the soil layers above the rock and the rigid foundation approximates the rock. To account for the energy loss due to the deformation of the rock a dashpot can be inserted between the foundation and the base of the shear beam. This model is shown in Fig. 49. Closed form solutions can be obtained for the response at any depth beneath the surface for harmonic excitation of the rock, and solutions by

numerical integration can be obtained for transient inputs.

For convenience, it is assumed that the damped shear beam possesses classical normal modes; thus, the model in Fig. 49 becomes equivalent to the model, shown in Fig. 50, used in the analysis.

To apply the model to the three sites, pre-construction soil borings were examined to determine appropriate values of soil layer depths, densities, and earthquake shear wave velocities (41). Table II summarizes the choices. The total depth of the layers is the distance between the rock and the foundation. At 3550 Wilshire the rock was assumed to be 100 ft. beneath the foundation.

The natural frequencies of the layered systems are relatively high at sites, such as 3407 W. 6th and 3470 Wilshire, with shallow depths of the soil layers. For a one layered system, such as 3470 and 3550 Wilshire, the natural frequencies are $f_r = \frac{2r - 1}{4} \left(\frac{C_1}{H_1} \right)$ c.p.s., where C_1 and H_1 are the shear wave velocity and depth of the layer, respectively. Substituting the values from Table II for 3470 Wilshire gives the natural frequencies, $f = 6.0, 18.0, 30.0, \dots$ c.p.s. The natural frequencies of the much deeper layer at 3550 Wilshire are considerably less, i.e., $f = 1.75, 5.25, 8.75, \dots$ c.p.s. The natural frequencies of the two layered system, such as 3407 W. 6th, are obtained by solving the transcendental equation, $(\rho_1 C_1 / \rho_2 C_2) \times \tan(H_1 \omega / C_1) = \cot(H_2 \omega / C_2)$, where ρ_i is the density of the i^{th} layer and ω is the circular natural frequency. For the 3407 W. 6th site the first two natural frequencies are 4.79 c.p.s. and 13.4 c.p.s. These calculations show that only the fundamental mode could affect

the response at 3407 W. 6th and 3470 Wilshire, since the frequency content of the earthquake accelerograms is negligible beyond 10 c.p.s. On the other hand the first three modes could contribute to the response at the 3550 Wilshire site.

The EW basement accelerogram from the 3411 Wilshire site (Fig. 42) was chosen as the rock motion. The resulting surface motions were then calculated for the three sites for 0% and 5% critical damping in each mode of the shear beams. The rock and computed surface accelerations are compared in Fig. 51 (0% critical damping) and Fig. 52 (5% critical damping).

Comparisons of Figs. 51 and 52 show that the computed ground and rock motions are virtually the same for the 3470 Wilshire and 3407 W. 6th sites. The 0% critically damped ground accelerations (Fig. 51) at these two sites contained slightly larger peaks than the input rock accelerogram. The peak acceleration of the rock motion was 0.13 g, while the peaks for the computed surface motion at these two sites were 0.15 g for 0% modal damping. For 5% damping (Fig. 52) the peak accelerations for the two sites were the same as the input motion.

Differences between the computed ground motion at 3550 Wilshire, the site where the rock was assumed to be 100 ft. beneath the surface, and the assumed rock motion are readily apparent. The higher frequency accelerations present in the rock motion are absent in the computed surface response. The peak accelerations of the computed ground motions are 0.10 g and 0.08 g for 0% and 5% modal damping, respectively. The amplitudes of nearly all peaks are smaller in the computed response.

The results of the analysis confirm a general conclusion of Seed et al. (39) discussed previously; namely, that peak accelerations at the surface can be much greater for shallow deposits (30 ft.-40 ft.) than deeper deposits (100 ft. or more) of similar soil. The shear beam analysis indicates that the response at the 5 easternmost sites, where the buildings either rest on the rock or are separated from the rock by shallow alluvial deposits, would be virtually the same for a common rock motion. Substantial differences could be expected at 3550 Wilshire, where the rock layer is much deeper. However, although 3550 Wilshire is the most atypical site of the group, its accelerogram, F.A.S., and response spectra for the San Fernando earthquake are relatively average by comparison. The 3550 Wilshire site recorded the second largest peak acceleration in both horizontal directions, whereas the theory predicted it should have been the smallest.

Comparing the results of the analysis and the data suggest that differences in the recorded accelerograms cannot be attributed to shearing modifications from differences in the local site conditions. The theory predicted significant differences in the accelerograms at 3550 Wilshire, which did not, in fact, exist in the data.

III.3 Basement Accelerograph Records in the Vicinity of the Wilshire Blvd.-Normandie Ave. Area

Seven basement accelerograms from buildings surrounding the Wilshire Blvd.-Normandie Ave. group were studied to see if there were any general similarities present for the entire array, and to determine the nature of the differences as a function of distance from the center of the earthquake.

Fig. 31 shows the locations of the selected buildings, 2 to 3 miles from the clustered group in the Wilshire-Normandie district, which contained basement accelerographs that triggered during the earthquake. In some instances buildings from a given area were chosen on the basis of acceleration data available at the time of the study.

Table III summarizes the pertinent information for each site (42). Three buildings are located to the north of the Wilshire-Normandie area; two of these buildings are only about 200 yards apart. Another building is directly west on Wilshire Blvd. while the building to the south is located on the campus of the University of Southern California. To the east of the Wilshire-Normandie group in downtown Los Angeles are the Union Bank building, 39 stories and the tallest of the seven, and the L.A. Department of Water and Power building, approximately a half mile northeast of the Union Bank building. Although the soil conditions vary from site to site, the seven sites have basically the same geologic formation as the Wilshire-Normandie area, i.e., Pleistocene deposits over Miocene sedimentary rock. At three of the sites, 4867 Sunset, Union Bank, and Department of Water and Power, the sedimentary rock is near the surface. At the other sites the rock layer is much deeper and was not encountered in soil borings except at 3440 University, where borings discovered the rock at a depth of 400 ft. The depth of the soil borings at the sites where rock was not found was not investigated.

Accelerogram Comparisons

Comparisons were made of similar 13 second portions of the accelerograms; each record beginning at the start of the hard shaking. To be consistent, portions of the accelerograms chosen were similar to those portions of accelerograms analyzed from the Wilshire-Normandie group.

Figs. 53, 54, 55 show the vertical, NS, and EW accelerograms, respectively. The strongest shaking in the vertical accelerograms was observed in the three buildings furthest north, i.e., closest to the center of the earthquake. Peak accelerations near 0.1 g were recorded at 6430 Sunset and 4867 Sunset. The 6464 Sunset vertical record, by comparison, had no peaks larger than 0.08 g and the overall amplitude level in the hard shaking was smaller. The smallest acceleration amplitudes were recorded at 3440 University, the site furthest south. This vertical component did not exhibit the high frequency accelerations typical of the other vertical records.

The same trends noted in the vertical accelerograms can be seen in the lateral components as well. The strongest shaking is found at 4867 Sunset and 6430 Sunset, while the weakest accelerations were found at 3440 University. The lateral motion at 6464 Sunset does not have large high frequency peaks as do the neighboring accelerograms at 6430 Sunset. The longer period accelerations for these two buildings closely agree.

F.A.S. Comparisons

Comparisons were continued in the frequency domain with F.A.S. plots. Figs. 56, 57, 58 show the once smoothed F.A.S. of the vertical, NS, and EW accelerograms, respectively. Plots have been superimposed where the records were from buildings close together, i.e., Union Bank and the Department of Water and Power (DWP), and the buildings at 6464 and 6430 Sunset. As might be expected, the F.A.S. correlate poorly except for the buildings close together. There is good agreement between the F.A.S. for 6430 and 6464 Sunset for frequencies less than 2 c.p.s. for all components. Beyond 2 c.p.s. the amplitudes are larger for the 6430 Sunset spectra in the lateral directions. The Union Bank and DWP spectra agree quite well for frequencies below 0.5 c.p.s.

Response Spectra Comparisons

The 2% damped relative velocity response spectra are shown in Figs. 59, 60, 61. From previous comparisons of the F.A.S. it is not surprising that the response spectra for 6430 Sunset and 6464 Sunset agree closely for periods larger than 0.5 sec., and that the Union Bank and DWP spectra agree closely for periods larger than 1.5 sec.

All of the spectra attenuate to some level beyond 8 sec. except the vertical and EW spectra for 3440 University. The amplitude in both of these spectra continuously increases between 8 sec. and 10 sec. and does not give any indication of leveling off. This anomaly is probably due to a spurious 13 sec. period inherent in the processed accelerogram trace. The standard correction of the acceleration data is to filter all periods above 15 sec.; thus, the spurious 13 sec.

motion would be unaffected by the correction process.

In general the lateral spectra exhibit roughly the same character as the Wilshire-Normandie spectra, i.e., narrow peaks in the neighborhood of 1 sec. and broader peaks centered between 4 sec. and 6 sec. An indication of the spread in the response spectra is shown in Fig. 62, where the maximum and minimum spectral values of the 7 buildings are plotted for each period. Superimposed on these graphs are the spreads in response spectra for the 6 buildings from the Wilshire-Normandie area. For the vertical and EW directions the spread in the Wilshire-Normandie spectra is contained within the spectral limits of the surrounding buildings. This result might intuitively be expected for all directions. However, in the NS direction the maximum and minimum values of the Wilshire-Normandie spectra are generally slightly larger than those of the spectra of the surrounding buildings for periods less than 3 sec. For periods larger than 4 sec. the spectral limits are roughly the same for each group of buildings.

III.4 Summary and Conclusions

Accelerogram, F.A.S., and response spectra comparisons for the 6 buildings in the Wilshire Blvd.-Normandie Ave. area indicate that the degree of similarity in the basement motion of any two buildings is mainly a function of the distance between them. Major differences in the accelerograms could not be explained by the theories of soil-structure interaction and vertically incident shear waves in a layered half space. There was no evidence of any correlation between similarities in the acceleration data and similarities in structural character-

istics, such as degree of embedment or size of the building.

The two accelerograms with the most in common were from 616 S. Normandie and 3411 Wilshire. These two buildings are the closest together but are very dissimilar structurally. The F.A.S. of their accelerograms agreed excellently for frequencies less than 1.2 c.p.s. (NS), 1.4 c.p.s. (EW), and 0.8 c.p.s. (vertical). The agreement was fair up to 2.2 c.p.s. (NS), 1.7 c.p.s. (EW), and 3 c.p.s. (vertical). The frequency content in all 6 accelograms was similar for frequencies less than 1.0 c.p.s. (NS and EW) and 0.6 c.p.s. (vertical). There was good agreement among the response spectra for each component; the best overall agreement occurred between the 616 S. Normandie and 3411 Wilshire spectra. All EW spectra had peaks near 1.0 sec. and 2.5 sec. and a broad hump centered around 5 sec., while the NS spectra had 2 peaks near 1 sec. and a broad hump centered around 3 sec. All vertical spectra had a small hump near 2 sec.

The 6 Wilshire-Normandie accelerograms had little in common with the 7 accelerograms, 2 to 3 miles from them. There was some general similarity in shape among the response spectra from the Wilshire-Normandie area and the larger circle of surrounding buildings. The spectra from the surrounding buildings, however, showed a wider range of variance than the spectra from Wilshire-Normandie.

Comparisons among the surrounding group again revealed that buildings closest together had accelerograms with the most in common. The next chapter offers some insight into the degree of similarity between two accelerograms as a function of their separation distance.

There is evidence of amplitude attenuation and dissipation of high frequency accelerations with increasing distance from the center of the earthquake. The dissipation of the higher frequency content from north to south is most obvious in the vertical accelerograms. It is less obvious in the lateral components, but F.A.S. comparisons between the 3 northern most sites on Sunset Blvd. and those roughly 3 miles to the south, including the Wilshire-Normandie group, establish this trend. The accelerogram furthest south, 6 miles from Sunset Blvd. and 24 miles from the center of the earthquake, had little high frequency content, and the acceleration amplitudes were considerably less than any of the records obtained further north. The effects of the epicentral distance over distances the size of the larger circle of buildings can therefore be significant for shorter period motions. The San Fernando data from this larger circle suggest that more than one design spectrum in the low period range could be used to reflect the distance from a known fault to sites within an area of this size.

Methods to modify design spectra, due to the effect of soil deposits on rock, are being proposed (67) based on the layered half space model developed by Seed et al. (39). In reference 67, two amplification curves for design spectra, one for alluvial deposits 20 ft. to 50 ft. deep and the other for deposits 80 ft. to 150 ft. deep, are considerably different. The response spectra from the Wilshire-Normandie area, which includes sites of these two types, suggest that local site conditions did not have any significant effect on the recorded basement motions. Any procedure for modifying a design

spectrum for this area based on the differences in local site conditions would not be consistent with what actually happened during the earthquake. The earthquake data indicates that only one spectrum for an area of this size would be necessary from the standpoint of design. However, to specify a representative spectrum for this area from the response spectra of the San Fernando event for future design would be incorrect even if it is unlikely that any future earthquake could generate stronger motion. The shapes of the spectra from Wilshire-Normandie and the larger area are similar to variable degrees. Thus, the shape of the response spectra is probably attributable to details of the source mechanism and the travel paths of the earthquake waves. Therefore, a future earthquake of the same size would conceivably produce response spectra with peaks at different periods. Given the additional uncertainty of size of the earthquake, along with the unpredictable nature of the location and source mechanism, it must be assumed in specifying design spectra that the size of the major peaks and their periods is unknown.

The use of peak acceleration in specifying overall levels of design spectra is not advisable. Acceleration peaks are usually high frequency spikes occurring in the hard shaking portion, and the amplitude of one such peak will not affect the response spectrum. The peak accelerations in the lateral accelerograms from the Wilshire-Normandie area varied by as much as a factor of almost two in some instances; however, the response spectra were nearly identical for the longer period motion greater than 1 sec. For periods less than 1 sec., the

F.A.S. gave a reasonable idea of the intensity of hard shaking. However, there was no absolute correlation between peak g and the amplitude levels of the F.A.S. for the Wilshire-Normandie data. Thus, peak acceleration, per se, is not a reliable yardstick in determining the intensity of the strong motion, except in a very general sense, and it is not recommended as a tool for determining design spectra.

BLDG.	DEPTH OF ROCK BENEATH SURFACE	DISTANCE OF INSTRU. ABOVE ROCK	DEPTH OF BLDG. BENEATH SURFACE, z	AREA OF BLDG AT SURFACE a_s	AREA OF BLDG BENEATH SURFACE, a_t	DIMENSION-LESS EMBEDMENT		MAXIMUM RECORDED ACCELERATION		
						z/a_s	z/a_t	V	EW	NS
616 S. Normandie	30 ft.	20 ft.	10 ft.	1.00×10^4 s.f.	1.26×10^4 s.f.	.100	.089	.06g	.12 g	12 g
3407 W. 6 th	40	35	<5	2.17	2.17	.034	.034	NR	.18	17
3345 Wilshire	30	20	30	1.30	2.75	.263	.183	.07	.10	12
3411 Wilshire	30	25 below	55	2.45	9.10	.352	.165	.06	.13	11
3470 Wilshire	40	25	20	2.39	2.91	.129	.117	.05	.12	14
3550 Wilshire	100+	90+	10	2.52	2.52	.063	.063	.07	.13	17

TABLE I

SITE	SOIL LAYER	SOIL LAYER PARAMETERS		
		DEPTH	DENSITY	EST. SHEAR VEL.
3407 W. 6 th	1	10 ft.	110 p.c.f.	500 f.p.s.
	2	25	100	700
	rock		90	1000
3470 Wilshire	1	25	105	600
	rock		90	1000
3550 Wilshire	1	100	115	700
	rock		90	1000

TABLE II

BLDG. NO. (FIG. 31)	ADDRESS	INSTRUMENT & LOCATION	LOCAL GEOLOGY	BLDG. TYPE	NO. OF STORIES	DISTANCE FROM 3411 WILSHIRE	DISTANCE FROM CENTER OF E.O.
1	4867 Sunset	AR-240, Bsmt.	shallow alluvium over Miocene sedimentary rock	R.C.	8	2.6 mi.	18.5 mi.
2	6430 Sunset	MO-2, 1st floor	alluvium	steel	14	3.1	18
3	6464 Sunset	MO-2, Bsmt.	alluvium	steel	11	3.1	18
4	4680 Wilshire	AR-240, Bsmt.	alluvium	R.C.	7	2.0	21
5	3440 University	MO-2, Bsmt	400' of alluvium over sed. rock	R.C.	12	3.0	24
6	445 Figueroa (Union Bank)	AR-240, Sub-Bsmt.	Miocene sed. rock	steel	39	2.5	22.5
7	111 N. Hope L A Dept. of Water & Power	AR-240, Bsmt.	Miocene sed. rock	steel	15	2.8	22.5

TABLE III

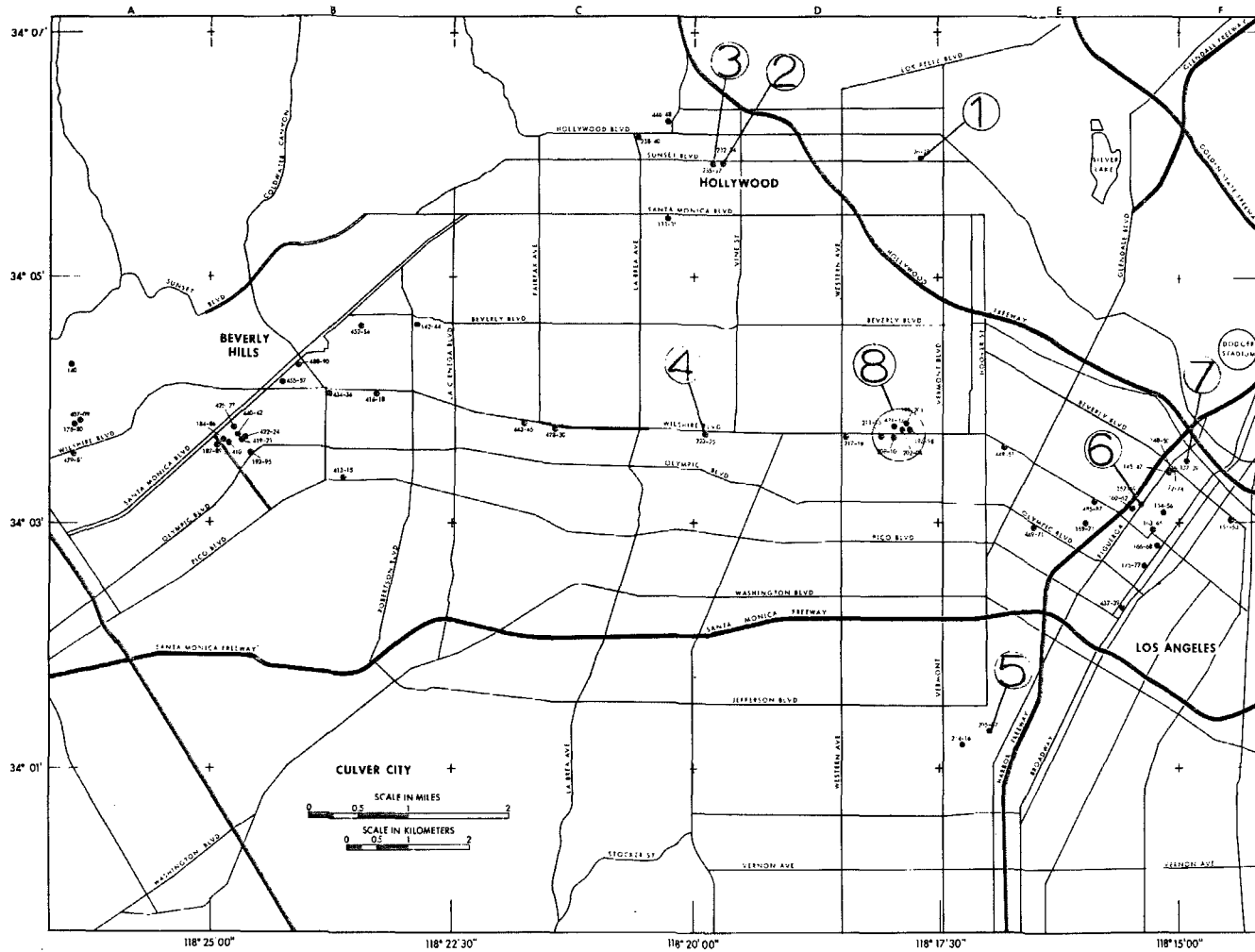


Fig. 31 Accelerograph Locations. 1: 4867 Sunset. 2: 6430 Sunset. 3: 6464 Sunset. 4: 4680 Wilshire. 5: 3440 University. 6: 445 Figueroa. 7: 111 N. Hope. 8: Six Buildings Near Wilshire Blvd. and Normandie Ave.



Fig. 32 Aerial View Looking Northwest. 3345 Wilshire Not Visible.

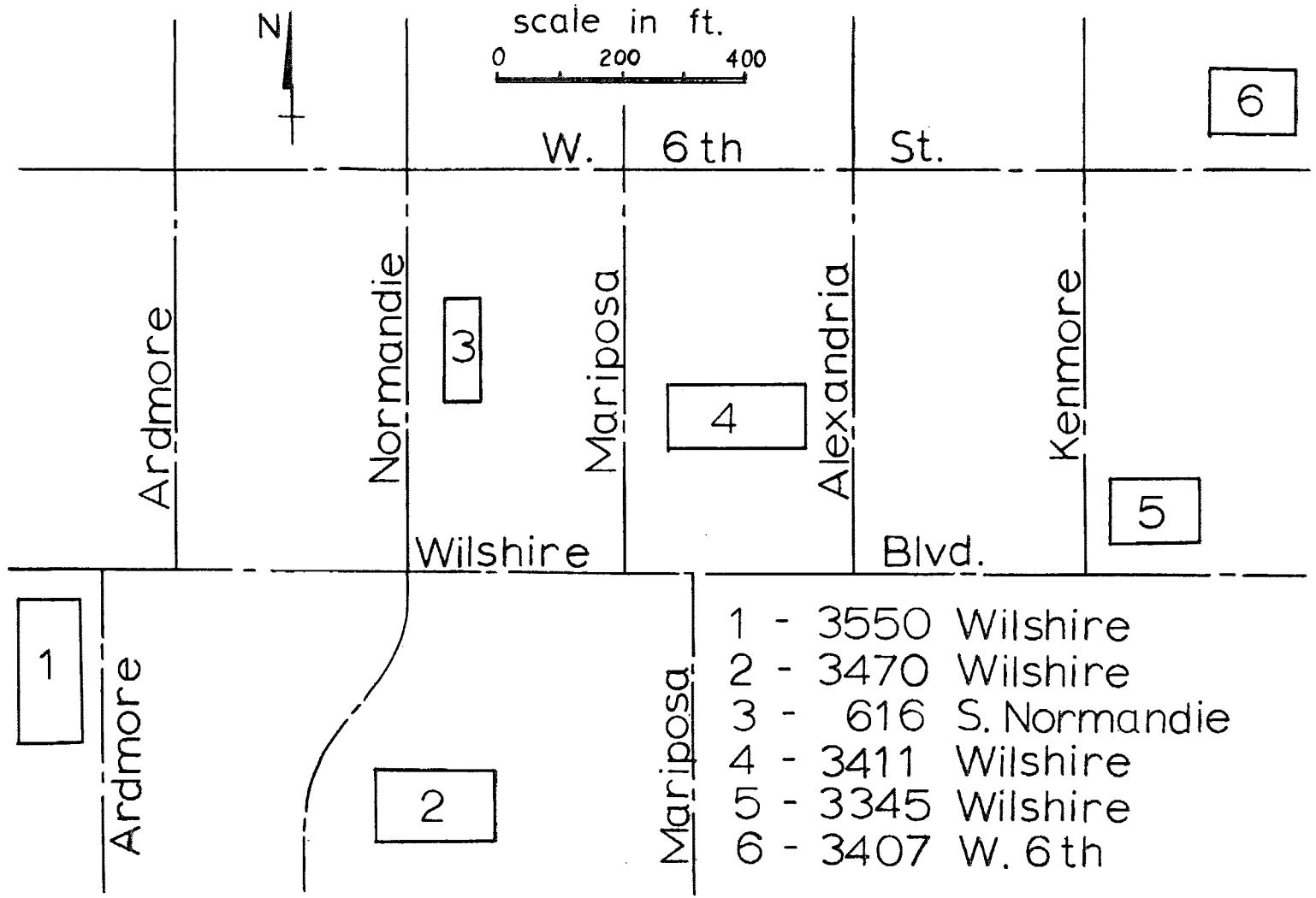


Fig. 33 Locations of Buildings.

3407 W. 6th

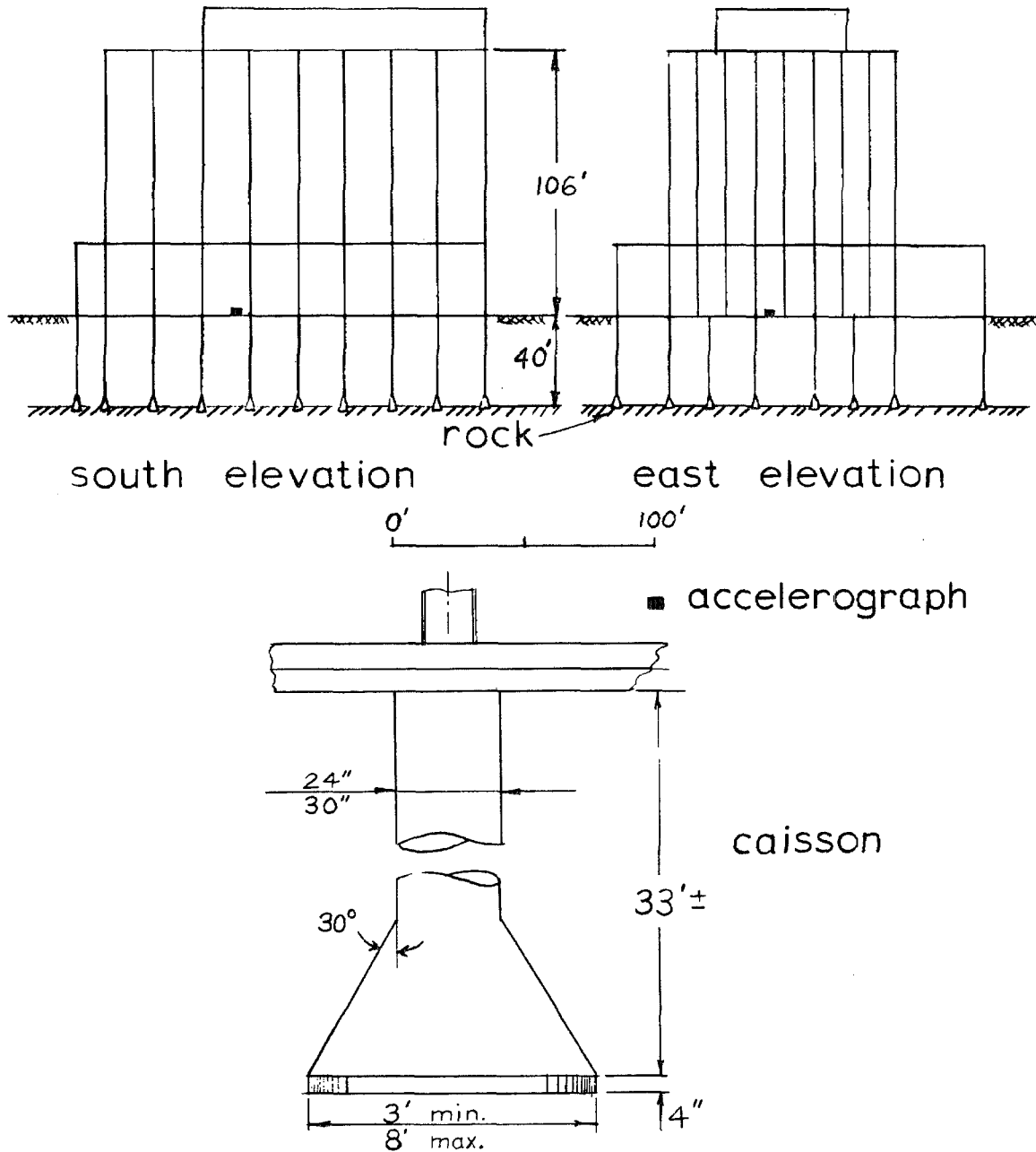


Fig. 34 3407 W. 6th.

3411 WILSHIRE

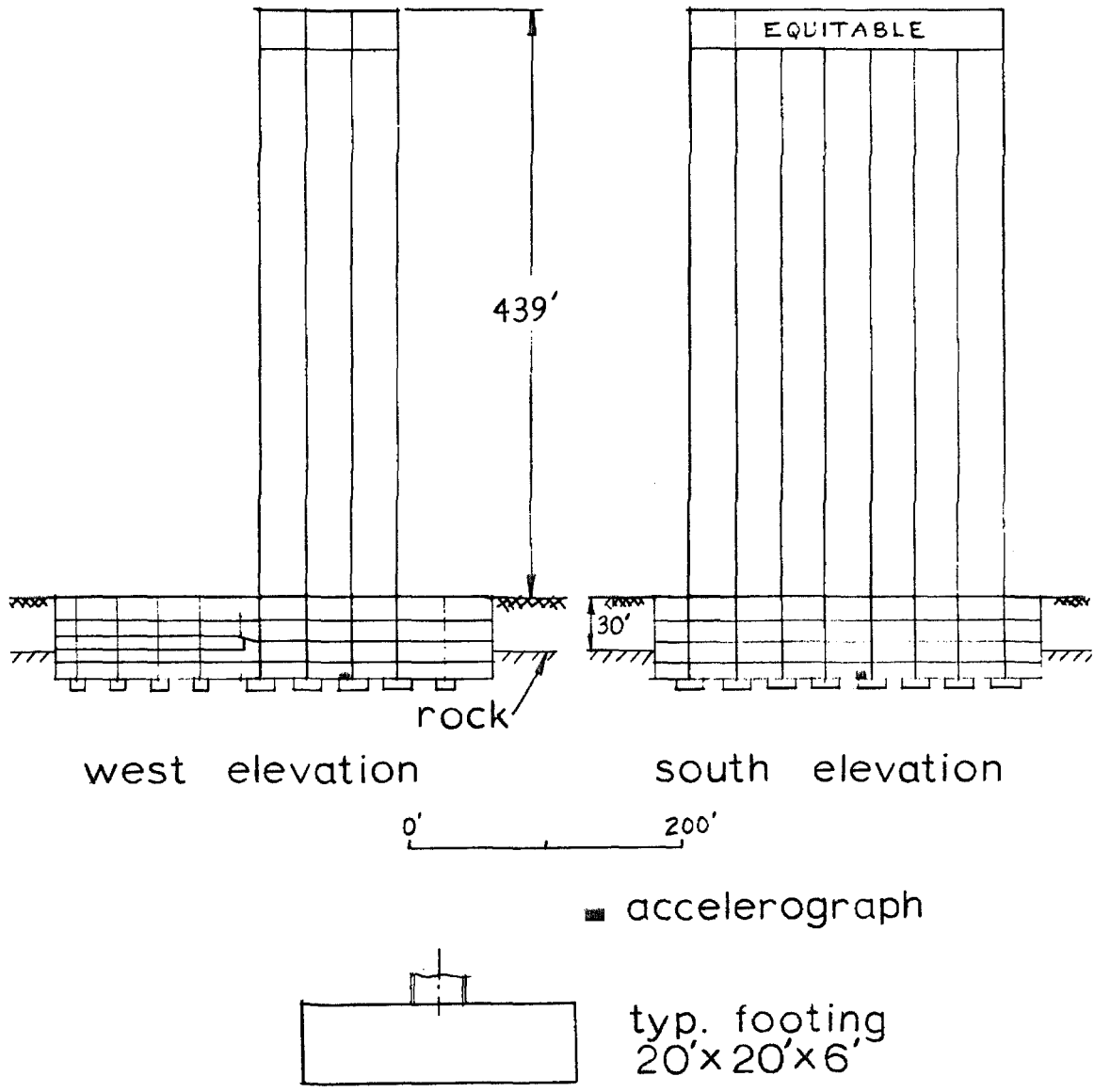


Fig. 35 3411 Wilshire.

616 S. NORMANDIE

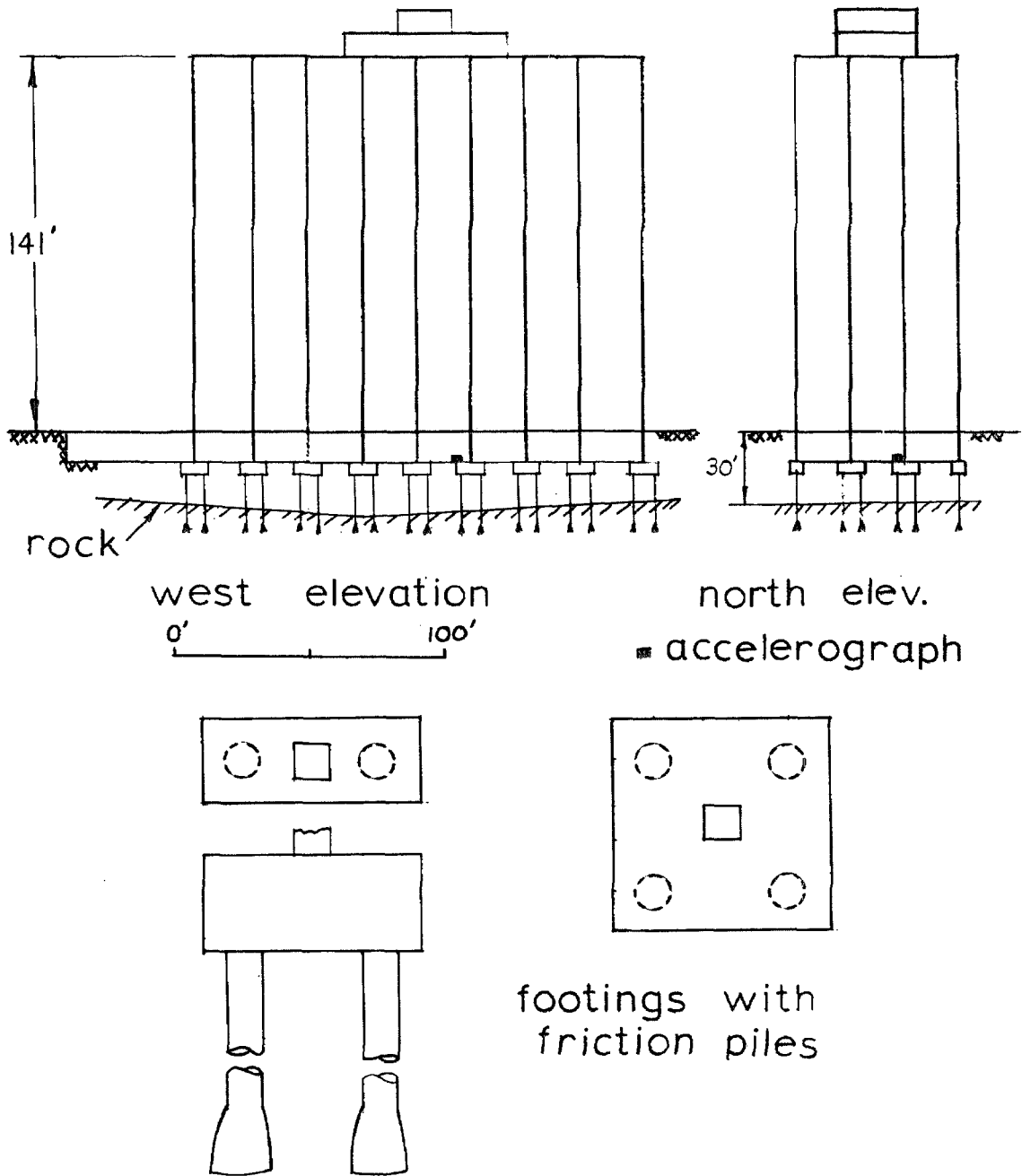
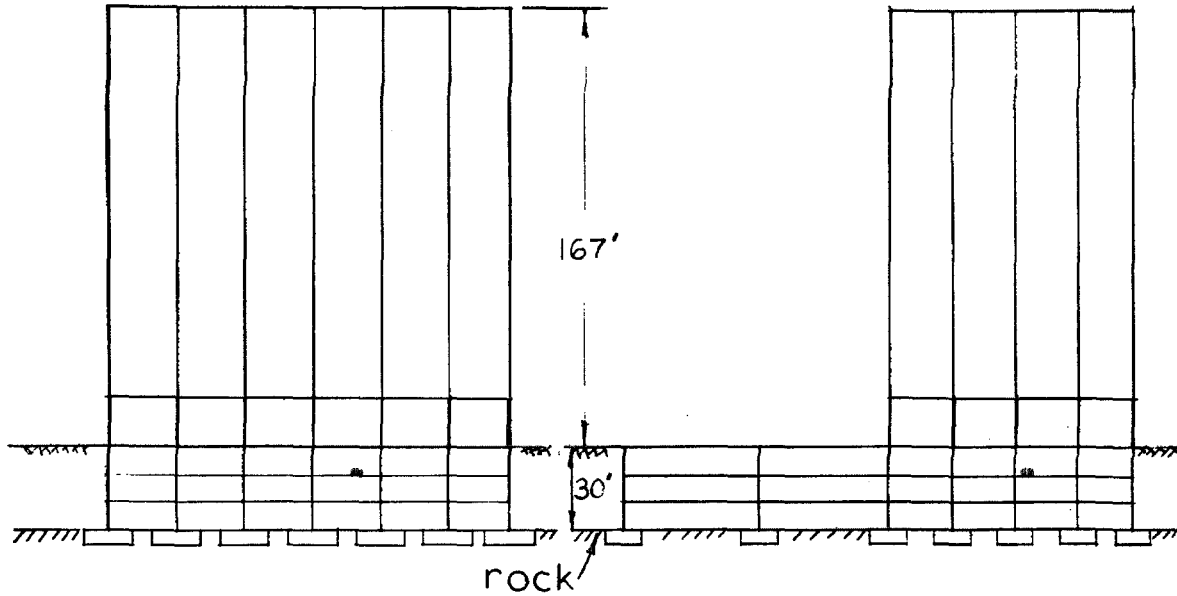


Fig. 36 616 S. Normandie.

3345 WILSHIRE

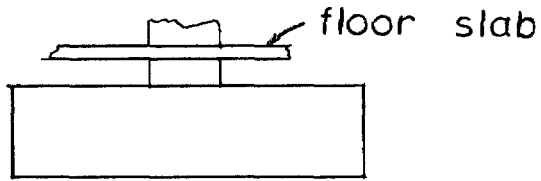


south elevation

west elevation

0' 100'

■ accelerograph



typ. interior footing
13' x 18' x 3' 4"

Fig. 37 3345 Wilshire.

3550 WILSHIRE

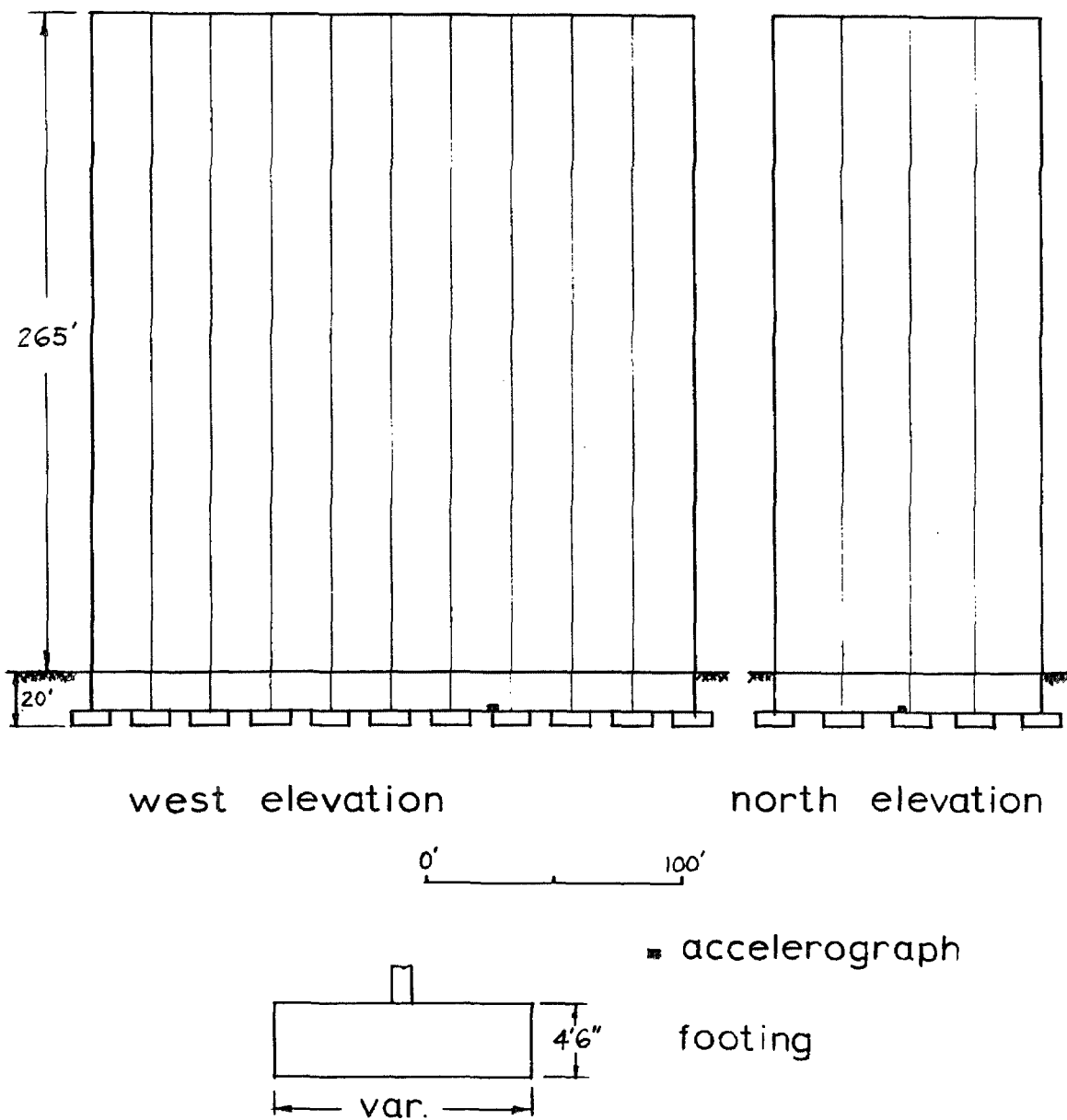
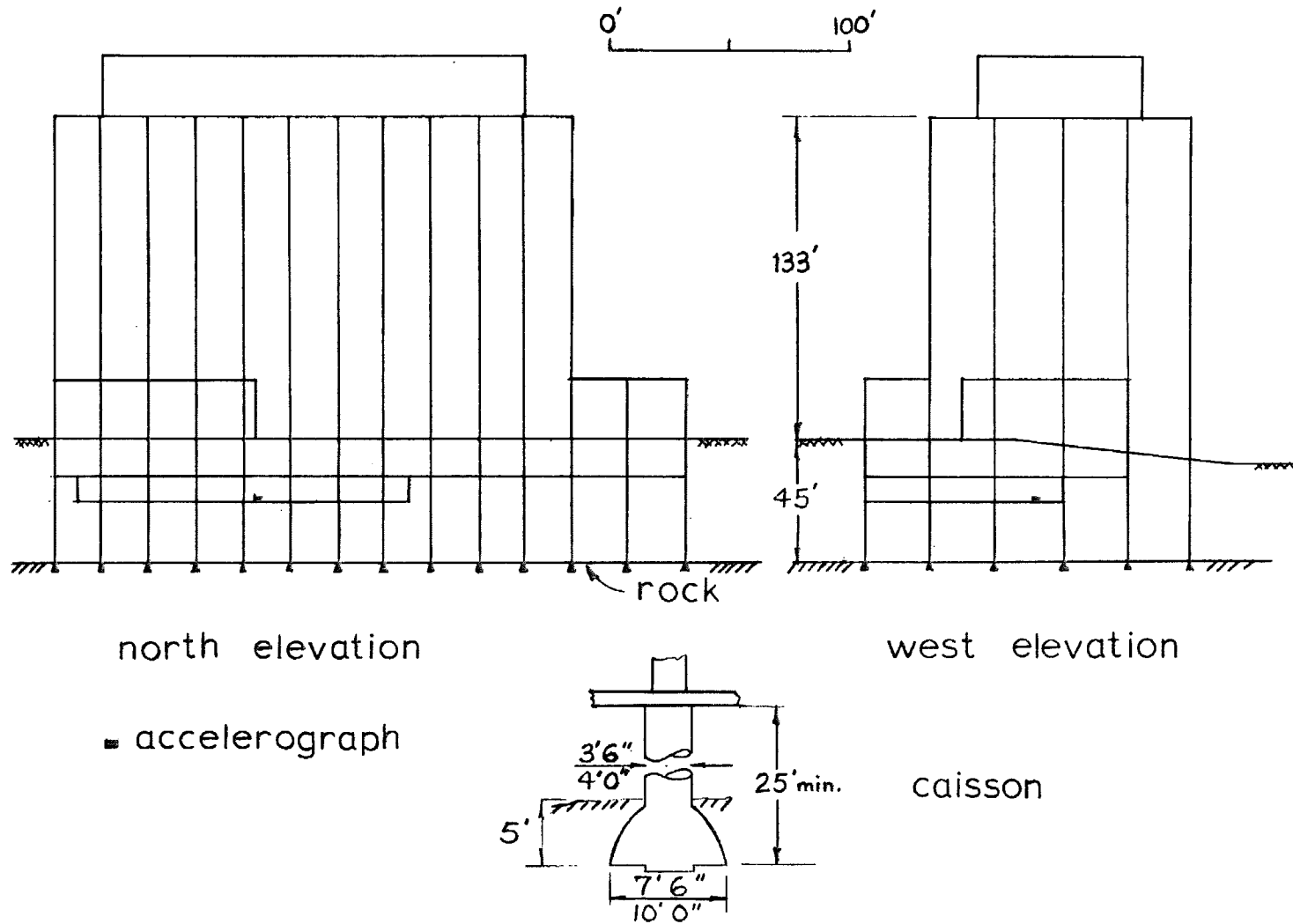


Fig. 38 3550 Wilshire.

3470 WILSHIRE



-102-

Fig. 39 3470 Wilshire

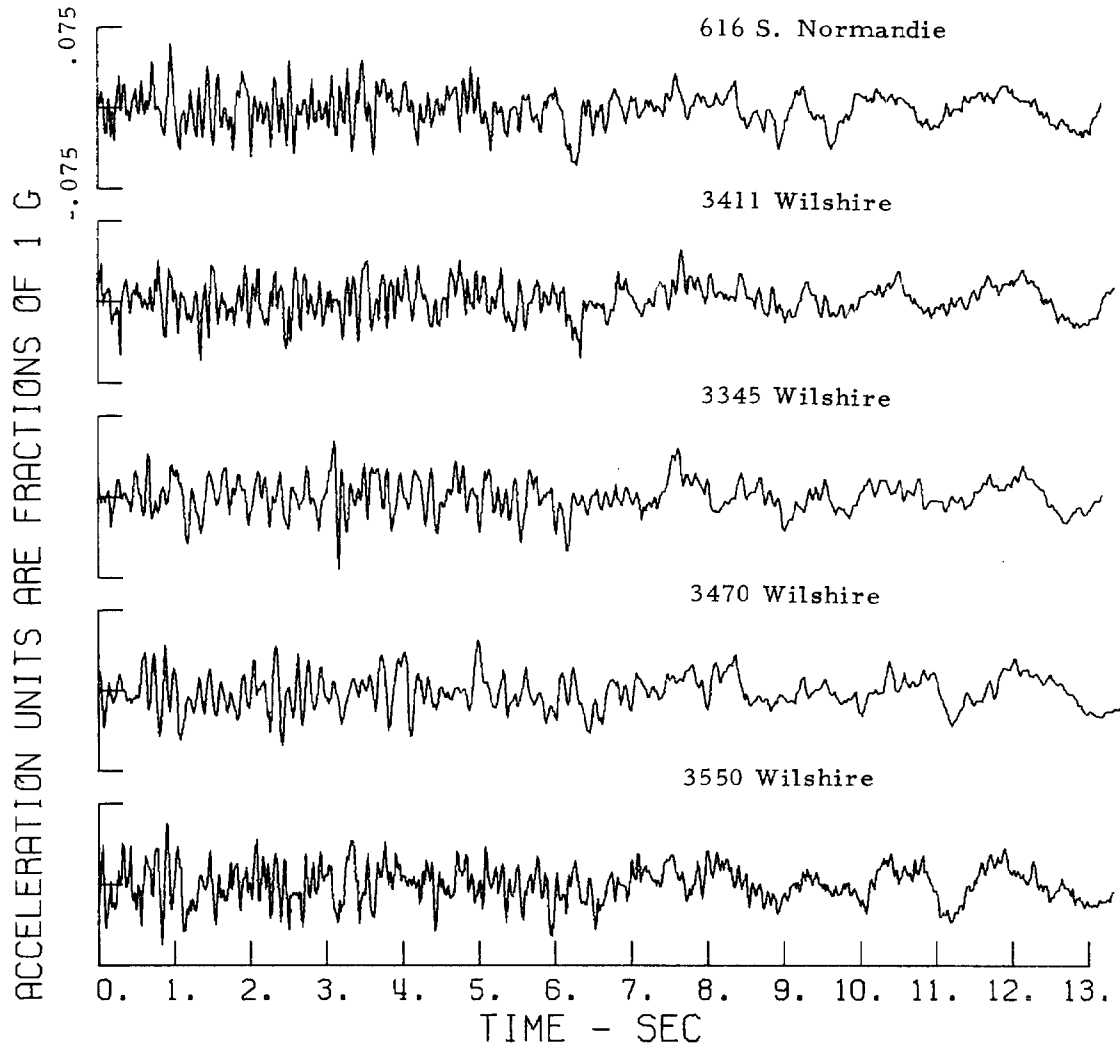


Fig. 40 Vertical Accelerations.

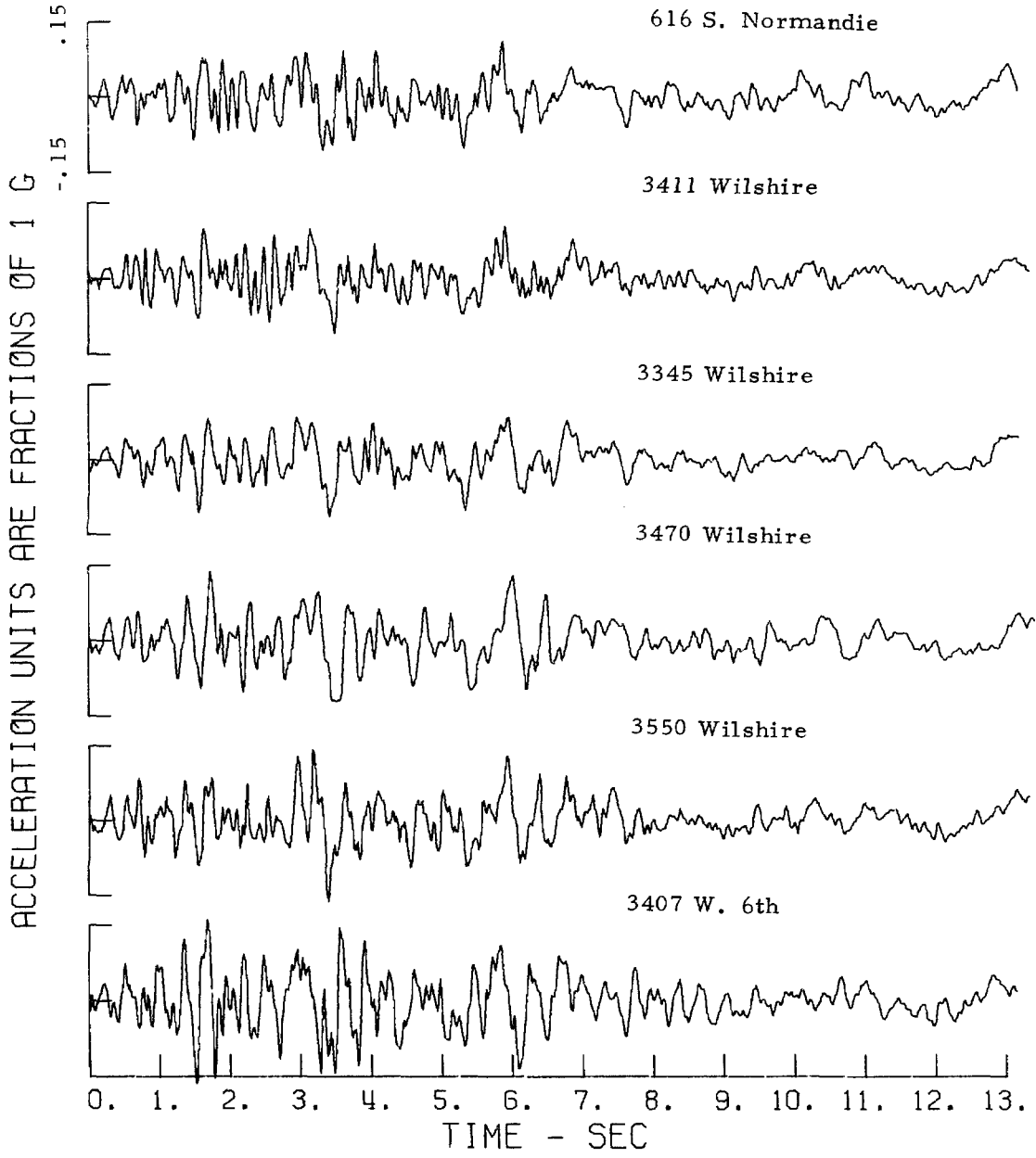


Fig.41 NS Accelerations.

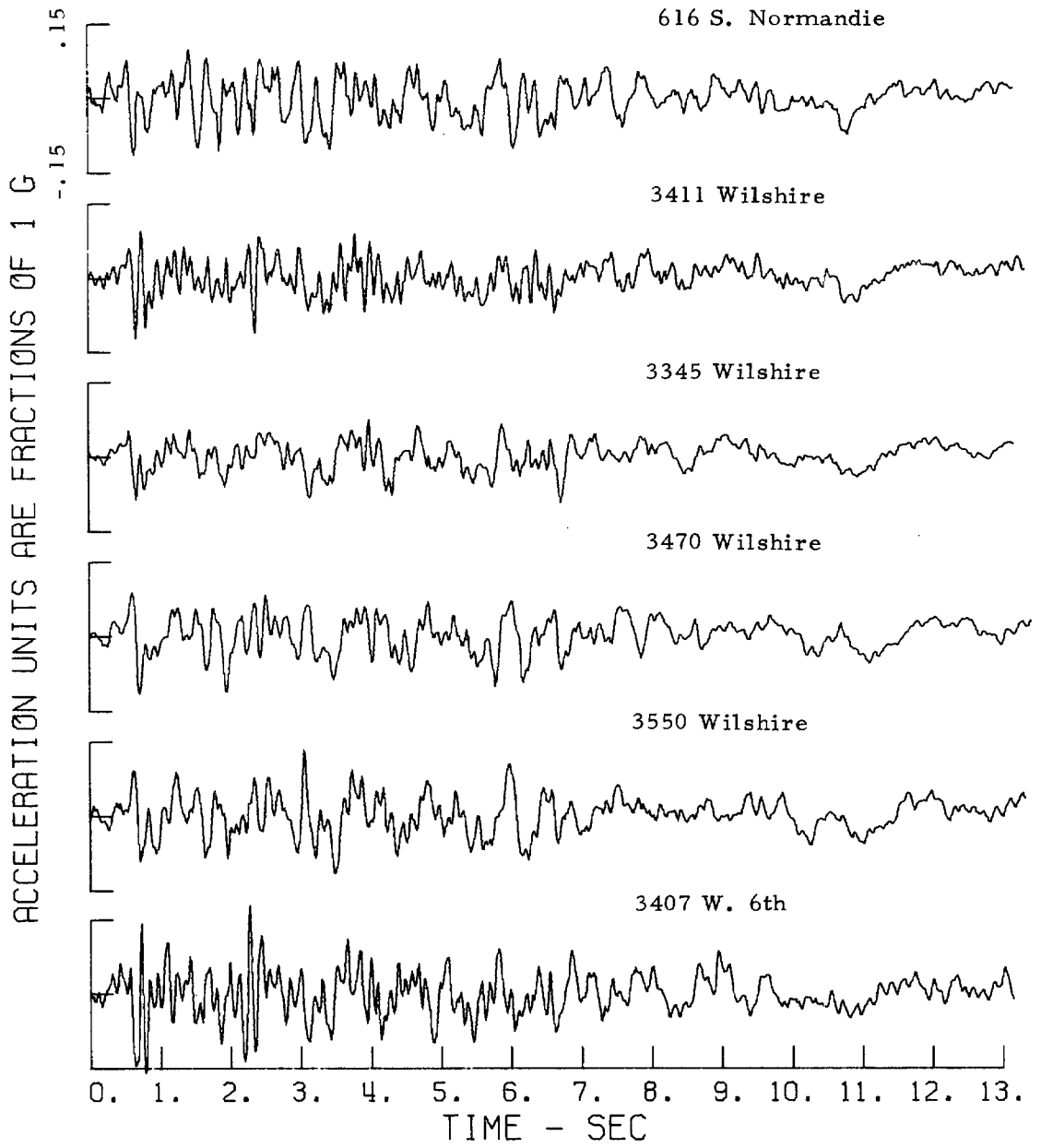


Fig. 42 EW Accelerations.

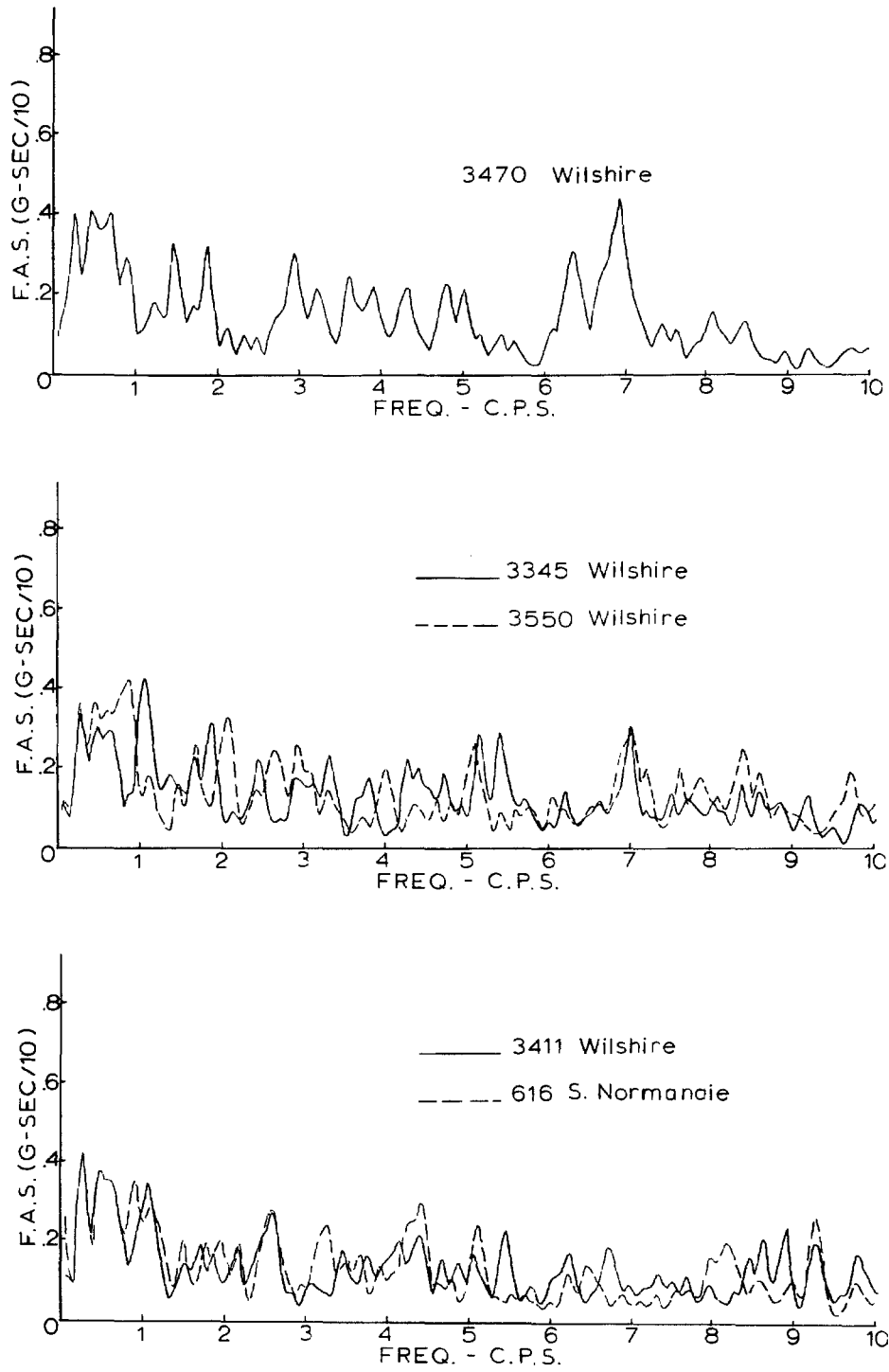


Fig. 43 Fourier Amplitude Spectra. Vertical Direction.

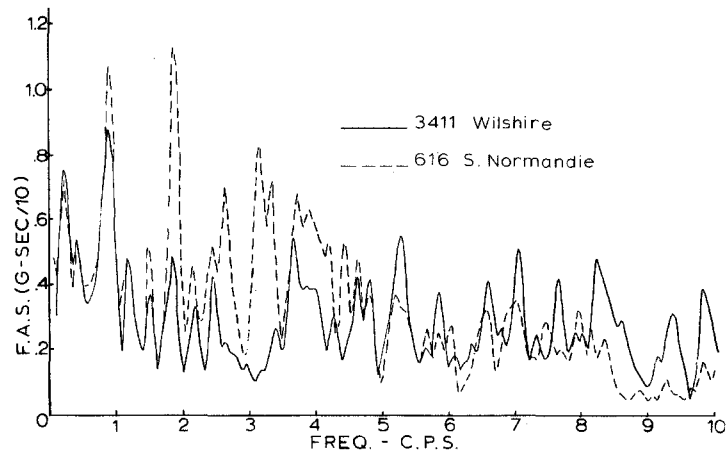
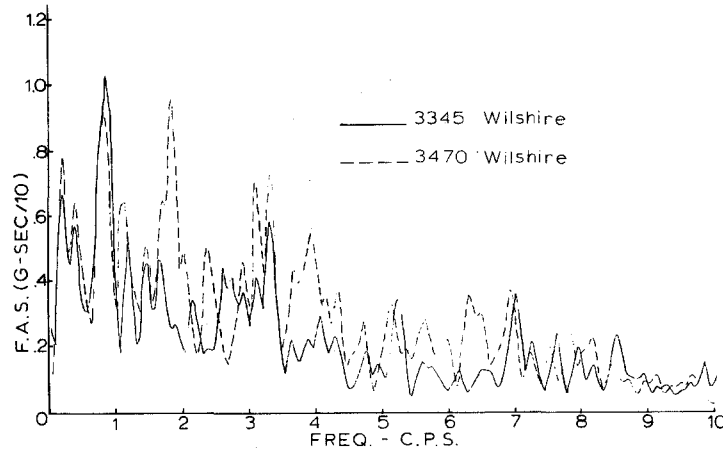
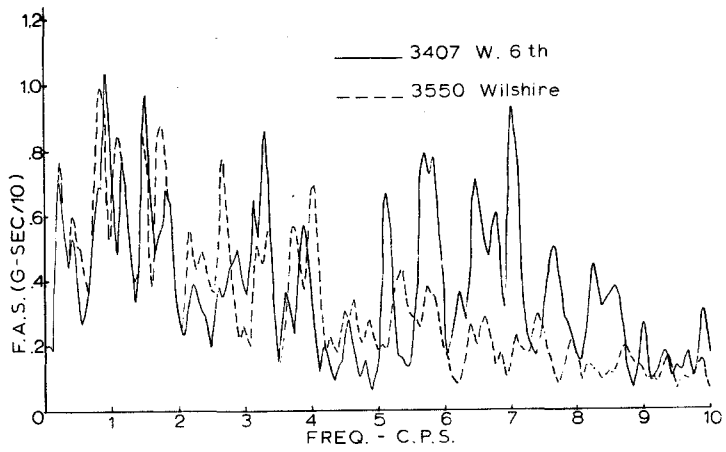


Fig. 44 Fourier Amplitude Spectra. EW Direction.

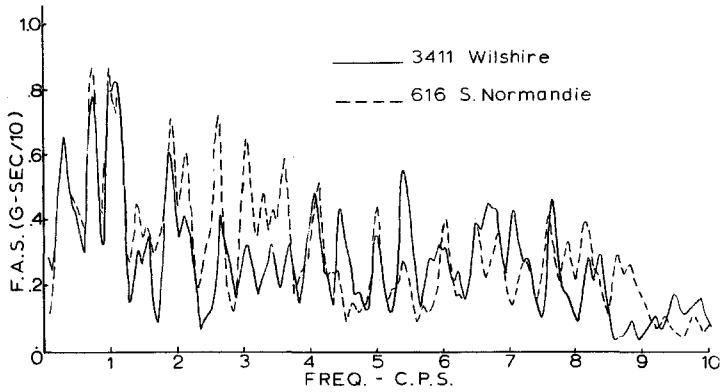
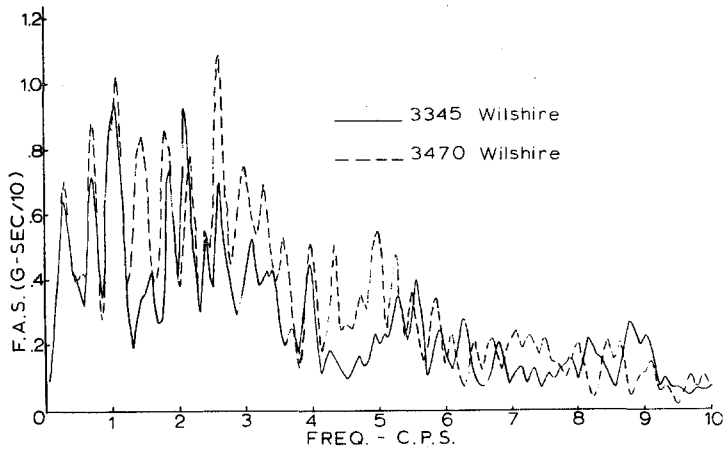
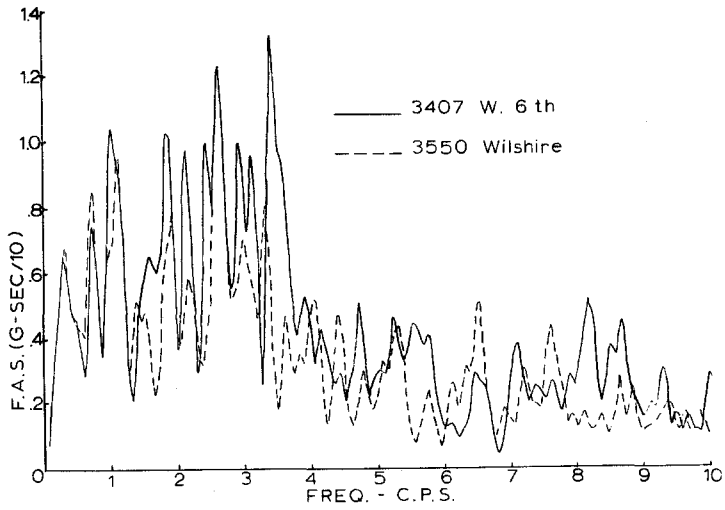


Fig. 45 Fourier Amplitude Spectra. NS Direction.

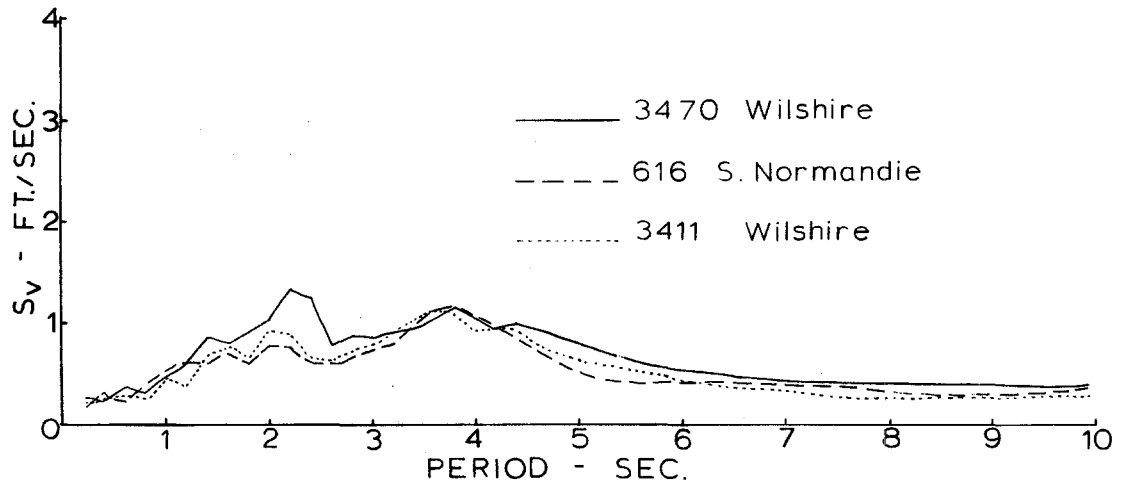
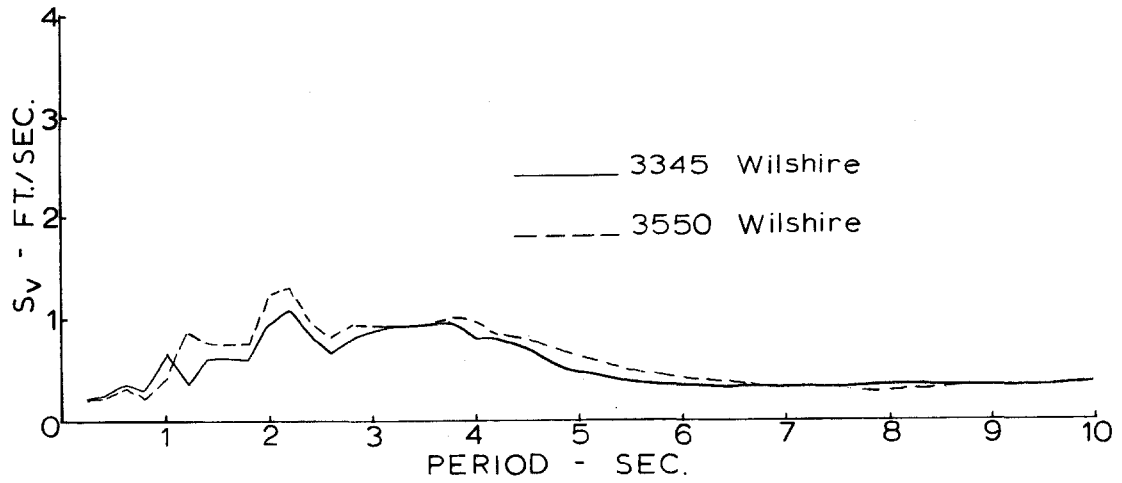


Fig. 46 Relative Velocity Response Spectra. Vertical Direction. 2% Damping.

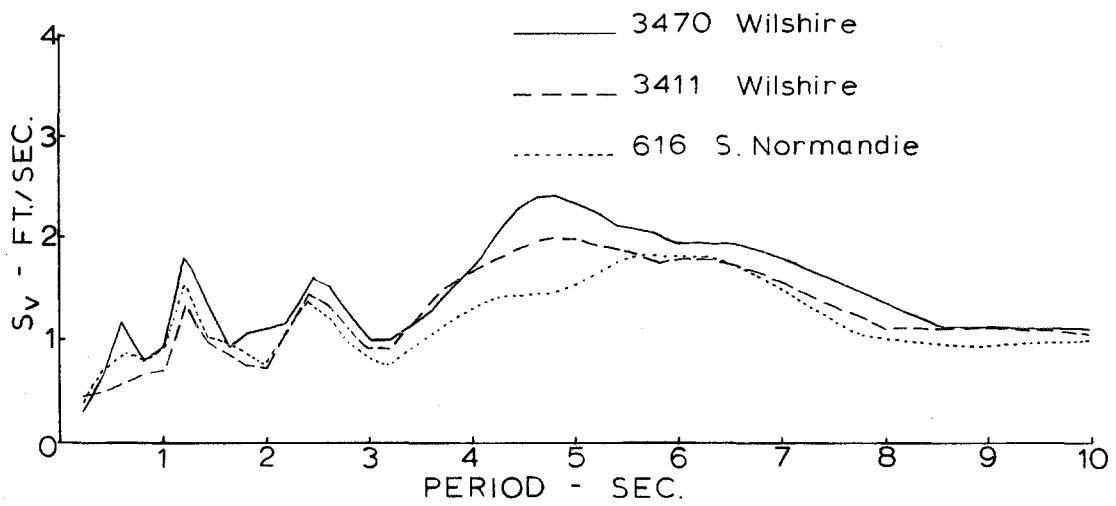
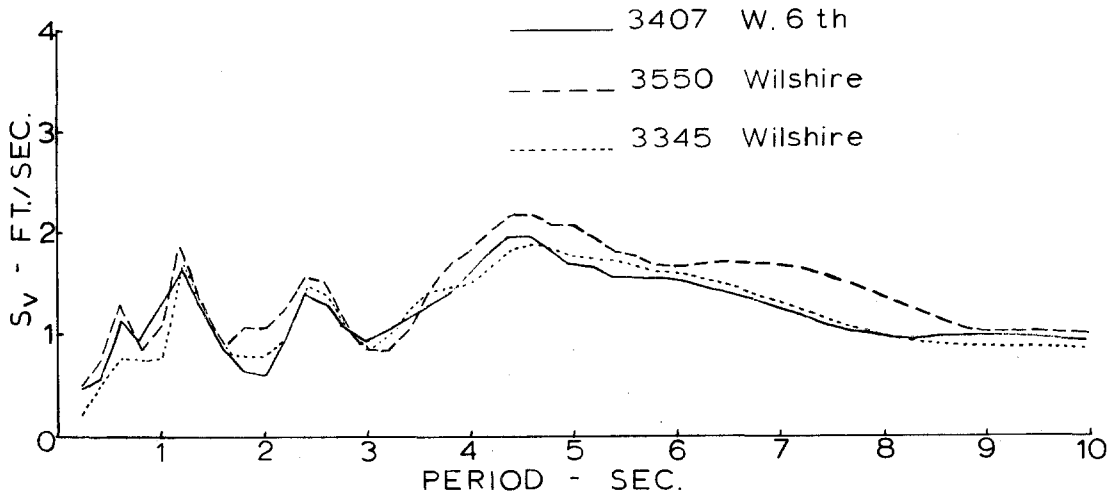


Fig. 47 Relative Velocity Response Spectra. EW Direction. 2% Damping.

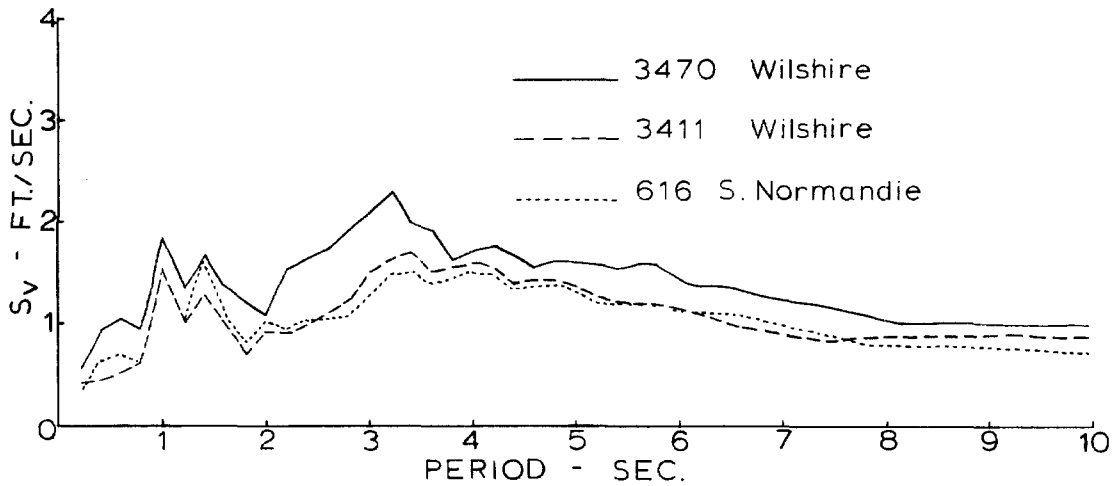
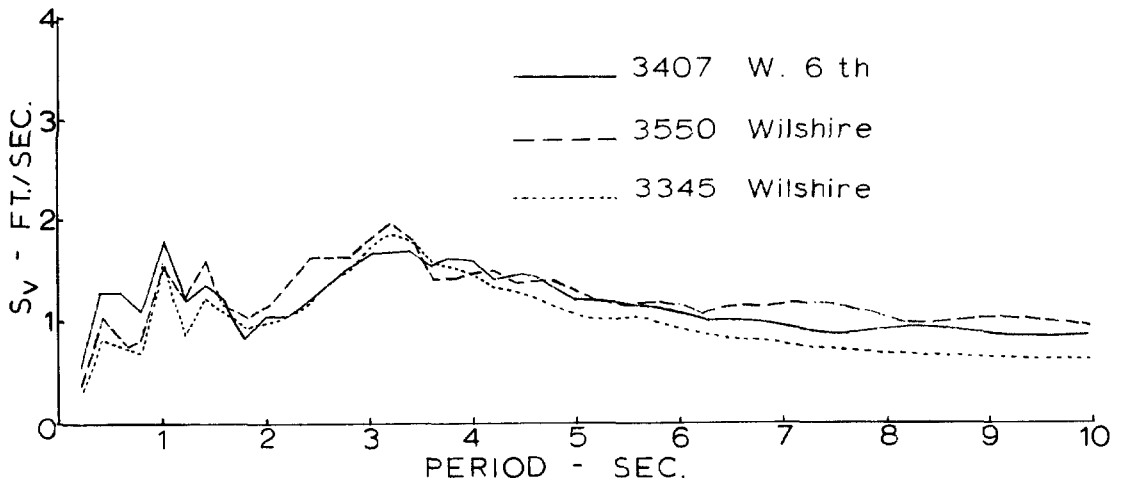


Fig. 48 Relative Velocity Response Spectra. NS Direction. 2% Damping.

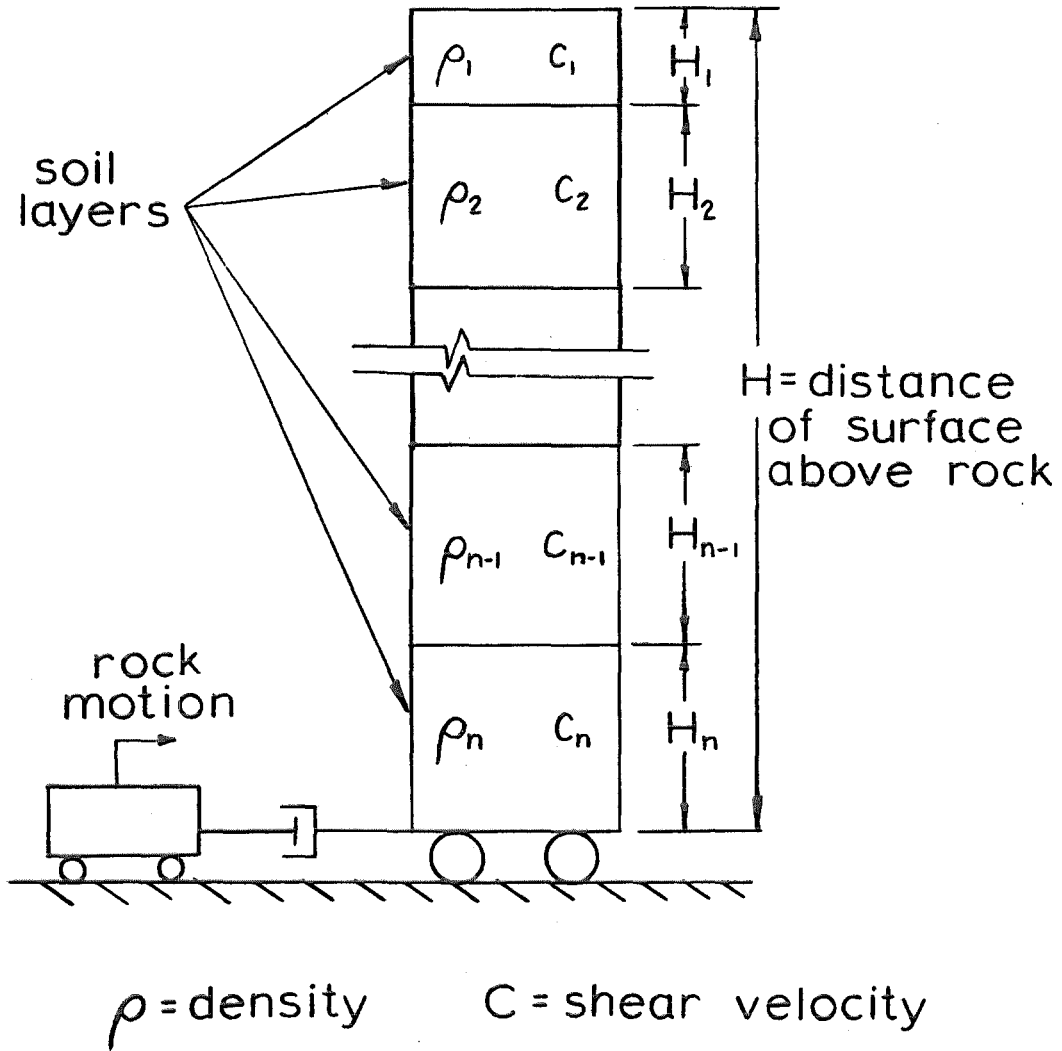


Fig. 49 Shear Beam Model of Layered Half Space.

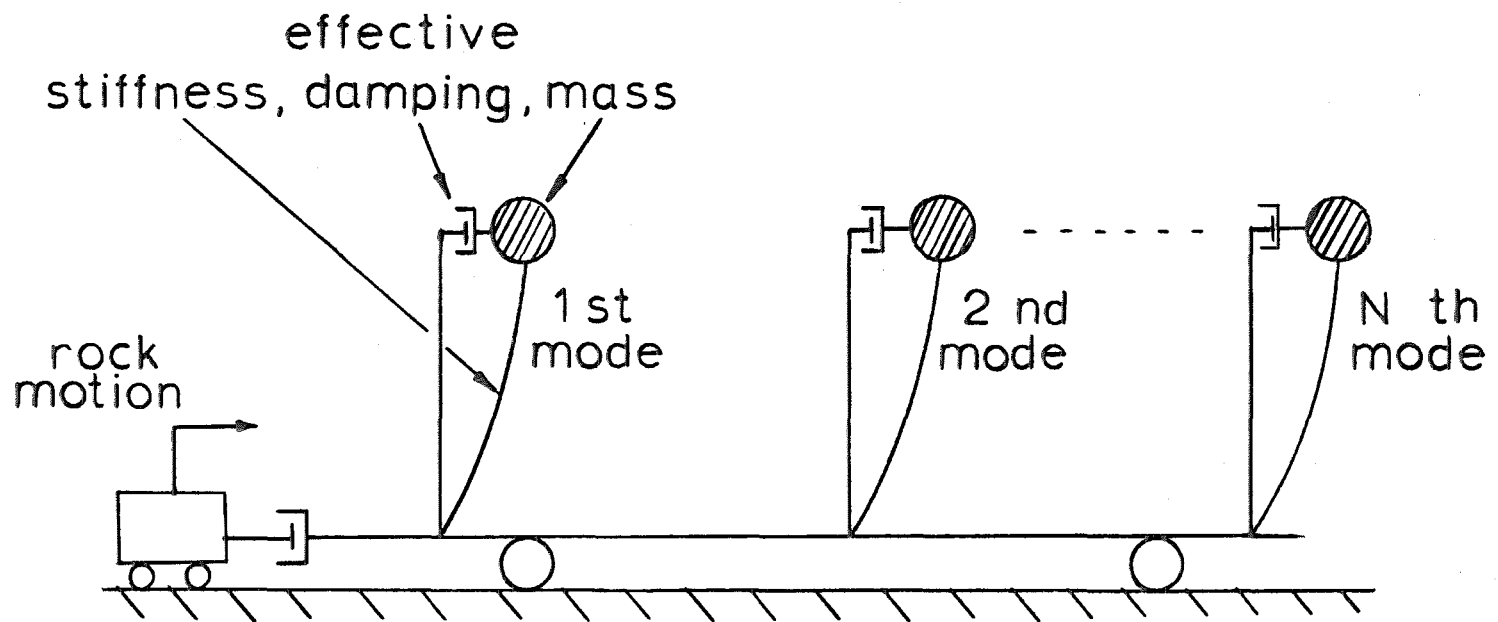


Fig. 50 Modal Representation of Shear Beam Model under Assumption of Classical Normal Modes.

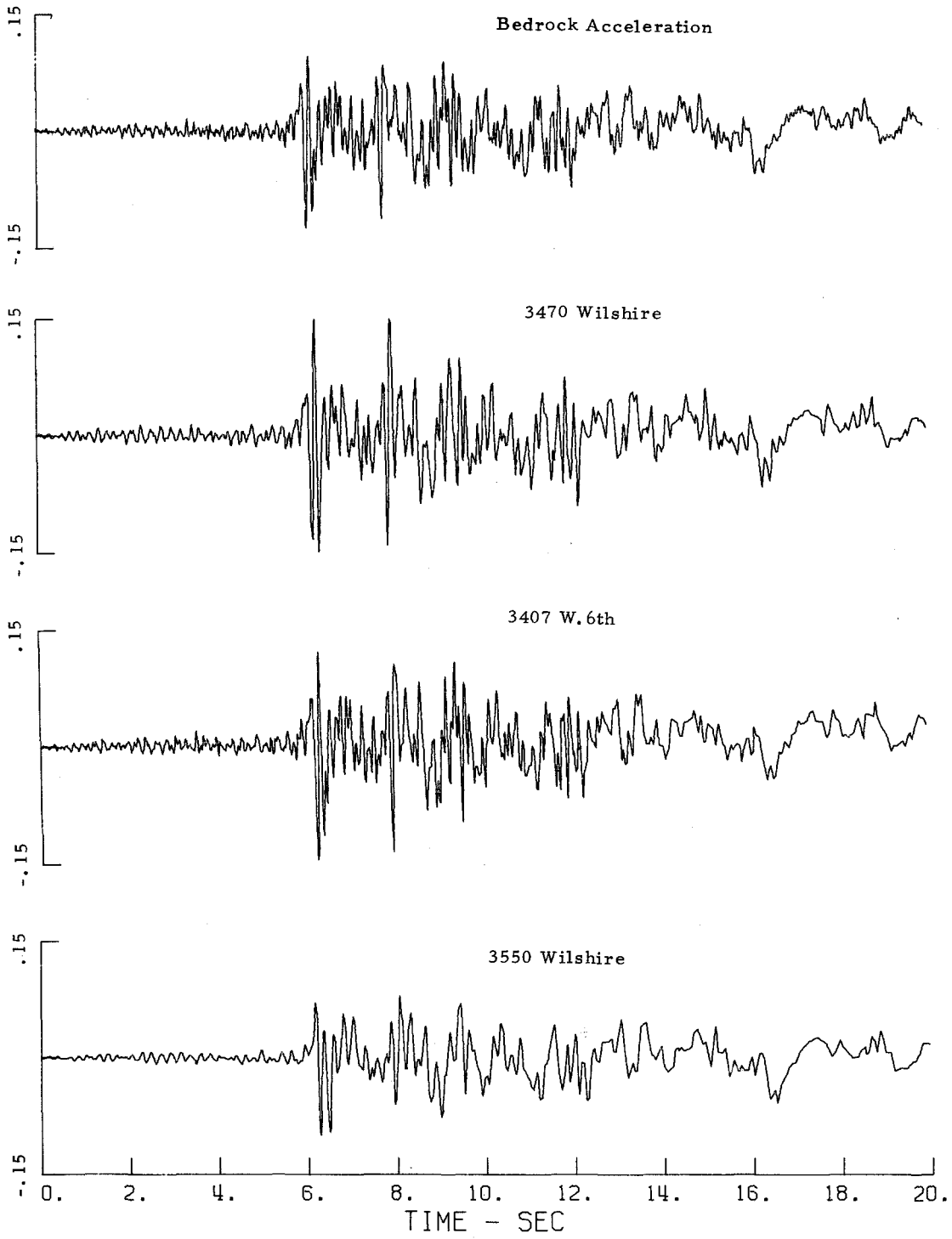


Fig. 51 Bedrock (Input) vs. Computed Surface Accelerations.
0% Damping.

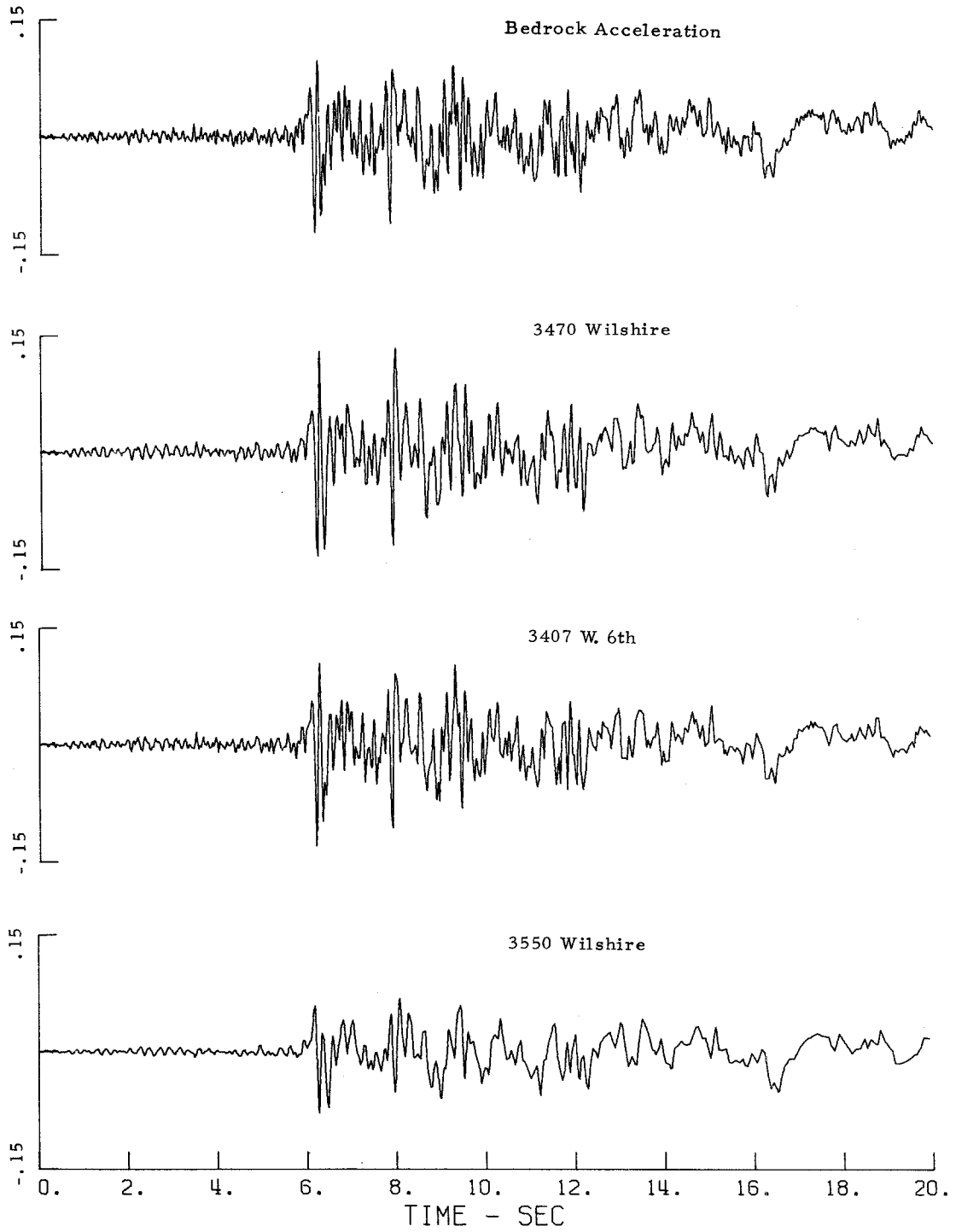


Fig. 52 Bedrock (Input) vs. Computed Surface Accelerations.
5% Damping.

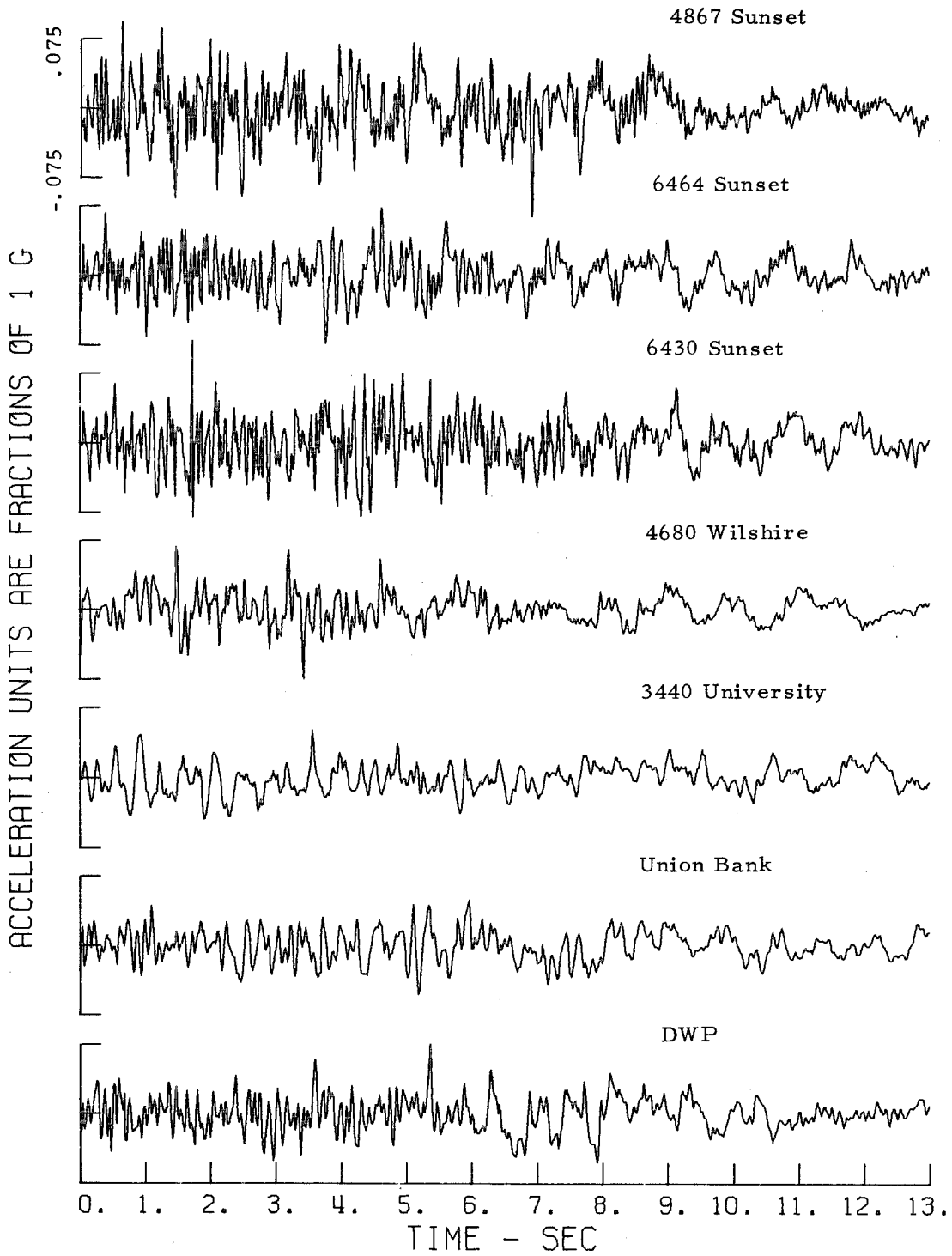


Fig. 53 Vertical Accelerations.

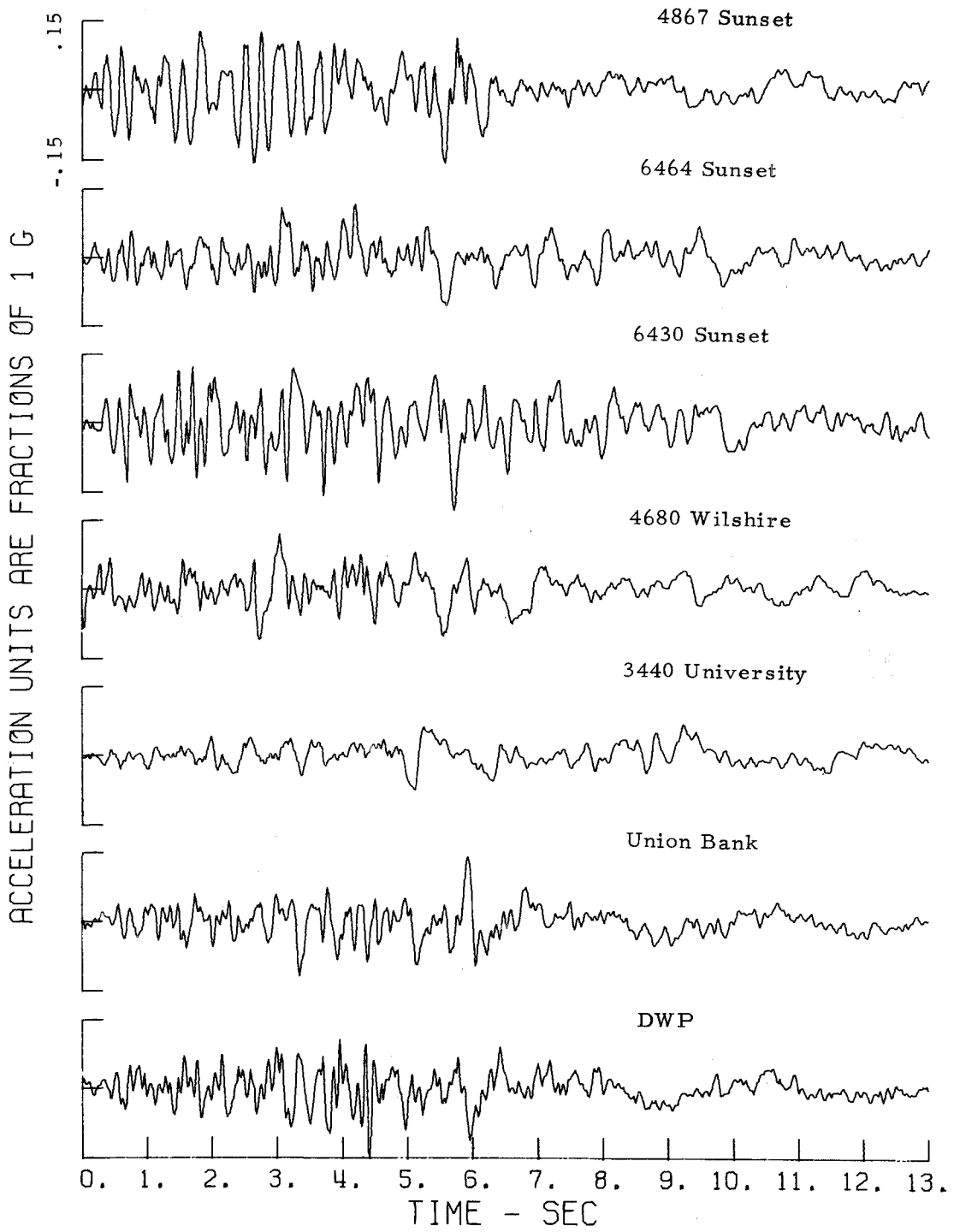


Fig. 54 NS Accelerations.

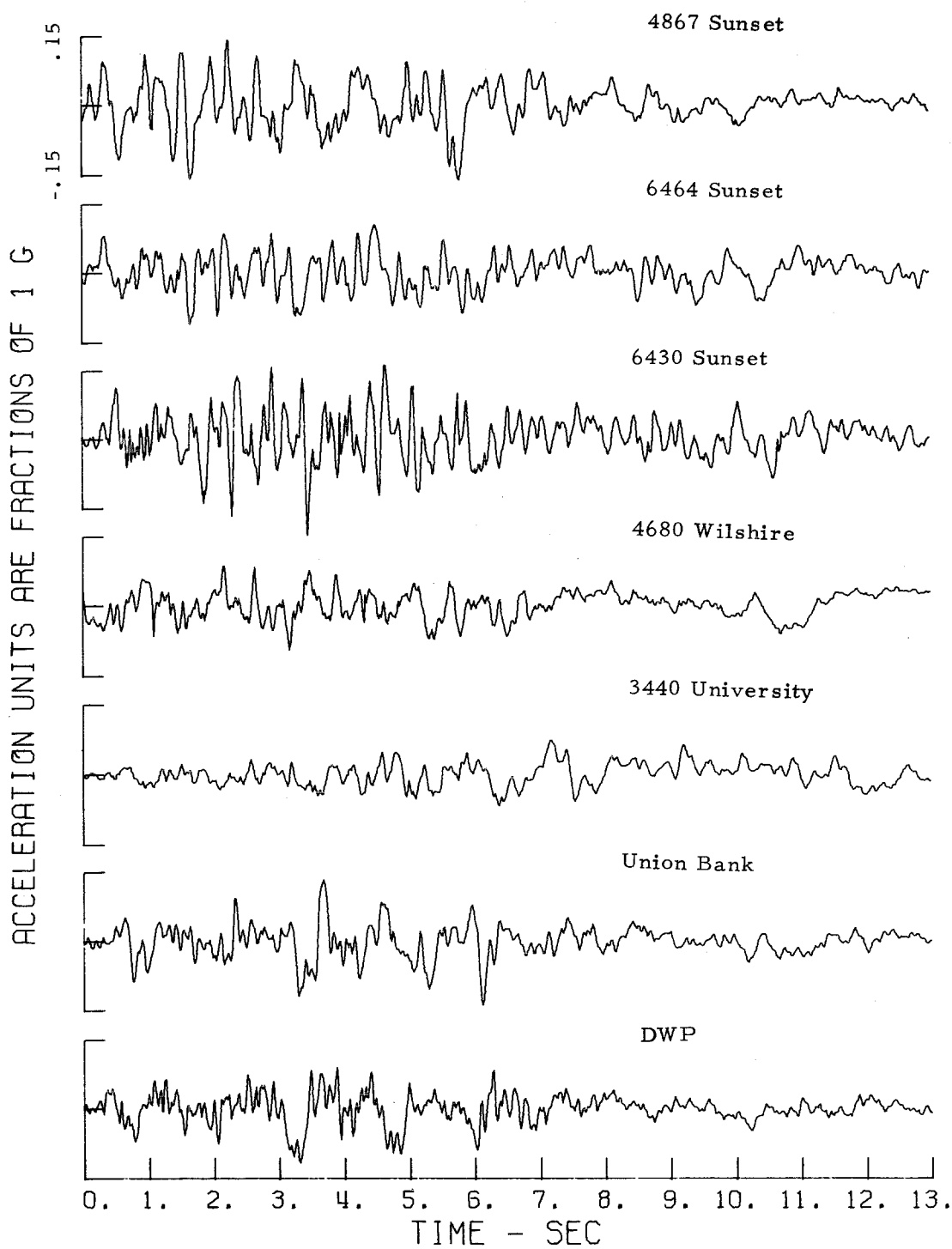


Fig. 55 EW Accelerations .

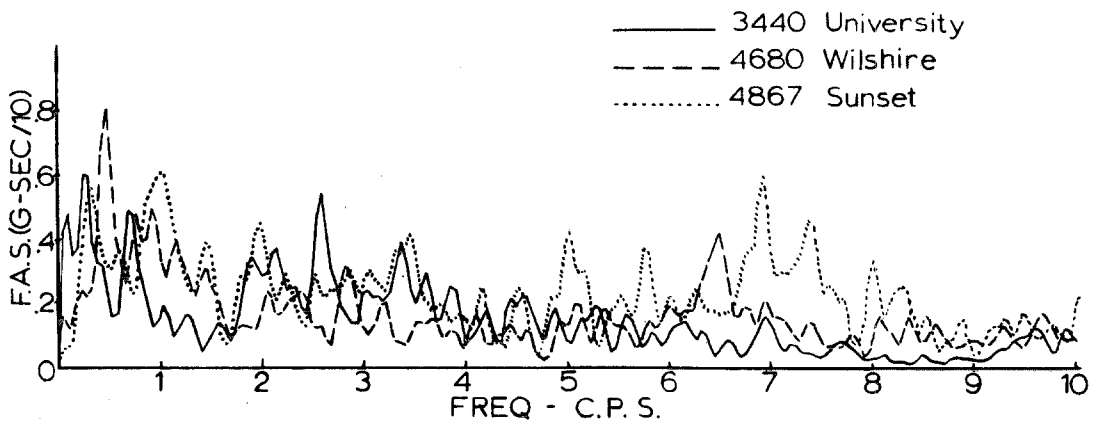
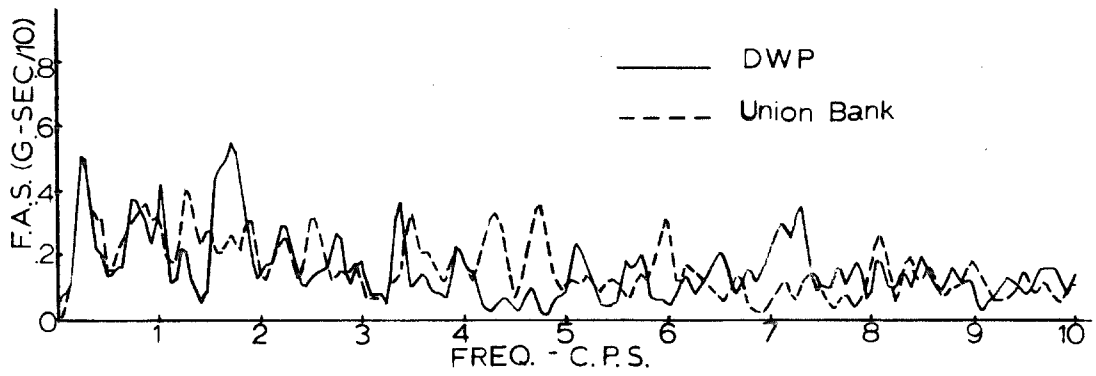
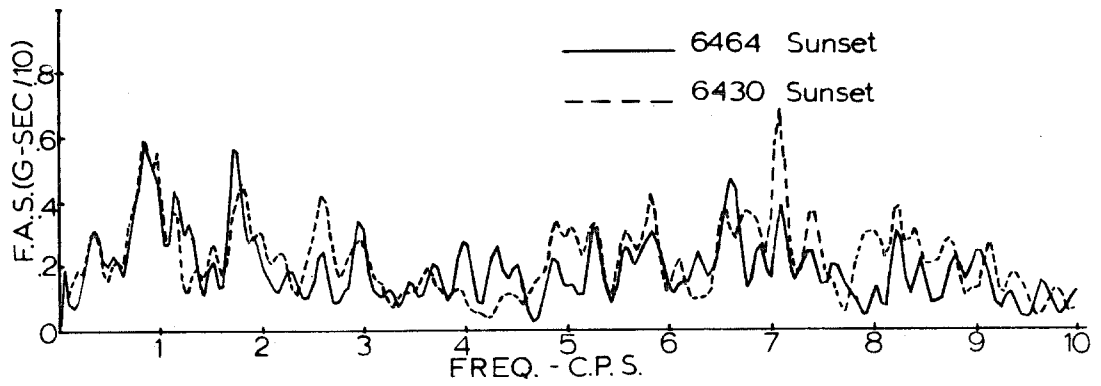


Fig. 56 Fourier Amplitude Spectra. Vertical Direction.

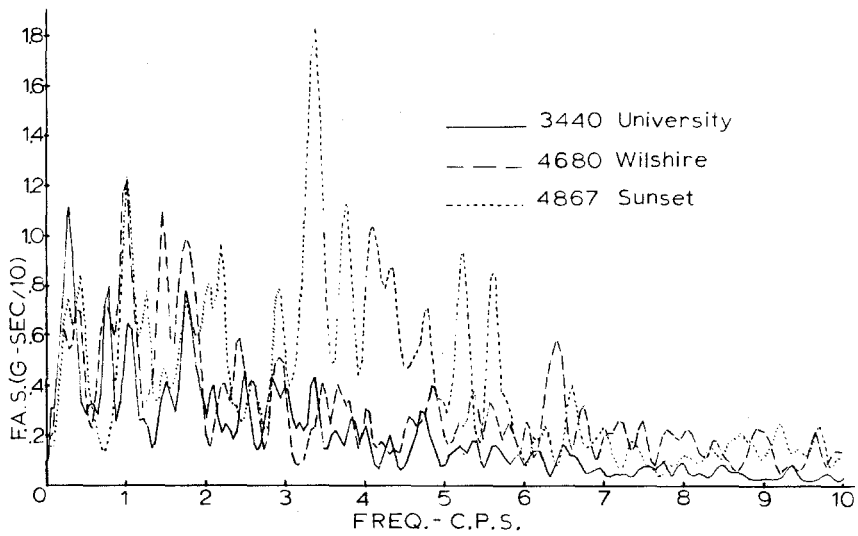
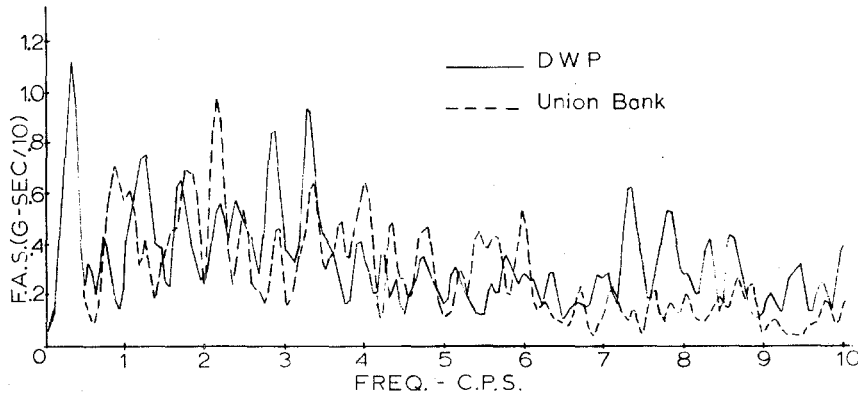
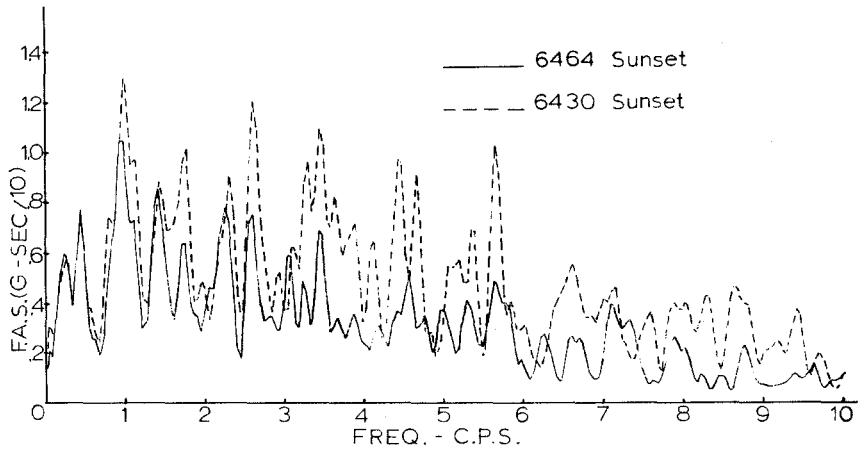


Fig. 57 Fourier Amplitude Spectra. NS Direction.

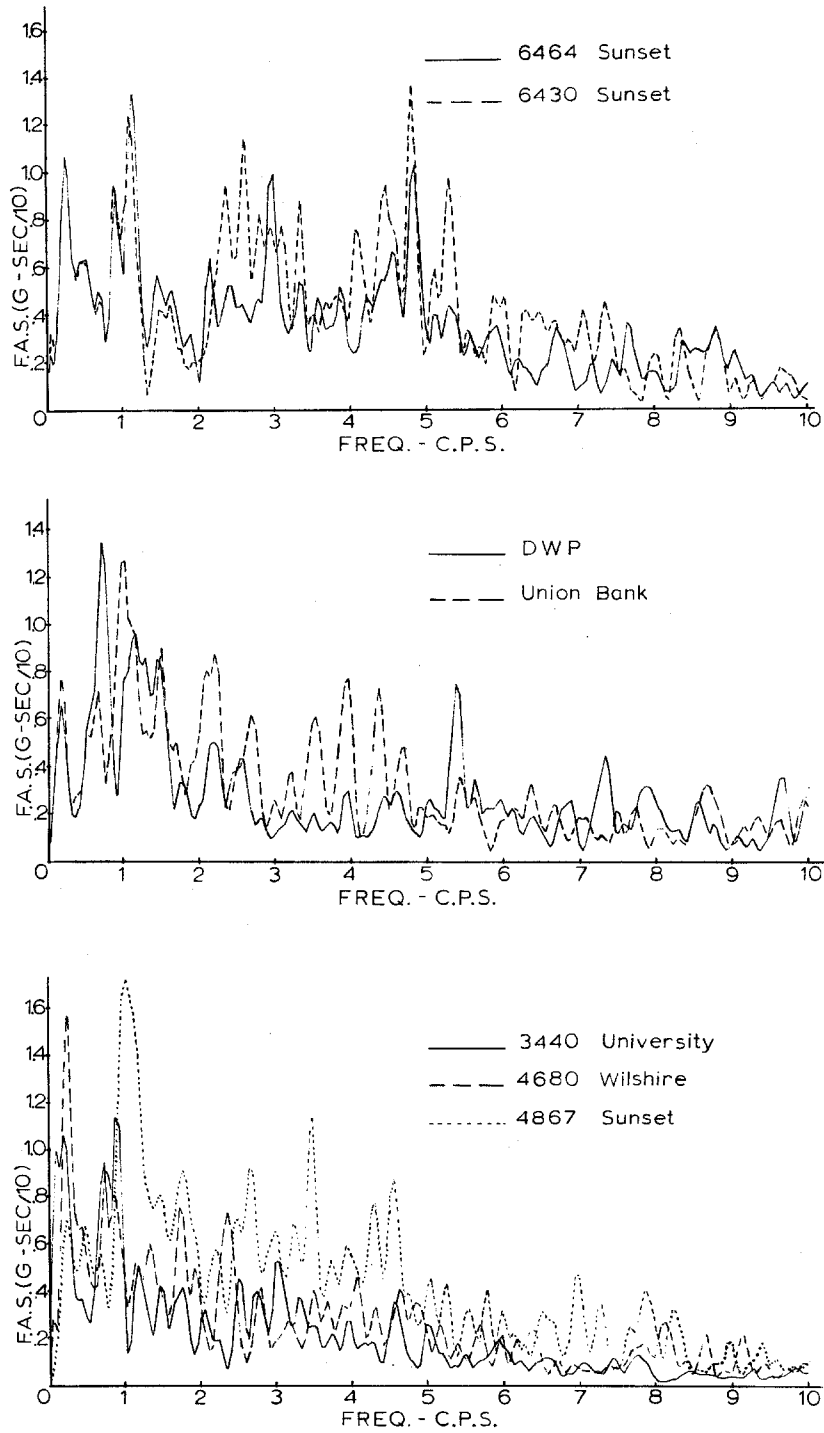


Fig. 58 Fourier Amplitude Spectra. EW Direction.

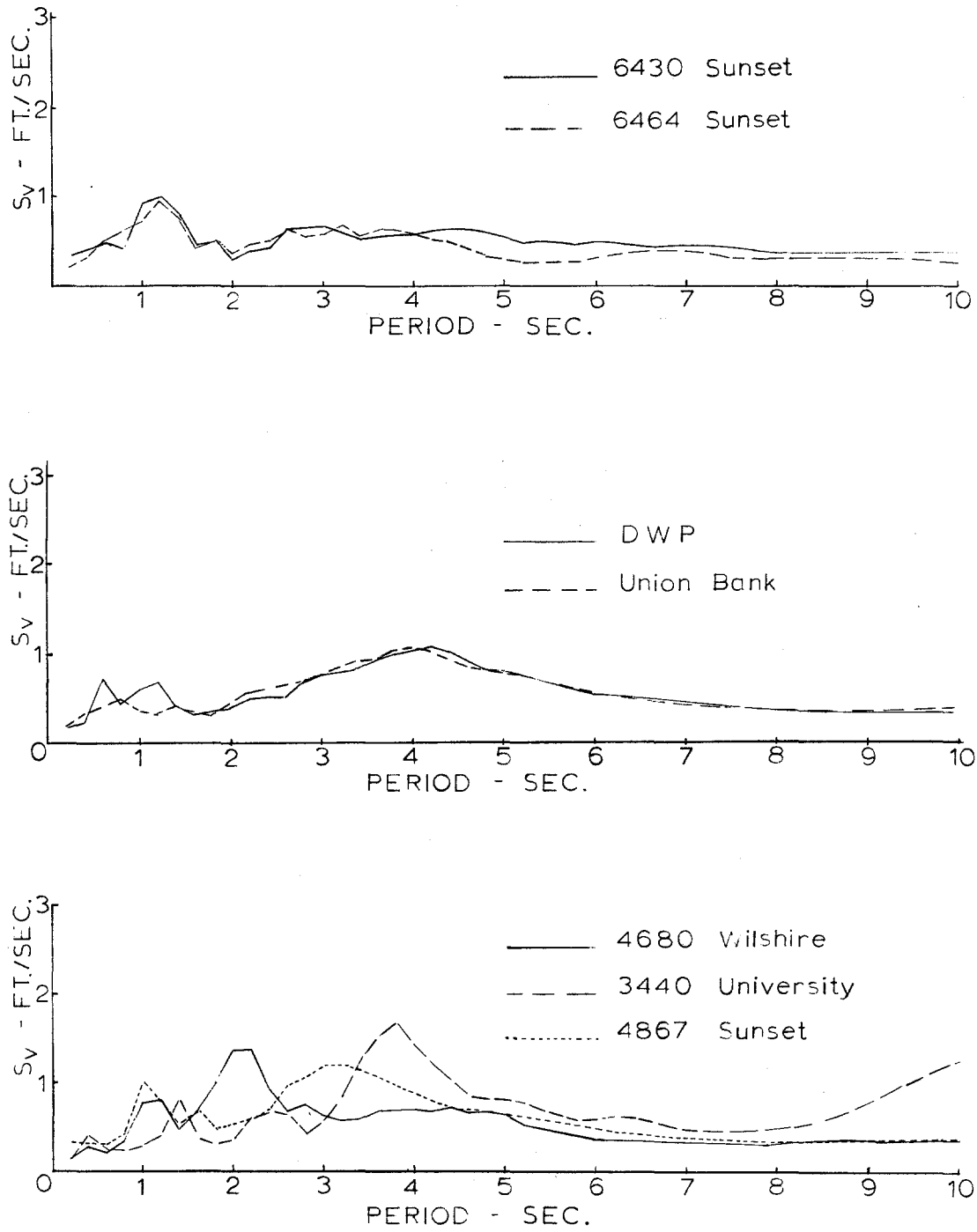


Fig. 59 Relative Velocity Response Spectra. Vertical Direction. 2% Damping.

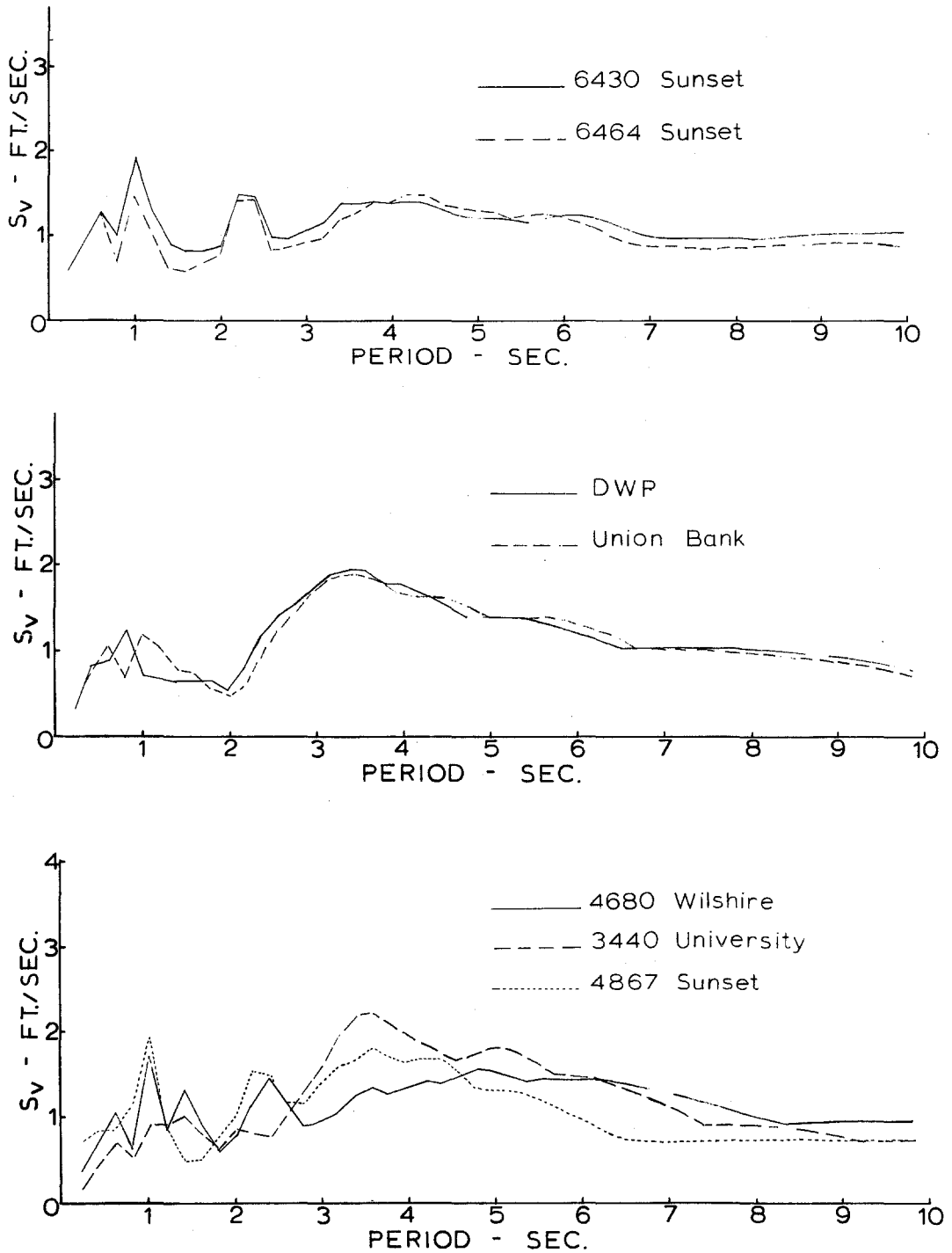


Fig. 60 Relative Velocity Response Spectra. NS Direction. 2% Damping.

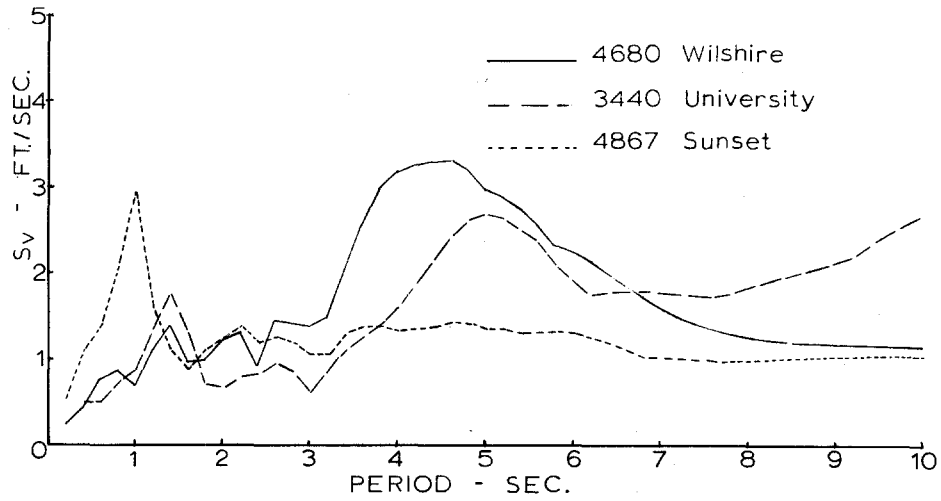
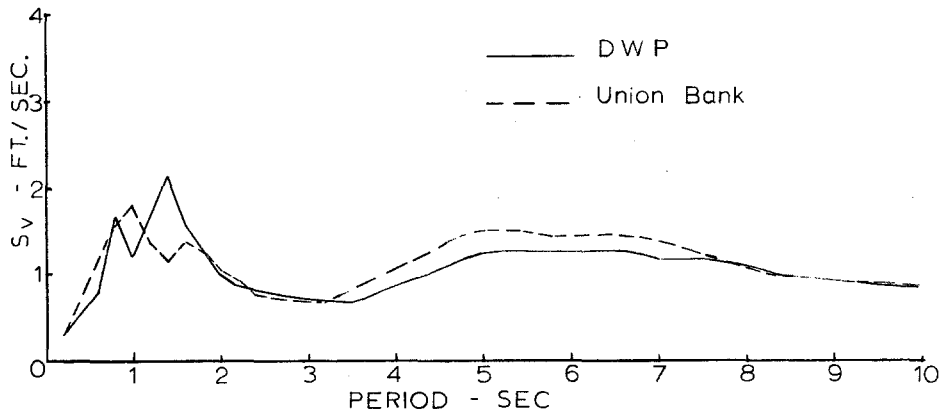
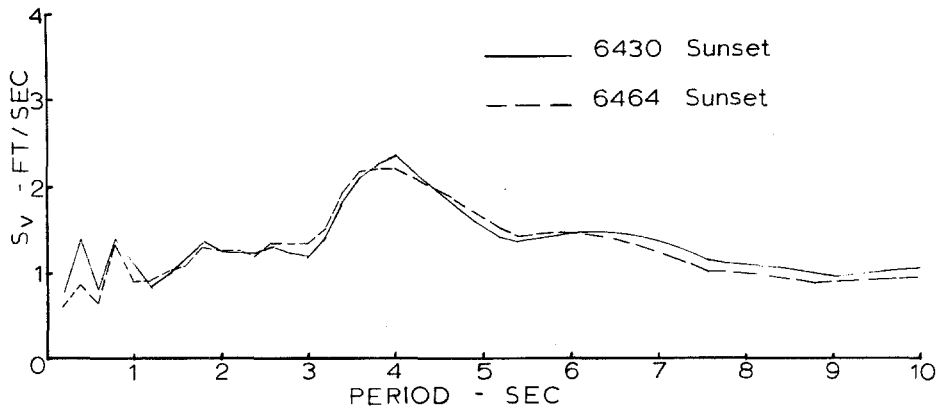


Fig. 61 Relative Velocity Response Spectra. EW Direction. 2% Damping.

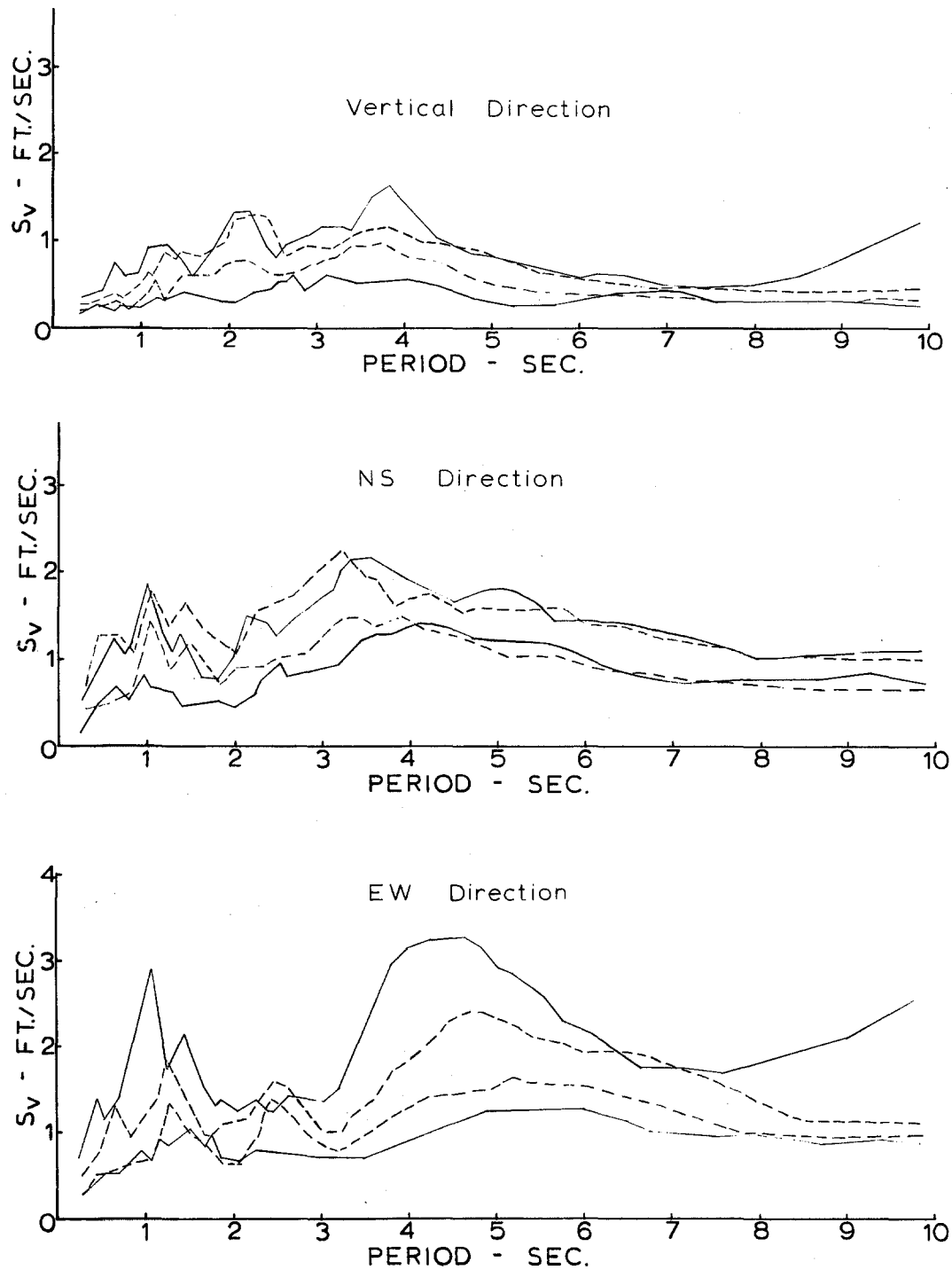


Fig. 62 Maximum and Minimum Response Spectra for Wilshire-Normandie (----) and Surrounding Buildings (—).

IV. STUDIES OF WAVE SUPERPOSITION AND INTERPRETATION
OF DIFFERENCES IN THE ACCELEROGRAMS

IV.1 Introduction

A number of theoretical investigations have been performed to explain variations in accelerograph records at different sites. Theoretical studies on the modification of earthquake waves due to variations in local geology are limited to the cases of horizontally stratified elastic sub-surface layers (43), (44), (45), (46), a semi-cylindrical inclusion at the surface of an elastic half space (47), and a medium having an irregular interface (48). Variations in surface topography have been studied for the special cases of a harmonic surface (49) and surfaces with a step discontinuity (50), semi-cylindrical canyon (51), and a protruding wedge (52). These studies indicate that the effects of surface topography become important for seismic wavelengths comparable to a characteristic dimension of the surface irregularity.

A number of investigators have studied the influence of local site conditions by analyzing available seismic data (53), (54), (55), (56). None of these studies conclusively revealed the presence of any local site periodicities. Clough et al. (57) used a three-dimensional finite element model to investigate the effects of local site conditions on the Pacoima Dam accelerogram obtained during the San Fernando earthquake. They concluded that the local topography was responsible for the extraordinarily large accelerations that were recorded.

The differences observed in the accelerograms from the Wilshire Blvd.-Normandie Ave. area could not be attributed to the minor differences in local geology revealed by the soil borings. Topography was not a factor since the area is fairly flat. Soil-structure interaction, based on the theory, was also ruled out. Wave scattering due to isolated inhomogeneities in the soil, such as the granite boulders encountered at 3411 Wilshire, would not be expected to contribute to differences in the frequency range, 0 to 10 c.p.s., because the earthquake wavelengths in this frequency range are much larger than a typical length of the granite inclusion.

In the previous chapter it was noted that some major differences in accelerograms were associated with distance from the center of the earthquake. On the other hand for sites very close together, such as the buildings in the Wilshire Blvd.-Normandie Ave. area, 6430 and 6464 Sunset, the Union Bank and DWP buildings, and the Hollywood Storage building and adjacent parking lot, it was observed that the degree of similarity in accelerograms was correlated with the separation distance between the sites. This observation suggests that differences in speeds and travel paths of earthquake waves and the resulting differences from superposition or dispersion of these waves may account, at least partly, for the degree of similarity and nature of the differences in the accelerograms.

IV.2 Dispersion

Dispersion is a surface wave phenomenon whereby waves of different frequencies propagate at different speeds. Hence, the appearance of a surface wave with various frequency components is constantly changing with time. The various frequency components gradually separate or disperse and the surface wave consequently becomes longer in duration. A theoretical development of dispersion can be found in the literature (58), (59) and will not be presented herein. However, qualitative features of dispersion, which are relevant to the scope of this section, will be discussed.

The term dispersion applies to surface waves and can only occur in media with different elastic properties. Wave dispersion was first studied by Bromwich (60). Love (61) further developed the topic in an attempt to explain the duration and complexity of earthquake waves. The theory of dispersion for both Rayleigh and Love surface waves predicts that waves of different periods will propagate at different velocities, called phase velocities. The proper relationship between phase velocity and wavelength is determined from a frequency equation which involves the elastic constants, densities, and depths of each layer.

Solutions to the frequency equation have been obtained for specific choices of the parameters involved (62), (63), (64), (65). A plot of dimensionless phase velocity vs. wave period (after Kanai (64)) is shown in Fig. 63 for Rayleigh-wave dispersion in a two layered system, the second layer having infinite depth. The Love-wave

dispersion curve for this case is basically the same (64) except that the phase velocity approaches the shear-wave velocity of the top layer for infinitely small wave periods. The phase velocity always approaches some limiting value as the period increases. For a two-layered system the phase velocity cannot exceed the shear wave velocity of the second layer or substratum (58).

In order for dispersion to account for the differences in the accelerograms from the Wilshire-Normandie group, a significant portion of the energy from the San Fernando earthquake must have been in the form of surface waves. Unfortunately, it does not appear possible, with any degree of confidence, to identify clearly the P (dilatational), S (shear), and surface wave motions in the hard shaking portions of the accelerograms, which exhibit the higher frequency accelerations. This is primarily due to the relatively short distance between the earthquake source region and the accelerograph stations. The duration of the faulting was long enough and the mechanism and propagation so complex that the P, S, and surface waves appear to arrive simultaneously during much of the hard shaking portion. Hence, it does not seem possible to separate their contributions to the strong motion.

The local geology must be known to depths on the order of half wavelengths of the surface waves (58) before any approximate model for dispersion can be formulated. Soil boring depths in the Wilshire-Normandie area were between 40 ft. and 100 ft.; typical half wavelengths for frequencies around 2 c.p.s. and wave speeds around 1,000 f.p.s. would be about 250 ft. A surface wave of this kind would be

influenced by soil properties to this depth; hence, the nature of the dispersion would be determined by some average soil properties over this depth and to a lesser extent by the soil properties at greater depths. Therefore, an informative dispersion model for the Wilshire-Normandie area cannot be constructed on the available soil boring data for frequencies between 2 c.p.s. (half wavelength = 250') and approximately 10 c.p.s. (half wavelength = 50'). It was noted in the previous chapter that differences in the accelerograms from the Wilshire-Normandie area occur for frequencies greater than $2 \pm$ c.p.s.

A study of Kanai's dispersion curves (58) for different combinations of soil layer depths and properties does indicate that dispersion in some cases can account for differences in the appearance of a wave-form for frequencies larger than 2 c.p.s. over distances comparable to the site-to-site distances in the Wilshire-Normandie area. Thus, if the majority of the waves comprising the strong motion were surface waves, dispersion could possibly be a cause of the differences. However, the uncertainty associated with any reliable estimates of the relative energy from surface waves coupled with a lack of knowledge of the soil properties to depths greater than 50 ft. at most sites, precludes any definite claims about the relative importance of dispersion in explaining the observed differences in the accelerograms.

IV.3 Wave Superposition Studies

An earthquake accelerogram is composed of a number of different transient wave pulses of varying types, travel paths, duration, amplitudes, propagation speeds, and frequency content. The super-

position of these waves at a particular location determines the character of the accelerogram recording the motion. In an early study (66) on the composition of accelerograms, Housner assumed a theoretical accelerogram formed by the superposition of a large number of elemental acceleration pulses, random in time, and showed that this accelerogram had much the same character as actual recorded accelerograms. The purpose of this section is to illustrate how the principle of superposition might affect the character of two accelerograms at a given distance apart. Some numerical examples illustrate to a certain extent some of the basic differences encountered in the Wilshire-Normandie accelerograms.

Suppose two accelerograph stations are located a distance, d , apart, and each accelerogram records the same number of transient waves. However, because of different travel paths and/or wave speeds, the waves superimpose differently at the two stations. Intuitively, one would expect accelerograms to exhibit more and more nearly the same character as the distance between the station decreases.

Assuming the recorded accelerations, $a_1(t)$ and $a_2(t)$, at stations 1 and 2 respectively, are composed of a superposition of acceleration pulses, g_i , then

$$a_1(t) = \sum_{i=1}^n g_i(t - \alpha_i)$$
$$a_2(t) = \sum_{i=1}^n g_i(t - \beta_i)$$

(4.1)

where α_i and β_i are the arrival times of the waves, g_i . It is assumed

that the distance between stations is small enough so that the pulse shapes are not modified significantly. Thus, the differences in appearance of $a_1(t)$ and $a_2(t)$ are due to the differences in arrival times, α_i and β_i .

One common method of measuring differences in the accelerograms is the Fourier Amplitude Spectrum (F.A.S.), used in the previous chapters. Let the Fourier transforms of $a_1(t)$ and $a_2(t)$ be $\tilde{a}_1(\omega)$ and $\tilde{a}_2(\omega)$, then by the Fourier shift theorem,

$$\tilde{a}_1(\omega) = \sum_{i=1}^n \tilde{g}_i(\omega) e^{-i\omega\alpha_i} \tag{4.2}$$

$$\tilde{a}_2(\omega) = \sum_{i=1}^n \tilde{g}_i(\omega) e^{-i\omega\beta_i}$$

where $\tilde{g}_i(\omega)$ is the Fourier transform of $g_i(t)$. The F.A.S. is given by the modulus of the Fourier transform. Thus, the differences in the F.A.S. of the two accelerograms, Δ , is given by

$$\Delta = |\tilde{a}_1(\omega)| - |\tilde{a}_2(\omega)| . \tag{4.3}$$

An upper bound on Δ is

$$\begin{aligned} \Delta &\leq |\tilde{a}_1(\omega) - \tilde{a}_2(\omega)| \\ &\leq \left| \sum_{i=1}^n \tilde{g}_i(\omega) (e^{-i\omega\alpha_i} - e^{-i\omega\beta_i}) \right| \\ &\leq \sum_{i=1}^n |\tilde{g}_i(\omega)| |e^{-i\omega\alpha_i} - e^{-i\omega\beta_i}| \end{aligned}$$

which can be written as

$$\Delta \leq 2 \sum_{i=1}^n |\tilde{g}_i(\omega)| \left| \sin \frac{\omega(\beta_1 - \alpha_1)}{2} \right|. \quad (4.4)$$

Thus, the upper bound on the differences, Δ , is a function not only of the frequency of the motion and the difference in arrival times, but also on the F.A.S. of the individual acceleration pulses, $g_i(t)$. If the argument, $\omega(\beta_1 - \alpha_1)/2$, is less than $\pi/2$, equation (4.5) shows that as the distance between two stations increases, i.e., the difference, $\beta_1 - \alpha_1$, increases, the frequency range where the two accelerograms, $a_1(t)$ and $a_2(t)$, exhibit reasonable agreement becomes smaller.

In the examples that follow only two acceleration pulses were considered. It was assumed for convenience that both pulses arrived at station 1 at the same time. At station 2 only the relative time lag between the pulses was considered in the superposition. This relative time lag is a function of the distance between the stations and the apparent velocities of the wave pulses. The apparent velocity is simply the distance between the accelerograph stations divided by the travel time between stations. The apparent velocity as opposed to the actual wave speed reflects the possibility of waves arriving from arbitrary directions and with arbitrary angles of incidence, as well as waves with inherently different wave speeds, owing to wave type or propagation through different soil media in the vicinity of the accelerograph stations. If the apparent velocities of two acceleration pulses are v_1 and v_2 , where $v_1 > v_2$, then the relative time lag, τ ,

between the pulses at station 2 is $\tau = d/v_2 - d/v_1$, where d is the distance between the stations.

The acceleration pulses, $g_1(t)$ and $g_2(t)$, were arbitrarily constructed and are 3 sec. and 2 sec. duration, respectively; their apparent velocities were taken as 1600 f.p.s. and 800 f.p.s., respectively. The distance, d , was varied from 64 ft. to 480 ft. Fig. 64 shows the two acceleration pulses and their F.A.S. The superposition of $g_1(t)$ and $g_2(t)$ at stations 1 and 2 for various values of d are shown in Fig. 65. Comparisons of the F.A.S. of the resultant accelerations, $a_1(t)$ and $a_2(t)$, are shown in Fig. 66a and Fig. 66b.

As expected the resultant accelerations become increasingly dissimilar as d increases. The F.A.S. comparisons of the resultants verify these observations and are consistent with the expected theoretical behavior indicated by equation (4.4). Figs. 66a and 66b show periodic frequency intervals where the F.A.S. of the resultants, $a_1(t)$ and $a_2(t)$, closely agree. This phenomenon is a consequence of the relevant form of equation (4.4) for the numerical examples. For these examples equation (4.4) reduces to, $\Delta \leq 2 |\tilde{g}_2(\omega)| |\sin \frac{\omega T}{2}|$, which shows the periodicity in Δ .

Close agreement exists between the F.A.S. of the resultants for frequency ranges between (0, 1.8 c.p.s.) and (0, 1.0 c.p.s.) for station to station distances from 160 ft. to 480 ft. Similar agreement in these frequency ranges was observed in the Wilshire-Normandie F.A.S. The two F.A.S. which agreed over the largest frequency range were the 616 S. Normandie and the 3411 Wilshire spectra. The agreement varied

up to 1.8 c.p.s. to 3.0 c.p.s. depending on the component compared. The distance between the buildings is approximately 450 ft., but their projected distance apart on a line from the epicentral region is around 200 ft. This distance is the closest to $d = 160$ ft. in the example where the F.A.S. agreement existed for frequencies less than 1.8 c.p.s. The agreement between all of the Wilshire-Normandie F.A.S. was reasonable up to about 1 c.p.s. The examples showed agreement up to about 1 c.p.s. for station to station distances of 320 ft. and 480 ft.

IV.4 Conclusions

If some of the differences in the Wilshire-Normandie accelerograms can be attributed to surface wave dispersion, more information is necessary before any definite claims can be made. Soil data to depths up to 1000 ft. are required to construct a reasonable mathematical model. Even if this model indicated that major differences in accelerograms could be expected, there still remains the question of how much surface wave energy comprised the hard shaking portions of the accelerograms. It does not appear possible to resolve this question based just on an examination of the accelerograms. The P, S, and surface waves are not separated in the hard shaking to permit identification. The alternative involves the formulation of an accurate model of the faulting. So far nothing has been published concerning P, S, and surface wave composition of the main shock of the San Fernando earthquake. Until more information is made available the role of dispersion must remain questionable.

An elementary model, consisting of two acceleration pulses with different apparent velocities, showed to a certain degree the behavior noted in the F.A.S. comparisons of the Wilshire-Normandie accelerograms. The examples graphically illustrated the extent superposition can affect the character of two accelerograms as their distance apart increased. Although imprecise, the model provides a semi-qualitative way of telling what wavelengths are susceptible to modifications between two stations.

The general model developed in the theory, namely, that the accelerograms were composed of a number of wave pulses with different arrival times at each station, assumes that the shape of the pulses remains unchanged in traveling from one station to another. The acceleration data from the Wilshire-Normandie area do not suggest that the shapes of the earthquake waves were modified significantly within this area. Therefore, it appears possible that major differences in accelerograms could be due to differences in the arrival times of the waves because of differences in travel paths and speeds. Comparisons made in the previous chapter among accelerograms 2 to 6 miles apart, however, definitely indicates that the shape of the waves were appreciably modified.

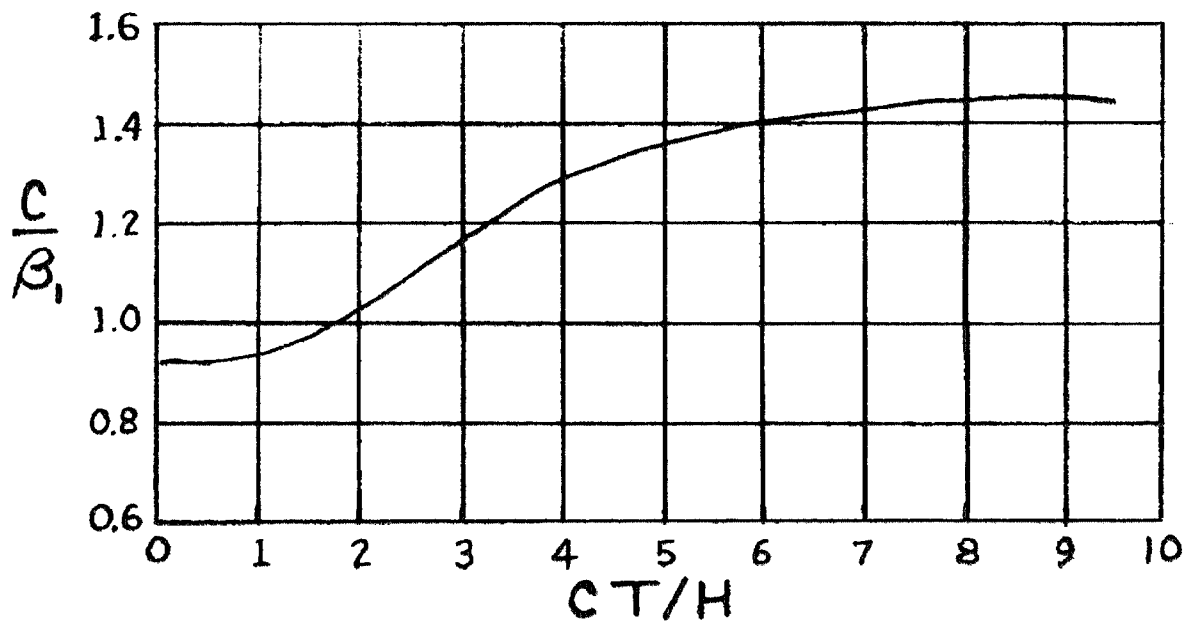


Fig. 63 Rayleigh-Wave Dispersion. c = phase velocity; β_1 = shear-wave velocity of top layer; layer density ratio, $\rho_2/\rho_1 = 1$; shear velocity ratio, $\beta_2/\beta_1 = \sqrt{3}$, T = wave period, H = depth of top layer.

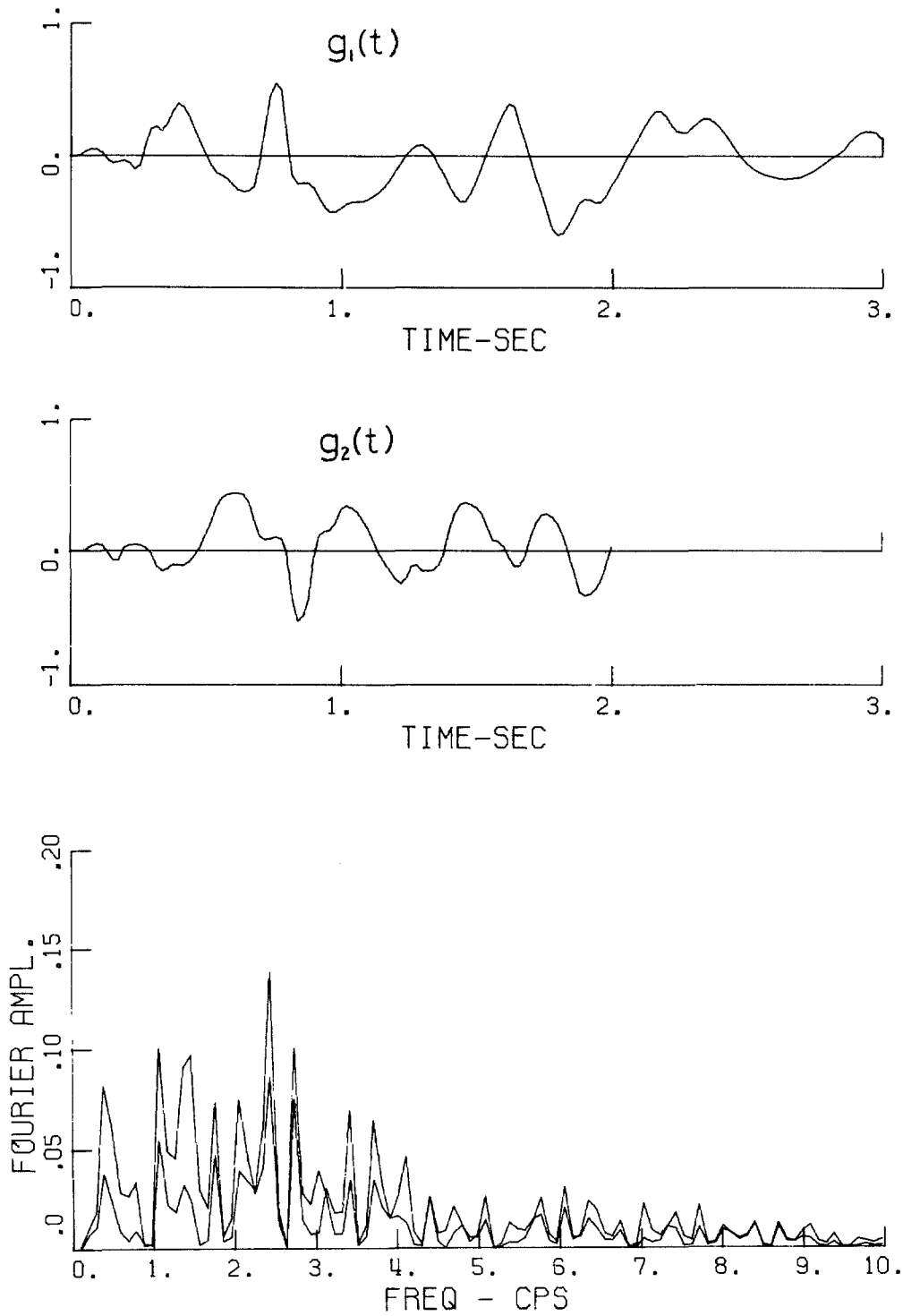


Fig. 64 Accelerations, $g_1(t)$ and $g_2(t)$, and a Comparison of their F.A.S.

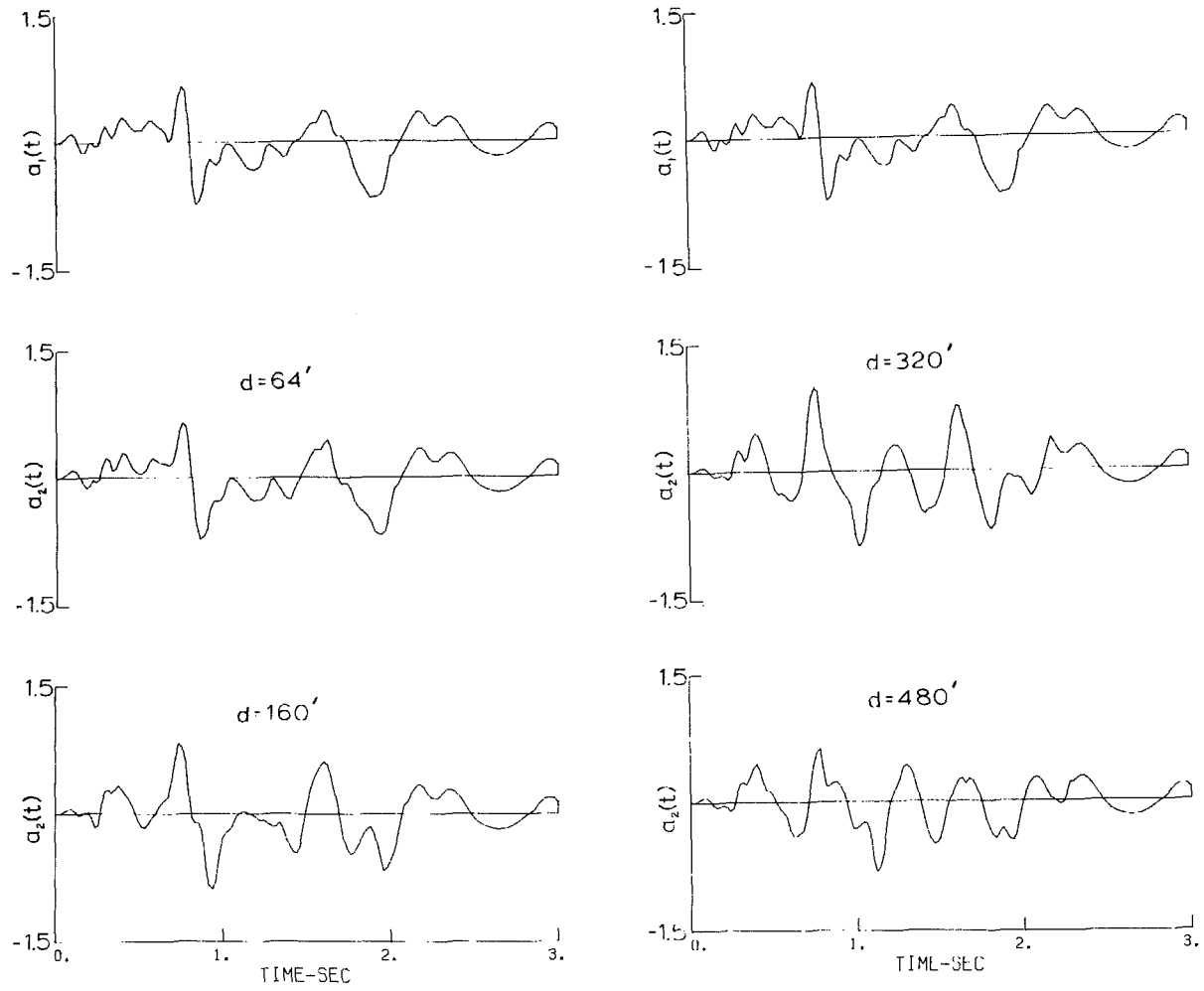


Fig. 65 Comparison of Resultant Accelerations.

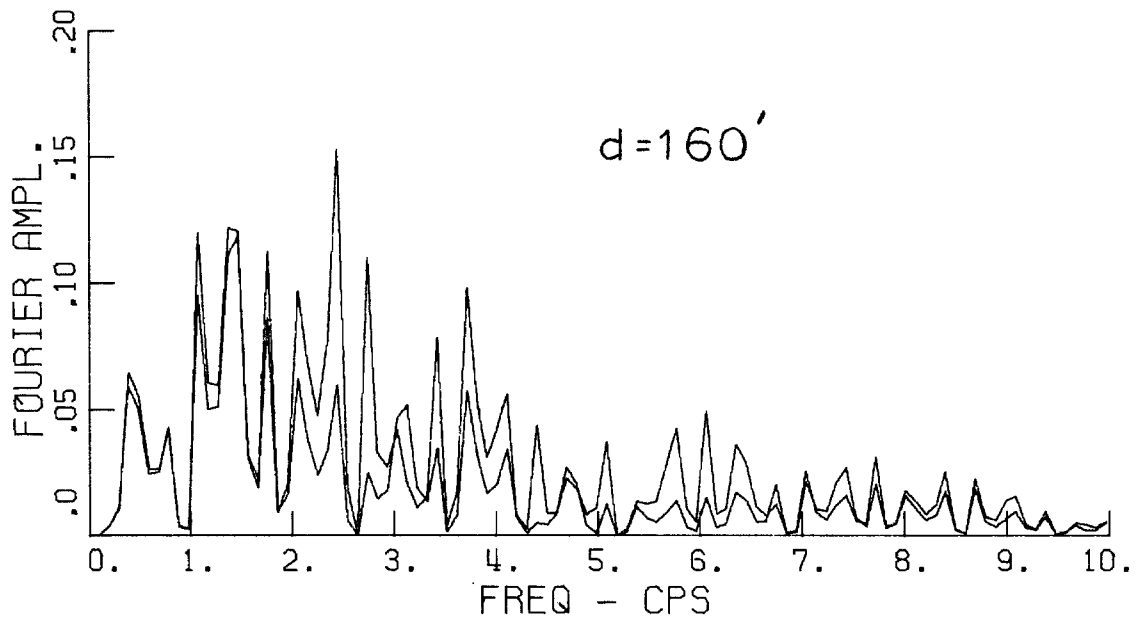
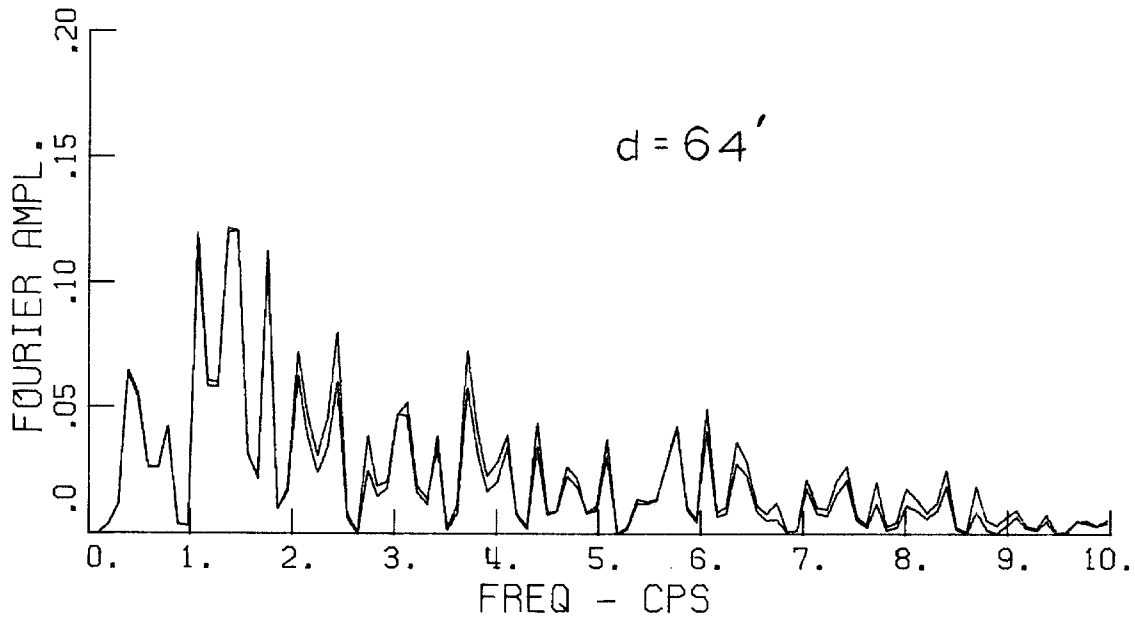


Fig. 66a Comparisons of Fourier Amplitude Spectra.

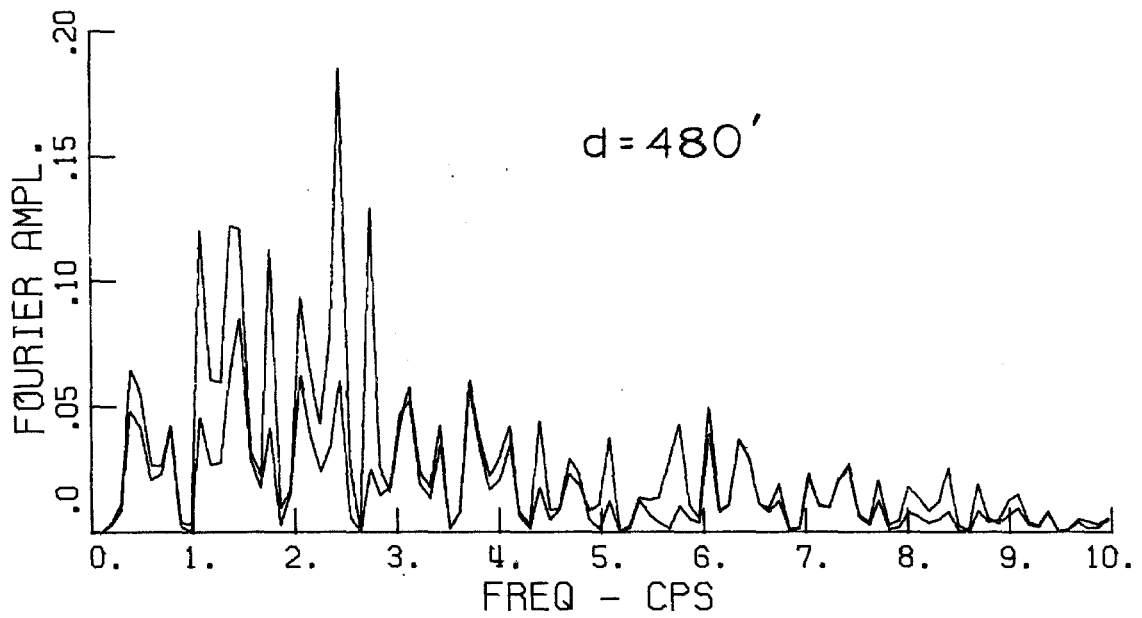
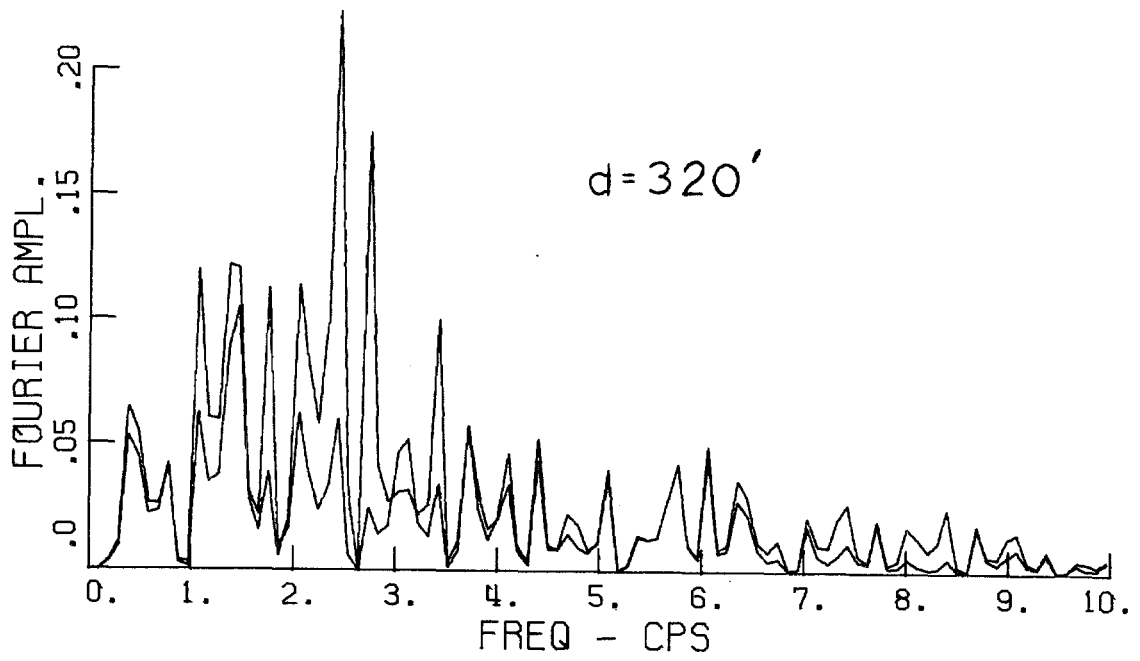


Fig. 66b Comparisons of Fourier Amplitude Spectra.

V. GENERAL CONCLUSIONS

The local effects at the sites studied in this report were not thought to be the major sources of differences observed in the accelerograms from the San Fernando earthquake. Theories of soil-structure interaction and a layered half space subjected to vertically incident shear waves could not account for these differences. Although there was evidence of soil-structure interaction from the fundamental mode of the Hollywood Storage building in one direction, the theoretical model could not predict differences in the accelerograms from the basement and nearby parking lot for higher frequencies. If soil-structure interaction of some form did contribute to major differences in any of the accelerograms, then the general character of the interaction phenomenon must be different from the present theory.

Differences in the ground motion predicted by the theory of a layered half space for the six sites in the Wilshire Blvd.-Normandie Ave. area were not consistent with what actually happened during the earthquake. The response spectra indicated that one design spectrum would be sufficient for buildings in this area. Thus, proposed modifications in design spectra which reflect differences in the sub-soil conditions of the type existing at this location should be seriously questioned, based on the ground motions during the San Fernando earthquake. The data also reaffirm that peak acceleration per se, is not a reliable means for determining design spectra.

The data indicated that the character of the ground motion

was probably most dependent on the source mechanism and the travel paths of the earthquake waves. Differences in travel paths of incoming waves along with differences in wave speeds can substantially modify the ground motion at two sites fairly close together. It was generally observed that the degree of similarity between two accelerograms increased as their separation distance decreased. This phenomenon can be predicted theoretically without the assumption that the shapes of the waves change in traveling between the sites. For sites the same direction from the center of the earthquake but at different distances, differences in the intensity of hard shaking were easily recognized over site-to-site distances as small as 3 miles at an average distance of 21 miles from the center of the earthquake. The higher frequency energy in the hard shaking diminished noticeably over 3 miles. This attenuation was greater for vertical motions than horizontal.

To obtain a better understanding of the soil-structure interaction phenomenon and the nature of the ground motion at a given site during an earthquake, a thorough array of accelerographs is necessary. For example, on the campus of the California Institute of Technology, more accelerographs to measure actual ground motion in addition to the accelerographs already located in the basements of Millikan Library and the Athenaeum, would be helpful in resolving these issues during future earthquakes. Instruments located near these buildings would give a better insight into: (1) the actual interaction phenomenon, (2) the relative importance of soil-structure interaction versus the

effect of the distance between the buildings on the free field motion, (3) variations in ground motion with distance, and (4) the existence and nature of any site periodicities.

APPENDIX

Description of Symbols for Fig. 2a and Eqns. (2.1)

- M = mass matrix of rigid base structure
- C = damping matrix of rigid base structure
- K = stiffness matrix of rigid base structure
- \ddot{v}_g = free field acceleration
- v_j = horizontal displacement of superstructure at j^{th} floor relative to the base mass excluding rotations
- v_o = translation of base mass relative to free field motion
- h_j = height of j^{th} story above base mass
- \underline{v} = $\{v_j\}$, a column vector
- ϕ = rotation of base mass
- $v_j^t = v_g + v_o + h_j\phi + v_j$
- m_j = mass of j^{th} story
- I_j = centroidal moment of inertia of j^{th} mass
- m_o = base mass
- I_o = centroidal moment of inertia of base mass
- $I_t = I_o + \sum_{j=1}^n I_j$
- $P(t)$ = horizontal interaction force between base mass and soil
- $Q(t)$ = interaction moment between base mass and soil
- ρ = mass density of soil
- σ = Poisson's ratio of soil
- V_s = shear wave velocity of soil
- a = radius of base mass
- $\mu = V_s^2 \rho$
- \underline{X}_k = k^{th} mode shape of rigid base structure
- X_{jk} = j^{th} component of \underline{X}_k

Soil-Structure Interaction Transfer Functions for eqn. (2.6).

The transform parameter, s , has been replaced by $i\omega$.

$$\begin{aligned} \Delta &= \omega^4 \sum_{\substack{j,k=1 \\ j \neq k}}^n (M_j \bar{I}_k - Z_j Z_k) \hat{F}_{jk}(\omega) \\ &- \omega^2 (-\omega^2 I_t + \mu a^3 K_{mm}) \left(\sum_{j=1}^n \hat{F}_j(\omega) M_j \right) \\ &- \omega^2 (-\omega^2 m_o + \mu a K_{hh}) \left(\sum_{j=1}^n \hat{F}_j(\omega) \bar{I}_j \right) \\ &+ \prod_{k=1}^n (-\omega^2 + \omega_k^2 + i 2\eta_k \omega \omega_k) [\omega^4 m_o I_t - \mu a^3 \omega^2 m_o K_{mm} \\ &\quad - \mu a \omega^2 K_{hh} I_t + \mu^2 a^4 K_{hh} K_{mm}] . \end{aligned}$$

$$\begin{aligned} \Delta_o &= - \left[-\omega^2 \sum_{\substack{j,k=1 \\ j \neq k}}^n (M_j \bar{I}_k - Z_j Z_k) \hat{F}_{jk}(\omega) \right. \\ &+ (-\omega^2 I_t + \mu a^3 K_{mm}) \left(\sum_{j=1}^n \hat{F}_j(\omega) M_j \right) \\ &- \omega^2 m_o \left(\sum_{j=1}^n \hat{F}_j(\omega) \bar{I}_j \right) \\ &\left. + m_o (-\omega^2 I_t + \mu a^3 K_{mm}) \prod_{k=1}^n (-\omega^2 + \omega_k^2 + i 2\eta_k \omega \omega_k) \right] . \end{aligned}$$

The compliance functions K_{hh} and K_{mm} are

$$K_{mm} = \frac{8\mu a^3}{3(1-\sigma)} \beta_m + i \frac{8\mu a^4 \omega}{3(1-\sigma)V_s} \beta_m \xi_m$$

$$K_{hh} = \frac{8\mu a}{2-\sigma} \beta_h + i \frac{8\mu a^2 \omega}{(2-\sigma)V_s} \beta_h \xi_h$$

where β_m , β_h , ξ_h , ξ_m are functions of $a_o \left(= \frac{\omega a}{V_s} \right)$.

The modal quantities M_j , Z_j , \bar{I}_j are

$$M_j = \frac{\left(\sum_{i=1}^n m_i X_{ij} \right)^2}{\sum_{i=1}^n m_i X_{ij}^2}, \quad \bar{I}_j = \frac{\left(\sum_{i=1}^n m_i h_i X_{ij} \right)^2}{\sum_{i=1}^n m_i X_{ij}^2}$$

$$Z_j = M_j H_j = \frac{\left(\sum_{i=1}^n m_i X_{ij} \right) \left(\sum_{i=1}^n m_i h_i X_{ij} \right)}{\sum_{i=1}^n m_i X_{ij}^2}.$$

The j^{th} undamped natural frequency, ω_j , of the rigid base structure is

$$\omega_j^2 = \frac{\underline{X}_j^T K \underline{X}_j}{\underline{X}_j^T M \underline{X}_j}.$$

The critical damping ratio of the j^{th} mode of the rigid base structure is defined by

$$2\eta_j\omega_j = \frac{\underline{X}_j^T \underline{C} \underline{X}_j}{\underline{X}_j^T \underline{M} \underline{X}_j} .$$

The functions $\hat{F}_j(\omega)$ and $\hat{F}_{jk}(\omega)$ are

$$\hat{F}_j(\omega) = (\omega_j^2 + i 2\eta_j\omega_j\omega) \prod_{\substack{k=1 \\ k \neq j}}^n (\omega_k^2 - \omega^2 + i 2\eta_k\omega_k\omega)$$

$$\hat{F}_{jk}(\omega) = (\omega_j^2 + i 2\eta_j\omega_j\omega)(\omega_k^2 + i 2\eta_k\omega_k\omega) \prod_{\substack{l=1 \\ l \neq k, l \neq j}}^n (\omega_l^2 - \omega^2 + i 2\eta_l\omega_l\omega) .$$

REFERENCES

1. Merritt, R. G. and Housner, G. W., "Effect of Foundation Compliance on Earthquake Stresses in Multistory Buildings," Bull. Seism. Soc. of Amer., Vol. 44, No. 4, Oct., 1954.
2. Housner, G. W., "Interaction of Building and Ground During an Earthquake," Bull. Seism. Soc. of Amer., Vol. 47, No. 3, July, 1957.
3. Reissner, E., "Stational axialsymmetrische durch eine schuttelnde Masse erregte Schwingungen eines homogeneu elastischen Halbraumes," Ingenieur-Archiv, Vol. 7, Dec., 1936.
4. Arnold, R. N., Bycroft, G. N., and Warburton, G. B., "Forced Vibrations of a Body on an Infinite Elastic Solid," Journal of Applied Mechanics, Vol. 22, No. 3, Sept., 1955.
5. Bycroft, R. N., "Forced Vibration of a Rigid Circular Plate on a Semi-Infinite Elastic Space and on an Elastic Stratum," Philos. Trans. Roy. Soc. London, Ser. A, Vol. 248, Jan., 1956.
6. Warburton, G. B., "Forced Vibration of a Body on an Elastic Stratum," Journal of Applied Mechanics, Vol. 24, No. 1, March, 1957.
7. Veletsos, A. S. and Wei, Y. T., "Lateral Rocking Vibration of Footings," Journ. of Soil Mech. and Found Div., ASCE, Vol. 97, No. SM9, Sept., 1971.
8. Lucco, J. E. and Westmann, R. A., "Dynamic Response of Circular Footings," Journ. of the Eng. Mech. Div., ASCE, Vol. 97, No. EM5, Oct., 1971.
9. Lysmer, J. and Richart, F. E., "Dynamic Response of Footings to Vertical Loading," Journ. of Soil Mech. and Found. Div., ASCE, Vol. 92, SM1, Jan., 1966.
10. Novak, M., "Vibrations of Embedded Footings and Structures," Meeting Preprint 2029, ASCE National Structural Engineering Meeting, San Francisco, Ca., April, 1973.
11. Kobori, T., Minai, R., Suzuki, T., Kusakabe, K., "Dynamical Ground Compliance of Rectangular Foundations," Proceedings of Sixteenth Japan National Congress for Applied Mechanics, 1966.
12. Thomson, W. T. and Kobori, T., "Dynamical Compliance of Rectangular Foundations on an Elastic Half-Space," Journal of Applied Mechanics, Vol. 30, Ser. E., No. 4, Dec., 1963.

13. Sarrazin, M. A., "Soil Structure Interaction in Earthquake Resistant Design," Research Report R70-59, Dept. of Civil Eng., Mass. Inst. of Tech., Sept., 1970.
14. Trifunac, M. D., "Surface Motion of a Semi-Cylindrical Alluvial Valley for Incident Plane SH Waves," Bull. Seism. Soc. of Amer., Vol. 61, No. 6, Dec., 1971.
15. Trifunac, M. D., "Interaction of a Shear Wall with the Soil for Incident Plane SH Waves," Bull. Seism. Soc. of Amer., Vol. 62, No. 1, Feb., 1972.
16. Luco, J. E., "Dynamic Interaction of a Shear Wall with Soil," Journ. of Eng. Mech. Div., ASCE, Vol. 95, EM2, April, 1969.
17. Sarrazin, M. A., Roesset, J. M., and Whitman, R. V., "Dynamic Soil-Structure Interaction," Journ. of Structural Div., ASCE, Vol. 98, No. ST7, July, 1972.
18. Parmelee, R. A., Perelman, D. S., and Lee, S. L., "Seismic Response of Multiple-Story Structures on Flexible Foundations," Bull. Seism. Soc. of Amer., Vol. 59, No. 3, June, 1969.
19. Bielak, J., "Earthquake Response of Building-Foundation Systems," Ph.D. Thesis, Calif. Inst. of Tech., EERL 71-04, May, 1971.
20. Fagel, L. W. and Liu, S., "Earthquake Interaction for Multistory Buildings," Journ. of Eng. Mech. Div., ASCE, Vol. 98, EM4, Aug., 1972.
21. Wood, J. H., "Analysis of the Earthquake Response of a Nine-Story Steel Frame Building During the San Fernando Earthquake," Report No. EERL 72-04, Calif. Inst. of Tech., Oct., 1972.
22. Finn, W. D. L. and Reimer, R. B., "Effect of Soil Structure Interaction on Seismic Response," Proc. of Third Eur. Symp. on Earthquake Eng., Sofia, Bulgaria, Sept., 1970.
23. Warburton, G. B., Richardson, J. D., and Webster, J. J., "Forced Vibrations of Two Masses on an Elastic Half Space," Journal of Applied Mechanics, ASME, Vol. 38, Ser. E, No. 1, March, 1971.
24. Gladwell, G. M. L., "Forced Tangential and Rotary Vibrations of a Rigid Circular Disc on a Semi-infinite Solid," Int. Journal of Eng. Science, Vol. 6, 1968.
25. Jennings, P. C. and Bielak, J., "Dynamics of Building Soil Interaction," Bull. Seism. Soc. of Amer., Vol. 63, No. 1, Feb., 1973.

26. Duke, C. M., Luco, J. E., Carriveau, A. R., Hradilek, P. J., Lastrico, R., and Ostrom, D., "Strong Earthquake Motion and Site Conditions: Hollywood," Bull. Seism. Soc. of Amer., Vol. 60, No. 4, Aug., 1970.
27. Duke, C. M. and Leeds, D. J., "Site Characteristics of Southern California Strong-Motion Earthquake Stations," Dept. of Eng., Univ. of Calif. at Los Angeles, Report No. 62-55, Nov., 1962.
28. Seed, H. B. and Idriss, I. M., "Soil Moduli and Damping Factors for Dynamic Response Analysis," Univ. of Calif. at Berkeley, Report No. EERC 70-10, Dec., 1970.
29. Carder, D. W. (editor), Earthquake Investigations in the Western United States, U.S. Dept. Comm., Coast and Geodetic Survey, Pub. No. 41-2, 1964.
30. Jennings, P. C., Matthiesen, R. B., and Hoerner, J. B., "Forced Vibration of a 22-story Steel Frame Building," Earthquake Eng. and Struct. Dyn., Journ. of Int'l. Assoc. for Earthquake Eng., Vol. 1, No. 2, Oct.-Dec., 1972.
31. Kuroiwa, J. H. "Vibration Test of a Multistory Building," Degree of Civil Engineer Thesis, Calif. Inst. of Tech., May, 1967.
32. Nielsen, N. N., "Dynamic Response of Multistory Buildings," Ph.D. Thesis, Calif. Inst. of Tech., 1964.
33. Lung, R., and Proctor, R. (editors), Engineering Geology in Southern California, Special Publication, Association of Engineering Geologists, Oct., 1966.
34. Halverson, H. T., "A Technical Review of Recent Strong Motion Accelerographs," Proceedings Fifth World Conference on Earthquake Engineering, Rome, Italy, June, 1973.
35. Jennings, P. C., "Rapid Calculation of Selected Fourier Spectrum Ordinates," Caltech Earthquake Engineering Research Laboratory, Report No. EERL-72-05, Nov., 1972.
36. Wiegel, R. L., Earthquake Engineering, Prentice-Hall, Inc., Englewood Cliffs, N.J., 1970.
37. Nigam, N. C. and Jennings, P. C., "Digital Calculation of Response Spectra from Strong-Motion Earthquake Records," Caltech Earthquake Engineering Research Laboratory, June, 1968.
38. Beredugo, Y. O. and Novak, N., "Coupled Horizontal and Rocking Vibrations of Embedded Footings," Canadian Geotechnical Journal, Vol. 9, No. 4, 1972.

39. Seed, H. B., Schnabel, P., and Lysmer, J., "Modification of Seismograph Records for Effects of Local Soil Conditions," Bull. Seism. Soc. Amer., Vol. 62, No. 6, Dec., 1972.
40. Tsai, N. C., "Influence of Local Geology on Earthquake Ground Motion," Ph.D. Thesis, Caltech, May, 1969.
41. Scott, R. F., private communication.
42. Hudson, D. E. (editor), "Strong-Motion Instrumental Data on the San Fernando Earthquake of Feb. 9, 1971," Caltech Earthquake Engineering Research Laboratory, Seismological Field Survey, Sept., 1971.
43. Kanai, K., "The Requisite Conditions for Predominant Vibration of Ground," Bull. Earthquake Research Inst., Vol. 35, 1957.
44. Herrera, I. and Rosenblueth, E. "Response Spectra on Stratified Soil," Proc. 3rd World Conf. Earthq. Eng., New Zealand, Vol. I, 1965.
45. Haskell, N. A., "Crustal Reflection of Plane P and SV Waves," Jour. Geoph. Research, Vol. 67, 1962.
46. Tsai, N. C., "A Note on the Steady-State Response of an Elastic Half-Space," Bull. Seism. Soc. Amer., Vol. 60, No. 3, June, 1970.
47. Trifunac, M. D., "Surface Motion of a Semi-Cylindrical Alluvial Valley for Incident Plane SH Waves," Bull. Seism. Soc. Amer., Vol. 61, No. 6, Dec., 1971.
48. Aki, K. and Larner, K., "Surface Motion of a Layered Medium Having an Irregular Interface Due to Incident Plane SH Waves," Journal Geophys. Res., Vol. 75, No. 5, Feb., 1970.
49. Abubakar, I., "Reflection and Refraction of Plane SH Waves at Irregular Interfaces I, II," Journal Phys. Earth, Vol. 10, 1962.
50. Sato, R., "Diffraction of SH Waves at an Obtuse Angled Corner," Journal Phys. Earth, Vol. 11, 1963.
51. Trifunac, M. D., "Scattering of Plane SH Waves by a Semi-Cylindrical Canyon," Earthquake Eng. and Structural Dyn., Vol. 1, 1973.
52. Boore, D., "A Note on the Effect of Topography on Seismic Waves," Bull. Seism. Soc. Amer., Vol. 62, 1972.
53. Gutenberg, B., "Effects of Ground on Earthquake Motion," Bull. Seism. Soc. Amer., Vol. 47, 1957.

54. Byerly, P., "The Periods of Local Earthquake Waves in Central California," Bull. Seism. Soc. Amer., Vol. 30, 1940.
55. Wiggins, J. H. "Effects of Site Conditions on Earthquake Intensity," Journal Structural Div., A.S.C.E., ST2, 1964.
56. Udawadia, F. E., "Investigation of Earthquake and Microtremor Ground Motions," Ph.D. Thesis, Caltech, Sept., 1972.
57. Clough, R. W., Reimer, R. B., and Raphael, J. M., "Evaluation of Pacoima Dam Accelerogram," Proceedings of Fifth World Conference on Earthquake Engineering, Rome, Italy, June, 1973.
58. Ewing, W. M., Jardetzky, W. S., and Press, F., Elastic Waves in Layered Media, Chapt. 4, McGraw-Hill, 1957.
59. Havelock, T. H., The Propagation of Disturbances in Dispersive Media, Stechert-Hafner Service Agency, 1964.
60. Bromwich, J. T. I'A., "On the Influence of Gravity on Elastic Waves, and, in Particular, on the Vibrations of an Elastic Globe," Proc. London Math Soc., Vol. 30, 1898.
61. Love, A. E. H., Some Problems of Geophysics, Cambridge University Press, London, 1911, 1926.
62. Haskell, N. A., "The Dispersion of Surface Waves in Multilayered Media," Bull. Seism. Soc. Amer., Vol. 43, 1953.
63. Jeffreys, H., "The Surface Waves of Earthquakes," Monthly Notices Roy. Astron. Soc.: Geophys. Suppl., Vol. 3, 1935.
64. Kanai, K., "On the Group Velocity of Dispersive Surface Waves," Bull. Earthquake Research Inst. (Tokyo), Vol. 29, 1951.
65. Sezawa, K., "Dispersion of Elastic Waves Propagated on the Surface of Stratified Bodies and on Curved Surfaces," Bull. Earthquake Research Inst. (Tokyo), Vol. 3, 1927.
66. Housner, G. W., "Properties of Strong Ground Motion Earthquakes," Bull. Seism. Soc. Amer., Vol. 45, No. 3, July, 1955.
67. Cassano, R. C., "Earthquake Codes - Poison or Panacea?" Meeting Preprint 1947, ASCE National Structural Engineering Meeting, San Francisco, Ca., April, 1973.